Spiracular control in moth pupae

Passive generation of respiratory patterns

D I S S E R T A T I O N

zur Erlangung des akademischen Grades

Doctor rerum naturalium
im Fach Biologie

eingereicht an der
Mathematisch-Naturwissenschaftlichen Fakultät I
Humboldt-Universität Berlin

von
Dipl. Biol. Thomas Daniel Förster
18.04.1977 in Hennigsdorf

Präsident der Humboldt-Universität Berlin:
Prof. Dr. Dr. h.c. Christoph Markschies

Dekan der Mathematisch-Naturwissenschaftlichen Fakultät I:
Prof. Dr. Lutz-Helmut Schön

Gutachter:
1. PD Dr. Matthias Hennig, Berlin
2. Prof. Dr. H. Arthur Woods, Missoula
3. Prof. Dr. Timothy J. Bradley, Irvine

eingereicht am: 25. März 2010
Tag der mündlichen Prüfung: 8. Juni 2010

Abstract

In conditions of low metabolic activity moth pupae of *Attacus atlas* show a triphasic, rhythmic pattern of CO_2 release (discontinuous gas exchange, DGC). The phases, *closed*, *fluttering* and *open* respectively, are labeled according to the behavior of the spiracles, which control gas exchange. However, a single spiracle only possesses two states, that is open or closed. *Fluttering* thus might be alternatively interpreted as a resonance phenomenon, which will cease to occur if endotracheal gas composition were held constant.

Experimentally, a constant composition could be achieved by perfusion of the tracheal system in live animals. Perfusion pressure served as a signal of spiracle opening state. The results of the experiment confirmed, that *fluttering* is not a steady state behavior. Spiracles are either continually closed or continually open during the perfusions. A plot of spiracle state *vs.* p_{O_2} and p_{CO_2} roughly confirms the conclusions of Burkett and Schneiderman (1974b). The observed thresholds for spiracle opening are lower though (p_{O_2} approx. 2-5 kPa, p_{CO_2} approx. 1-1.5 kPa) and, surprisingly, a distinct *fluttering* region is lacking completely. The higher resolution of the method suggested that the threshold curve is a bilinear function, supporting the emergent property hypothesis (Chown et al., 2006). According to this hypothesis two distinct feedback loops interact during the DGC and create the complex pattern of CO_2 release.

The second part of the thesis discusses possible mechanisms that may serve as the basis of the two required feedback loops. Mathematical modelling is used to show that these mechanisms are in accordance with the requirements posed by previous observation.

The most simplistic CO_2 based control uses pH as sensor input. In aqueous solutions CO_2 hydrates to carbonic acid which dissociates quickly and acidifies the hemolymph. This drop in pH can be detected and converted into an activation of the spiracle muscle (modelled as a sigmoidal dependence of spiracle aperture on pH). If pH is too high, the spiracles close, too low and the spiracles open. Neuronal pattern generaters like dedicated respiratory centers or specialized CO_2 sensing organs were obsolete in this model.

Interestingly even this simple model oscillates when physiologically meaningful parameters are fed into it. All that is required is a low metabolic rate combined with relatively large tracheal conductance. Furthermore the spiracle activation has to be relatively sensitive to small changes in pH, which is in accordance to the observed two state behavior of the spiracles. If metabolic rate is increased the CO_2 release pattern changes from discontinuous to continuous, as postulated by Bradley (2008). Reducing either internal conductance or spiracle conductance also resulted in a switch to continuiously open spiracles (Hetz, 2007). In contrast to the naturally observed rhythms (with period length up to 6 h) the cycles in the model were much shorter (10 - 20 min). The reasons for that are not fully understood at the moment.

The oxygen based control, which is most prominently evident during *fluttering*, was modelled as a metameric extension of the mechanism proposed by Burkett and Schneiderman (1974b). Multiple independently controlled segments were diffusively coupled in sequential order. This coupling resulted in a synchronisation between neighboring segments without higher order central nervous control. Depending on the coupling strength, that is the conductance of the longitudinally running tracheae, quite different patterns of *fluttering* could be observed. These ranged from regular single spiracle opening with strong coupling (as observed in beetles)

to nearly random behavior if coupling strength is low. The spatial arrangement of opening spiracles compares to data of Sláma (1988).

Both, the experimental results and the mathematical models provide strong support for the emergent property hypothesis of DGC. It could be shown that at least in lepidopteran pupae without active ventilation, the complex DGC might be the result of quite simple feedback loops without the need of elaborate pattern generators.

Zusammenfassung

Unter Bedingungen geringer metabolischer Aktivität zeigen Schmetterlingspuppen der Art *Attacus atlas* ein dreiteiliges, rhythmisches Muster der CO_2 Abgabe (*discontinuous gas exchange cycles*, DGC), welche durch die Stigmen kontrolliert wird. Die einzelnen Phasen sind dabei nach dem Verhalten der Stigmen *Closed*, *Fluttering* und *Open* benannt. Ein einzelnes Stigma besitzt allerdings nur zwei Zustände - offen oder geschlossen. Das Fluttern könnte demnach auch als Resonanzphänomen der Stigmenregulation gedeutet werden, welches bei erzwungener konstanter Gaszusammensetzung im Tracheensystem nicht aufträte.

Experimentell wurde die konstante Gaszusammensetzung durch eine Perfusion des Tracheensystems erreicht. Der Öffnungszustand der Stigmen konnte dabei durch den Perfusionsdruck überwacht werden. Es zeigte sich, daß das Fluttern in der Tat kein Gleichwichtszustand ist. Vielmehr kommt es bei konstanter endotrachealer Gaszusammensetzung entweder zu einer dauerhaften völligen Öffnung oder vollständigen Schließung der Stigmen. Trägt man den Öffnungszustand der Stigmen gegen den p_{O_2} und p_{CO_2} auf, folgt die Struktur dieses Phasenraums grob der von Burkett and Schneiderman (1974b). Allerdings sind die beobachteten Schwellwerte für die Stigmenöffnung wesentlich geringer (p_{O_2} ca. 2-5 kPa, p_{CO_2} ca. 1-1.5 kPa) und eine Flutter-Region fehlt völlig. Durch die höhere Auflösung zeigte sich, daß die Schwellwertkurve nicht einheitlich ist. Vielmehr besitzt sie eine bilineare Struktur, welche mit der "Emergent property hypothesis" (Chown et al., 2006) vereinbar ist. Demnach interagieren im DGC zwei getrennte Regelkreise für CO_2 und O_2 miteinander und erzeugen so das komplexe Muster der CO_2 Abgabe. Unter der Prämisse der *emergent property hypothesis* werden im zweiten Teil mögliche Mechanismen für die zwei geforderten Regelkreise diskutiert. Anhand von mathematischen Modellen wurde belegt, daß diese den sich ergebenden Anforderungen an eine Atemregulierung genügen.

Die einfachste vorstellbare auf CO_2 basierende Kontrolle ist ein von der pH Regulation abgeleiteter Mechanismus. Durch die Hydratation von CO_2 zu Kohlensäure in wässrigen Lösungen kommt es zu einer Ansäuerung der Hämolymphe und damit zu einem Abfall des pH. Dieser Abfall kann zellulär detektiert und als sigmoide Aktivierungsfunktion neuronal mit den Stigmen verschaltet werden. Bei zu hohem pH schließen die Stigmen, bei zu niedrigem pH öffnen sie. Neuronale Mustergeneratoren im Sinne von respiratorischen Zentren oder Schrittmachern sowie spezielle CO_2-Sinnesorgane würden hierbei nicht benötigt.

Dieses einfache Modell ist im physiologischen Parameterbereich zu Oszillationen fähig. Voraussetzung ist eine niedrige Stoffwechselrate, bei gleichzeitig relativ großer Konduktanz des Tracheensystems. Weiterhin mußte die sigmoide Aktivierungsfunktion sehr scharf sein, was sich mit der beobachteten binären Regelung der Stigmenöffnungsweite deckt. Eine alleinige Veränderung der Stoffwechselrate bewirkt im Modell einen Wechsel zwischen kontinuierlicher und diskontinuierlicher CO_2 Abgabe, genau wie von Bradley (2008) diskutiert. Ebenfalls traten im Modell immer dann Oszillationen auf, wenn die Stigmenkonduktanz gegenüber der Stoffwechselrate groß war (Hetz, 2007).

Im Unterschied zu den natürlichen Rhythmen mit Periodendauern von bis zu sechs Stunden, waren mit dem Modell nur Zyklen von wenigen Minuten Dauer zu realisieren. Die Gründe hierfür sind zur Zeit noch nicht vollständig verstanden.

Für die O_2-abhängige Stigmenregelung wurde der vorgeschlagene Mechanismus von Burkett and Schneiderman (1974b) auf mehrere unabhängige Segmente erwei-

tert. Das Modell zeigte, daß sich unterschiedliche und teilweise scheinbar zufällige Rhythmen der Stigmenöffnung in der Flutterphase durch das Zusammenwirken der Stigmenkontrolle mehrerer Segmente erklären lassen. Die diffusive Kopplung durch longitudinale Tracheenstämme bewirkt dabei eine Synchronisation der Stigmenöffnung zwischen benachbarten Segmenten, auch ohne übergeordnete, zentralnervöse Kontrolle. Die räumliche Verteilung der sich öffnenden Stigmen gleicht dabei den Messungen von Sláma (1988).

Die experimentellen Ergebnisse sowie die beiden mathematischen Modelle bieten starke Hinweise zur Unterstützung der emergent property hypothesis als möglicher Erklärung für das Auftreten diskontinuierlicher CO_2 Abgabe bei Schmetterlingspuppen. Die beiden geforderten Regelkreise wurden dabei als pH bzw. O_2 Regulation konkretisiert.

Contents

Part I.

Introduction

1. Insect respiration

Insects are a very unique group of animals. Not only do they differ in morphology from almost all other phyla, also many physiological structures and processes are only found in insects and closely related groups. One of them is the respiratory gas exchange which is the exclusive topic of this work.

Contrary to vertebrates with their gills and lungs, insects possess a distinct air-filled respiratory system which uses common distribution mechanisms for respiratory gases in a different way. The next section will present this tracheal system in more detail and highlight its apparent efficiency. Indeed the system is efficient enough that in special circumstances insects are able to employ it only intermittently, a phenomenon that became known as discontinuous gas exchange (DGC; see Lighton, 1996, for review).

1.1. The tracheal system

In contrast to most other animals insects do not rely on internal circulation to provide oxygen to their tissues (Chapman, 1998). They developed a respiratory system - the tracheal system - which is able to transport oxygen and carbon dioxide in the gas phase right to the tissues. This saves the energetically costly convective transport of gases dissolved in liquid.

The tracheal system of insects generally consists of gas-filled, branching tubes that ramify into all parts of the body. The distal ends of the tubes concentrate at lateral pores in the external cuticle which connect the tracheal system to the outside. These spiracles, as the pores are called, are augmented in most insects with a valve-like structure which allows to seal the tracheal system. This closing apparatus ultimately effects the changes in diffusive and convective conductance which are necessary to control the tracheal gas composition.

Peritreme and sieve plate are the only parts of the tracheal system that are visible externally. The former simply is a thickening of the cuticle which surrounds the spiracle aperture. It probably enhances the mechanical stability of the whole spiracle region.

A sieve plate covers the spiracle in most insects. Its dense network of trabeculae consists of exocuticular structures and prevents the entry of parasites, drops of water or dust into the tracheal system (Miller, 1974). It has been hypothesized that it also reduces bulk air flow due to the increased frictional drag, which in turn is thought to minimize respiratory water loss (Miller, 1974).

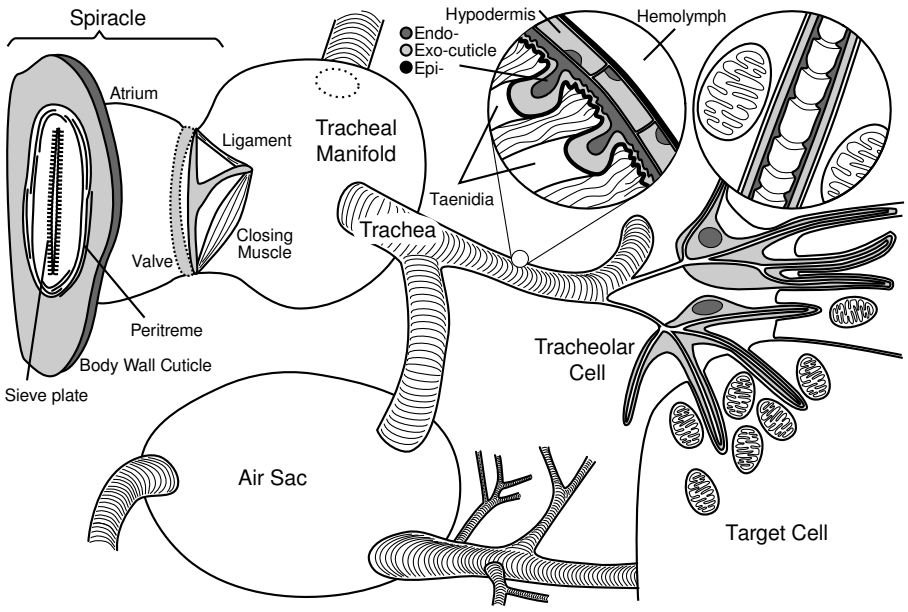

Figure 1.1.: Schematic view of the insect tracheal system. Not to scale. Adapted from Chapman (1998); Wigglesworth (1965); Miller (1974).

The closing apparatus of spiracles in Saturniidae like *Attacus atlas* is of the lever-and-bar type (Schmitz and Wasserthal, 1999). The single closing muscle, when contracted, presses the bar against the opposite wall of the spiracle and closes it. Possibly a thin liquid film (Burkett and Schneiderman, 1974b; Kestler, 1985) effects a gas tight seal (Bridges et al., 1980).

When the muscle relaxes, an elastic ligament made of connective tissue and having been tensed by the contraction pulls the lever back and stretches the closing muscle. The increasing spiracular aperture, when large enough, destroys the liquid film and allows gas exchange between the tracheal space and the surrounding air.

Tracheae constitute the nominal part of the tracheal system. They are gas-filled tubes that form a variably branched hierarchy. The branching is not strictly dichotomous and loops and interconnections between tracheae frequently occur.

The tracheal walls show the typical cross section of insect cuticle with a base epidermal layer which excretes the endo- and exocuticle. Chemical composition and morphology is similar to the respective layers of the body wall cuticle.

There is one exception though. Found only in the tracheae, taenidiae form helical rings of cuticle on top of the tracheal cuticle, i.e. in the tracheal lumen. They have been attributed to prevent the collapse of the tracheae in which they occur.

Interestingly, tracheal collapse has been observed regularly in some species. Herford (1938) described rhythmic pulsations in the flea. More recently these or similar pulsations have been rediscovered when looking at insects in synchrotron x-rays (Westneat

et al., 2003, 2008). To date, it is still unclear whether these rhythmic contractions of the whole tracheal system serve respiratory purposes and might be the cause of convective redistribution of air in the tracheal system.

Because of the relatively thick cuticle it has been assumed that no or only few lateral diffusion across the wall of larger tracheae does occur. The oxygen pathway is thought to follow the tracheal lumen up to the fine terminal branches before the gas dissolves in the hemolyph and tissue liquids. However, as Schmitz and Perry (1999) have shown, about 25 % of the oxygen might be delivered across the tracheal walls of larger tracheae in the stick insect *Carausius morosus*.

Tracheoles comprise the finest branches of the tracheal system with a diameter of less than 1 µm. The minimum diameter is probably bound by the mean free path length of diffusing gas molecules, as smaller diameters would impede O_2 diffusion along the tracheoles (Pickard, 1974).

Despite their smaller size tracheoles are very similar to tracheae in outer appearance. Notable distinctions include the structure of their wall and of their taenidial folds. The former lacks a wax layer (Beament, 1964) and underlying protein epicuticle (Miller, 1974). The tracheolar taenidiae also usually lack the typical infilling as is found in tracheae.

Another very significant difference to tracheae is the generation of these structures. Whereas the tracheal cuticule is secreted from a base epithelium, tracheoles are formed in a single tracheolar or terminal cell. This prevents the usual shedding of cuticular structures at molts. Therefore old tracheoles are glued to the newly secreted tracheal walls to reestablish the lost connection (Wigglesworth, 1959).

The tips of the tracheoles are filled with a fluid and are barely visible in a light microscope (Wigglesworth, 1965). Because the meniscus is dependent on local oxygenation status of the surrounding tissue, it is thought that the fluid serves as a kind of regulator of oxygen supply (Kestler, 1985; Wigglesworth, 1935). Locke (1966) described pores of 3 nm diameter which pierce the tracheolar intima which may have significance for this fluid transport across the wall. Recently, Woods et al. (2009) assumed that the same mechanism is used in larval *Manduca sexta* to eliminate the fluid from the tracheal system during the initial air filling which occurs when the embryo is still in the egg.

Air sacs are an auxiliary structure in the tracheal system. They serve various roles and probably not all of them are respiratory. Air sacs provide extra space for the tissues to grow into during development between molts, as the outer body volume is defined by the cuticle and cannot be increased. For example, Greenlee and Harrison (2004) observed a steady decrease in relative tracheal volume within single larval stages of *Manduca sexta* that supports this hypothesis.

However, air sacs do increase tracheal volume and also provide the tracheal system with sections of increased compliance. Therefore they might as well facilitate convective redistribution of air by their repeated collapse. Wasserthal et al. (2009) describe a

case of redistribution of air between abdomen and thorax in the blowfly *Calliphora*. Hemolymph transport to the head leads to compression of the air sacs in head and thorax. When the heart reverses flow direction the net hemolymph flow is out of the thorax and the air sacs reinflate.

One special type of air sac, the tracheal manifold, lies directly beneath each spiracle and connects it to the main tracheal trunks that run longitudinally along the body.

1.2. Discontinuous gas exchange

Probably the earliest report of the phenomenon that is now known as discontinuous gas exchange cycles (DGC) in insects can be found in Heller (1930), p. 449:

> "Der Gasaustausch erfolgt nicht ständig, sondern in Intervallen, deren Länge der Intensität des Stoffwechsels umgekehrt proportional ist. Es sieht so aus, als ob die Stigmen dicht geschlossen wären, um sich erst bei einer bestimmten CO_2-Spannung in den Tracheen zu öffnen."
>
> *Gas exchange is not continuous, rather in intervals, the length of which is inversely proportional to the intensity of metabolism. It seems as if the spiracles were tightly closed, only to open at a certain CO_2 tension in the tracheae.*

First seen as a source of error in respirometric measurements, a more systematic investigation started with Punt (1956). However, even though it seems that this year the 80th anniversary of discovery of DGC can be celebrated, the pattern still puzzles investigators working on it.

Usually DGCs are demonstrated using the release of carbon dioxide through the spiracles as a marker of their behavior and they manifest themselves as a peculiar rhythm in the external gas exchange (compare Fig. 1.2). Most often this patterned gas exchange is observed in resting insects at low temperatures or dormant life stages, with diapausing moth pupae being a classic example (e.g. Buck and Keister, 1955; Schneiderman and Williams, 1955).

Three phases can be distinguished in the pattern, which are described in more detail in the following. Afterwards, hypotheses about the origin and evolution of DGC will be presented.

1.2.1. CFO - The three phases

Discontinuous gas exchange cycles divide into three distinct phases which differ in the behavior of the spiracles. These are the 'constricted', 'fluttering' and 'open/burst' phase respectively. The names derive from the behavioral mode of the spiracles, fully closed during constriction, intermittent brief opening during flutter and prolonged opening during the burst. With respect to the initial letters of the three phases this kind of gas exchange is also called the 'CFO'-type.

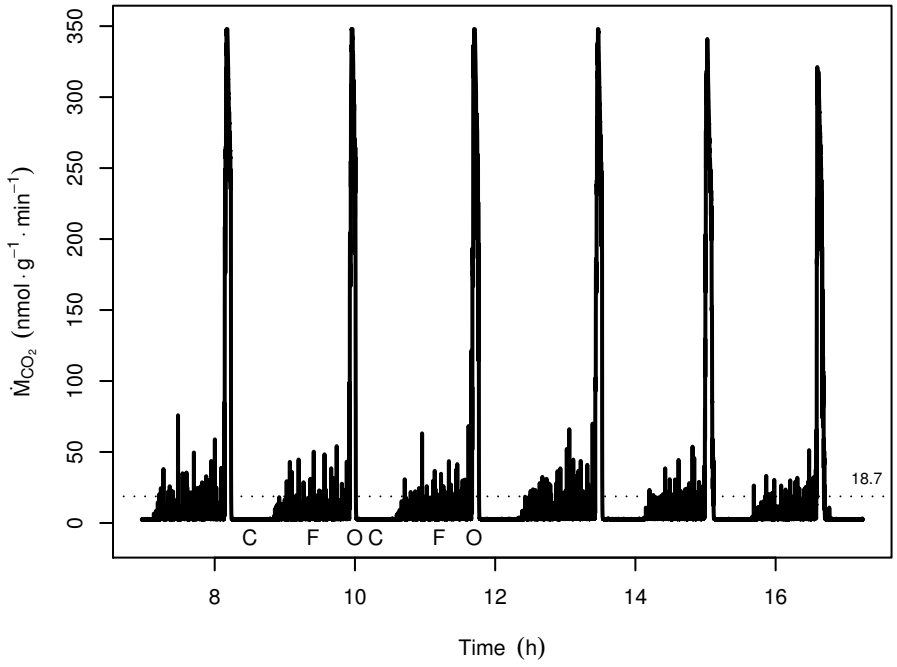

Figure 1.2.: CO_2 release of a diapausing *Attacus* pupa at 15 °C. The dotted line specifies the mean CO_2 release, C, F, and O stand for the constriction, fluttering and opening phase respectively. Unpublished data from S. K. Hetz.

All three phases serve different purposes in the exchange of respiratory gases, so they will be presented one by one.

Constriction phase (C) Using the above, arbitrarily defined, order of CFO, the first phase in a cycle is the constriction phase.

During the constriction phase the spiracles are hermetically sealed (Bridges et al., 1980; Wobschall and Hetz, 2004). No external gas exchange takes place and the oxygen demand of the aerobic metabolism is satisfied by depleting the O_2 in the tracheal system. Intratracheal oxygen partial pressure falls from nearly normoxic values down to about 5 kPa (Hetz, 1994) according to the metabolic rate and the compliance of the tracheal system (Förster and Hetz, 2008). CO_2 is buffered chemically in the form of bicarbonate in the hemolyph. Only a fraction of the metabolically produced CO_2 appears in gaseous form in the tracheal system and increases the partial pressure of that gas (Buck, 1958).

The different rates of removal of oxygen from and CO_2 release into the tracheal system result in a negative net balance of gas molecules in the tracheal system when the spiracles are closed. According to the ideal gas law, this must be compensated either by a decrease of total pressure or tracheal volume. Indeed both can be observed. Hydrostatic pressure falls from normobaric values by about 1 kPa.

However, this is much less than would be expected if the partial pressure differences

of oxygen and carbon dioxide are summed up. Assuming that the tracheal system is filled with ambient air initially (21 kPa O_2, 0 kPa CO_2), oxygen falls by about 15 kPa wheras CO_2 rises by only 4 - 6 kPa (Lighton, 1996), leaving an expected difference in pressure of about 10 kPa.

Therefore most of the pressure is compensated by volume decrease of the tracheal system. This deflation is externally visible in *Attacus* and other moth pupae as an abdominal shortening of the animal (Brockway and Schneiderman, 1967; Hetz, 1994; Wobschall and Hetz, 2004).

After some time the endotracheal O_2 partial pressure reaches a threshold which triggers spiracle opening (Schneiderman, 1960). The constriction phase ends and transitions into the flutter phase.

Flutter phase (F) Following the constriction phase, the flutter phase is characterized by continued brief spiracle openings, which, overall, still severely restrict external gas exchange. On average the spiracles are still closed most of the time (Schneiderman, 1960). Mean CO_2 release during flutter is less than the overall mean CO_2 release so there is still carbon dioxide accumulation albeit at a slower rate than during constriction. Mean oxygen uptake rate matches metabolic demand now, which stops the endotracheal p_{O_2} from falling further. Throughout the whole flutter phase it is regulated to values near the triggering threshold (Levy and Schneiderman, 1966c; Hetz and Bradley, 2005).

Comparing the CO_2 release and the endotracheal pressure the flutter phase might be subdivided into two parts. The first one, immediately following the constriction, is known as the pressure rise phase (Brockway and Schneiderman, 1967). During this phase the subatmospheric pressure gradient is reduced stepwise to normobaric levels. The convective inflow of air prevents significant loss of water and CO_2 so still no gas exchange is visible in CO_2 measurements. This evoked some discussion about the proper definition and distinction of the single phases in the absence of information about endotracheal pressure (Wobschall and Hetz, 2004; Terblanche et al., 2008).

The later, and according to duration, main part of the flutter phase is characterized by small fluctuations of endotracheal pressure, which indicate that the spiracles are closed most of the time. The developing pressure gradients are very small (few Pa only) and probably no significant convective flow occurs during the brief opening of spiracles.

Open phase (O) As the tracheal p_{CO_2} still increases during the flutter phase, eventually a threshold partial pressure for CO_2 is reached (Schneiderman, 1960). It results in prolonged opening of few or all spiracles and is distinctly visible in traces of CO_2 release as a huge burst of CO_2 coming out of the animal.

During the open phase all accumulated CO_2 is released from the tracheal system and the hemolymph. Depending on buffer values and the duration of opening up to 90 % of the total CO_2 released in a cycle is given off during the open phase (Schneiderman, 1960).

The CO_2 loss is visible in pH measurements as an increase of about 0.05 to 0.1 units (Hetz and Wasserthal, 1993; Matthews and White, 2009). The exact amplitudes depend on the buffer capacity of the hemolymph.

Oxygen partial pressure rises quickly to nearly normoxic values and stays high throughout the rest of the opening phase. Only when the spiracles close again in the subsequent constriction phase do oxygen levels begin to slowly decrease. The exact conditions that terminate the burst are not fully understood but likely depend on p_{CO_2} (Levy and Schneiderman, 1966c).

1.2.2. Internal and external factors that influence the DGC

Not all insects show DGC, in fact most of the investigated species do not (Marais et al., 2005). Several factors have been identified that are neccessary for DGC or at least favor it.

First of all, DGC is a phenomenom typical of resting insects. When they become active, the pattern vanishes and is replaced by continuous gas exchange to meet the increased metabolic demand. The aerobic scope of insects is unsurpassed and reaches to more than 100-fold increased metabolic rates during flight in honey bees (Stabentheiner et al., 2003).

DGC often occurs in connection with low temperatures and quiescent life stages like diapause. Again the crucial factor seems to be metabolic rate. As ectothermic animals insects show lower resting metabolic rates at lower temperatures. During dormancy there is likewise a typical depression of metabolic rate (U-shaped curve; Schneiderman and Williams, 1953).

The observation of metabolic rate as a key factor in the DGC lead Bradley (2008) to the conclusion that the pattern might solely be a result of a control that faces a change in metabolic rate. This idea is supported by a number of observations that a systematic change in the pattern occurs if temperature is artificially modified (Contreras and Bradley, 2009a,b).

However, other factors also determine the DGC pattern. Through the occlusion of spiracles the conductance of the spiracles and consequently the whole tracheal system can be artificially modified (Hetz, 2007). The results show that typically the spiracular conductance is high in moth pupae and the DGC pattern is retained for a large number of blocked spiracles. However, the proportions of the three subphases change with the number of sealed spiracles. Bursts tend to increase in duration at the expense of the flutter phase (Hetz, 2007; Mörbitz and Hetz, 2009). At one point subsequent bursts fuse and the pattern essentially becomes continuous.

One of the main explanations for the occurence of DGC is the reduction of respiratory water loss (see also next section). The influence of environmental relative humidity thus is well researched with inconclusive results. Whereas earlier studies concluded DGC to occur primarily in dry conditions (Cloudsley-Thompson, 1975; Edney, 1977), newer work cast some doubt on this simple water DGC interaction. Hadley and Quinlan

(1993) found an inverse relationship between hydration state and the occurence of DGC in grass hoppers. Dehydrated individuals were more likely to give up DGC even though this would have incurred an additional water cost. In a comparative study, Terblanche et al. (2008) likewise found only little evidence of a humidity effect on DGC. However, other authors found the opposite (White et al., 2007). In conclusion, the question whether environmental humidity directly influences the regulation of gas exchange in insects still has to be regarded open.

The discussion of several orders of insects in the last paragraph points to another possible source of influence, that is phylogeny. For many years research on DGC had concentrated on few key species often from closely related groups (moth pupae (e.g. Buck, 1958; Levy and Schneiderman, 1966c), ants (Lighton and Berrigan, 1995), beetles (Duncan and Byrne, 2000) or roaches (Kestler, 1985)). A broad scale phylogenetic study (Marais et al., 2005) thus came to the, then surprising, result that only few orders of insects show the typical CFO-type DGC as described earlier. Most others either show periodic fluctuations in the CO_2 release without ever fully closing their spiracles (cyclic gas exchange), or, alternatively, they simply use continuous gas exchange all the time.

1.2.3. Evolution of the DGC

Given the large diversity of gas exchange modes in the different orders and life stages of insects it is not surprising that a large number of explanations have been developed regarding the origin of DGC. Chown et al. (2006) sum up the current hypotheses that explain the evolution of discontinuous gas exchange. Most of them are adaptive in that they argue that DGC were the consequence of the selective pressure on a single trait. One hypothesis (the 'emergent property hypothesis') is nonadaptive with respect to the DGC pattern.

Hygric hypothesis Like all terrestric animals, insect also face the problem of increased water loss if compared to aquatic animals. Thus depending on local climate and humidity, a large range of adaptations occured to minimize water loss across all possible pathes. The respiratory system is no exemption.

However, as the primary function of a respiratory system is the exchange of respiratory gases, that is oxygen and carbon dioxide, all animals have to trade-off delivery capacity *vs.* possible water loss along the same pathway.

Given the generality of the above points it does not surprise that the first explanation which was developed for the DGC is that the pattern serves to minimize respiratory water loss by maximizing the time the spiracles are closed (Buck, 1958).

Strolling arthropods hypothesis Miller (1974) attributed the exclusion of tracheal mites as one of the functions of the spiracles. Mainly brought about by the dense sieve plate also the closing valve should play a role in this process. However, Miller (1974) did not postulate a causal role of mite prevention for the evolution of the DGC.

Promotion to an explanatory hypothesis has been done later (Chown et al., 2006) based on observations of Harrison et al. (2001), who could show that tracheal mite infestation reduces the flight metabolism safety margins for oxygen uptake in bees.

Though usually treated as an exotic alternative, this hypothesis on the origin of DGC has not been disproved so far (Chown et al., 2006).

Chthonic hypothesis The first direct competitor to the long standing hygric hypothesis had been developed when Lighton and Berrigan (1995) discovered that all insect species that show DGC spend at least some life stage subterranean. Often these habitats share hypoxic and hypercapnic conditions (depending on the specific geometry of the burrows this might not necessarily be the case though, see e.g. Tschinkel, 2004). Lightons idea was that the DGC pattern maximizes the external gas exchange by steepening the partial pressure gradients across the spiracle. Diffusive gas exchange will thus be enhanced on spiracle opening.

Since the mechanism in itself provides no adaptive explanantion, two different additional propositions were put forward. First that gas exchange rate had to be enhanced to minimize prolonged spiracle opening which would incur high respiratory water loss. This is basically the same assumption as the hygric hypothesis, so this particular interpretation of the chthonic hypothesis has later been refined as the chthonic-hygric hypothesis (Chown et al., 2006). In effect, it is a disguised version of the hygric hypothesis as the basic assumptions of the evolutionary driving forces are the same.

Later it was proposed that the increase of the CO_2 gradient per se is adaptive (Lighton, 1998; Chown et al., 2006). It balanced, especially in hypoxic conditions, the disparate rates of diffusion between O_2 and CO_2. A puzzling consequence of this idea is that a pattern would adaptively evolve, which results in the abandonment of the very same pattern, as balanced echange rates would be equivalent to continuous gas exchange.

However, again no disproof of this hypothesis exists yet (Chown et al., 2006).

Oxidative damage hypothesis When Hetz and Bradley (2005) found that the oxygen partial pressure is tightly controlled to low levels during the flutter phase, irrespective of the ambient p_{O_2}, they proposed that the adaptive value of the DGC was to keep internal oxygen levels right to the level that was needed for sufficient oxygenation of the tissues. It has long been known that oxidative damage occurs in tissues if they are well oxygenated (Fridovich, 1977; Landis and Tower, 2005). Animals therefore have developed oxygen detoxification mechanisms. That these are crucial is shown by experiments where a knock out or an overexpression of the particular proteins resulted in direct effects on adult life span (Sun et al., 2002).

In this interpretation the fluttering phase were the visible sign of the control process for O_2. The accumulation of CO_2 is deemed a side effect of keeping the oxygen levels low. Because eventually the CO_2 has to be released the open phase occurs with a massive burst of CO_2. Its purpose is to rid the animal of carbon dioxide as fast as possible because the endotracheal partial pressure of O_2 rise to nearly ambient values after a

short time of spiracle opening. The subsequent constriction serves to quickly lower p_{O_2} to less harmful levels.

Emergent property hypothesis A completely different approach was taken by Chown and Holter (2000). Instead of trying to explain some adaptive value of the pattern they attributed it to the interaction of multiple different control systems. The complex pattern of DGC therefore could be an emergent phenomenon with no immediate advantage in itself.

Because the hypothesis is not easily testable it has often been neglected in current research that comparatively tested multiple hypotheses (White et al., 2007; Terblanche et al., 2008).

However, on second look the emergent property hypothesis allows to disintegrate spiracular control into simpler 'modules'. The pattern is obviously dependent on O_2 and CO_2 (Schneiderman, 1960). Also a number of authers locate the sensing of CO_2 and O_2 in different regions of the body (e.g. Hoyle, 1960; van der Kloot, 1963; Burkett and Schneiderman, 1974b).

From an evolutionary viewpoint it might be much easier to find the driving forces that shaped each of these low complexity 'modules' with much simpler behavior than to try to find a single cause for the complex pattern of the DGC.

1.3. Spiracle control and innervation

Given the particular morphological arrangement of the lepidopteran closing apparatus with only a single closing muscle it is amazing how such a complex and coordinated pattern of opening as is represented by the DGC can be generated at the level of single spiracles. As the muscle is multiterminally innervated (Chapman, 1998), its action is most probably all-or-nothing. It becomes clear that neural or other forms of coordination between multiple spiracles are necessary to generate the DGC pattern by modulating their opening time.

During the discussion of the three phases of DGC it has been briefly mentioned that mainly endotracheal p_{CO_2} and p_{O_2} trigger the transition between the phases. Therefore it has to be assumed that these gases somehow exert an influence directly on the spiracle muscle or via neural mechanisms. This section will further detail the mechanism how these gases act on the function of the spiracle muscle.

A morphological study of the innervation of the spiracle muscle in *Hyalophora* (Beckel, 1955; Beckel and Schneiderman, 1957) revealed that the muscle is innervated by two branches of unpaired median nerves, the antero-lateral (ALN) and the medio-lateral (MLN) nerve respectively (compare Fig. 1.3). Both nerves originate in segmental ganglia, the ALN in the segment preceding the spiracle, MLN in the same segment. The unpaired axons bifurcate outside the ganglia and innervate both spiracles of a single segment.

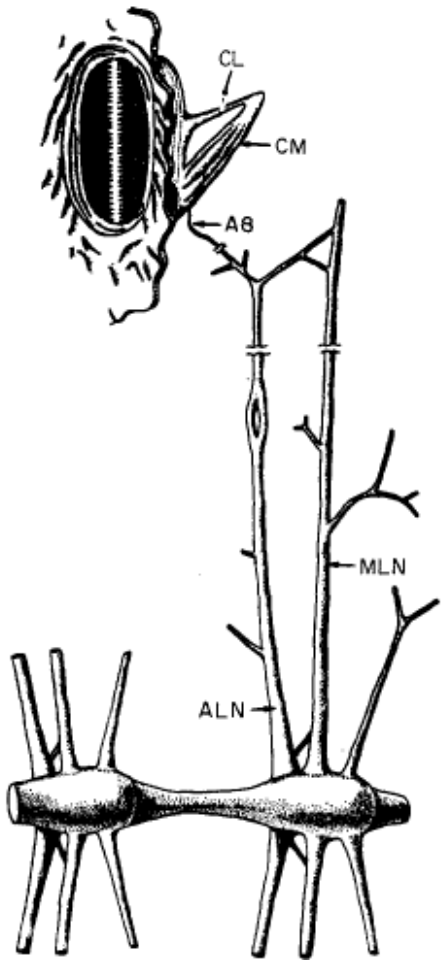

Figure 1.3.: Semi-diagrammtic view of the innervation of the spiracle muscle in *Hyalophora cecropia*. ALN - anterior lateral nerve, MLN - medio lateral nerve, A8 - nerve branch supplying the closing muscle, CL - closing lever, CM - closing muscle. From van der Kloot (1963)

From this arrangement of unpaired neurons and bifurcating axons it has been concluded that the opening of both spiracles in a single segment is synchronized though slight differences in latency due to differences in the length of the propagation pathway might occur (van der Kloot, 1963). However, on a behavioral basis the spiracles in a segment might still be independent (Sláma, 1988). So far no simultaneous records of electrical and mechanical activity of both spiracles in a segment exist.

Transsection of the median nerves resulted in prolonged constriction of the denervated spiracle (Beckel and Schneiderman, 1957). It has been concluded that the muscle is spontaneously active (myogenic contraction) and no central nervous input is necessary to close the valve. This was later confirmed by reports that the muscle fibres of *Hyalophora* pupae possess a pacemaker potential, which is possibly unique to this stage (van der Kloot, 1963).

Apart from the pacemaker potentials in the muscle membrane tonic activity has been decribed in the axons of the median nerves (ALN, MLN; van der Kloot, 1963; Hoyle, 1959, 1960). Perfusion experiments with separate tracheal and ganglionic flows revealed that the tonic firing most probably is releated to the oxygenation state of the ganglion, that is it provides an O_2 dependent signal to the spiracle (Burkett and Schneiderman, 1974b).

Direct electrical recording demonstrated a stopping of the electrical activity in ALN due to relatively high concentrations of CO_2 (10 %; van der Kloot, 1963), although no central behavioral effect of CO_2 at physiological concentrations has been found later in the perfusion experiments (Burkett and Schneiderman, 1974b).

However, a number of experiments revealed a direct effect of CO_2 on the neuromuscular transmission. First, no morphological evidence for a peripheral reflex network has been found (Beckel and Schneiderman, 1957). Further the sensitivity of the muscle to CO_2 persists after denervation and even after dissection of most of the fibres of the muscle (Beckel and Schneiderman, 1957; van der Kloot, 1963). Measurements of the postsynaptic activity and the mechanical force generation under the influence of CO_2 (Hoyle, 1960) led to the conclusion that the effect of CO_2 is direct and on the transmission at the neuromuscular junction.

A possible mechanistic explanation for this direct effect probably has been found in the properties of the postsynaptic receptors of the neurotransmitter. Like all insect skeletal muscles, the transmitter at the neuromuscular junction of the spiracle muscle is L-glutamate (Chapman, 1998). Investigating the narcotic effects of CO_2, Badre et al. (2005) found that the postsynaptic glutamate receptors are blocked by CO_2 in the heart and the intersegmental muscles in larvae of the fruit fly *Drosophila*. It is likely that this CO_2 inhibition also occurs in the neuromuscular junction of the spiracle muscles.

In conclusion, it can be said that, within a single segment, the action of CO_2 is directly on the spiracle muscle and therefore local, whereas the reaction to O_2 requires central nervous control of the spiracle.

Part II.

Experimental Work

2. Perfusion Experiment

2.1. Introduction

2.1.1. Working Hypothesis

As the introduction indicated, there are at least two interdependent perspectives on the phenomenon of discontinuous gas exchange. First there is the evolutionary perspective, asking for the reasons that ultimately led to the evolution of DGC. The other perspective is the mechanistic one, asking for the mechanism and the exact functioning of the internal control systems that generate the pattern. As a number of comparative studies have tried to tackle the first with varying success (e.g. Marais et al., 2005; White et al., 2007; Terblanche et al., 2008), this study will concentrate on the second aspect.

The first complete and still mostly valid mechanistic theory is that of Buck (1958). However, even though there is general consensus on the big picture (Chown et al., 2006), a number of details of this theory are under debate or have not been fully investigated.

One of these debated questions regards to the actual thresholds that trigger a particular behavior of the spiracles. First discussed in Schneiderman (1960) and Levy and Schneiderman (1966c) the interaction between CO_2 and O_2 thesholds was confirmed by the perfusion study of Burkett and Schneiderman (1974b). The latter produced a diagram which for every combination of endotracheal p_{CO_2} and p_{O_2} assigns a behavioral mode of the spiracles (see Fig. 2.1). For reasons that will become apparent in a minute, I call this interpretation the "three state phase space".

However, owing to experimental limitations the actual number of different gas mixtures that were tested was small and the diagram rests on few points only. Burkett and Schneiderman (1974b) placed the points where spiracular flutter occured in a distinct extended flutter region, probably based on the ideas given in Schneiderman (1960). However, the points lie close to an imaginary curve and could be alternatively thought as lying directly on the boundary between the 'open' and 'closed' region (Fig. 2.1B). Slight variations in perfusion rate (e.g. due to changes in flow resistance) would result in small fluctuations from the nominal gas composition. This in turn could repeatedly led into the open and closed regions of the diagram, also leading to intermittent brief spiracle openings or flutter. Because there are only two spiracle modes in the alternative diagram this is the "two state phase space".

The difference between both interpretations might seem marginal, yet it has implications for the mechanism of the DGC. In the original interpretation (Burkett and Schneiderman, 1974b) three behavioral modes of a single spiracle are assumed for *steady state*

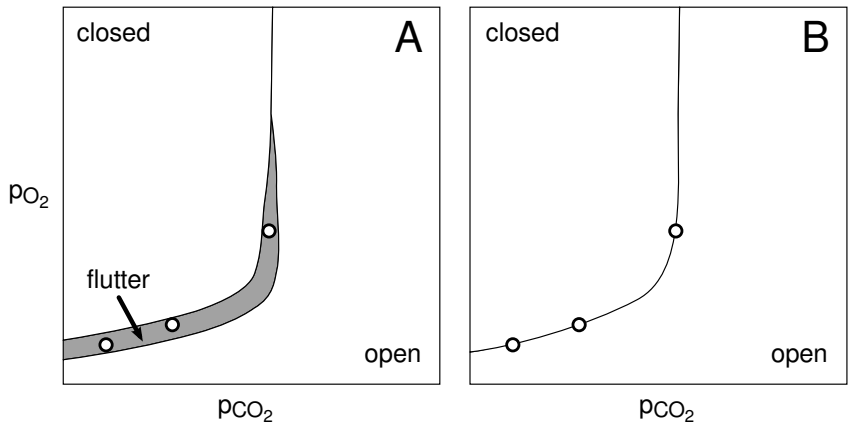

Figure 2.1.: Two alternative interpretations of the Burkett and Schneiderman (1974b) data (their Fig. 7). Shown is the spiracle behavior in response to p_{CO_2} (x-axis) and p_{O_2} (y-axis). Circles denote combinations of O_2 and CO_2 where fluttering was observed during perfusation. *left* - original interpretation with distict flutter region. *right* - alternative interpretation with only two regions, placing the data points on the boundary between the open and closed region. Redrawn from Burkett and Schneiderman (1974b).

conditions in the tracheal system. Fluttering as a behavioral mode was on par with the other two modes of open and closed spiracles.

On the other hand, the two state hypothesis assumes only two steady states of a spiracle. The closed and open states are consistent with the two modes of contraction and relaxation of the spiracle muscle. Fluttering would be a dynamic behavior resulting from non-steady state conditions in the tracheal system. Thus the behavior vanished when steady state conditions were enforced.

To decide between both interpretations an experiment has been devised that is a modern reevaluation of the classic experiment of Burkett and Schneiderman (1974b) using an observation method that enables long term measurement. This allows to sample the phase space at much higher resolution compared to the older experiment.

2.1.2. Principle of Measurement

To distinguish reliably between the two phase space structures that were presented in the previous section (Fig. 2.1) it is of crucial importance to increase the number of sampling points in a single individual. This requires automation of the observation of spiracle behavior.

Since visual methods are limited to single spiracles or maybe serial sampling of multiple spiracles (Burkett and Schneiderman, 1974b) another approach had to be taken. Alternative optical methods like reflex light barriers or photo diodes have given unsatisfactory results so far (Kaiser et al., 1996). They also share the limitation of allowing

only the observation of single spiracles.

On the other hand, tracheal pressure measurements by design observe the behavior of all spiracles simultaneously. Using a trick this approach might be used even when the tracheal system is being artificially perfused with air. The basic idea is as follows.

Perfusion of the tracheal system requires one to apply a pressure gradient over the tracheal system which will generate the bulk flow of air or any other mixture of gases through the animal. The mass flow will change according to the pressure gradient applied and the resistance of the tracheal system to the flow. The latter is most strongly influenced by the opening state of the spiracles and a measurement of the mass flow would reveal the spiracle state if the pressure gradient is fixed.

However, if on the other hand the mass flow were fixed, the pressure gradient over the tracheal system will adapt so as to generate the required flow. In other words, the pressure gradient is dependent on the current state of the spiracles and might be used to observe it.

Fig. 2.2 illustrates what happens during the perfusion. Initially all spiracles are closed. The flow has to pass a low conductance cannula (LCC) which is manufactured to generate a defined pressure drop for a given mass flow rate. The drop has been chosen to be about 500 Pa, which corresponds to the subatmospheric pressures experienced by *Attacus* during the constriction phase of DGC (Wobschall and Hetz, 2004). The outflow cannula (HCC) has high conductance, so the pressure drop it generates is negligible. In sum the observed perfusion pressure drop will be that of the LCC.

If, on the other hand, some or all spiracles open, they will provide additional flow paths. These bypass LCC and lower the overall resistance to the flow. Consequently the resulting pressure gradient over the tracheal system will be much smaller and the opening of spiracles would manifest as a breakdown in the (negative) pressure signal.

Because internally the tracheal system is interconnected this effect will occur independently of the specific spiracle that is to open. Thus this method allows observation of all spiracles at once.

2.2. Material & Methods

2.2.1. Animals

Eggs of Attacus Silk moths (*Attacus atlas*), obtained from a local breeder, were reared on Cherry Laurel (*Prunus laurocerasus*, L.) at 25 °C with L/D-cycles of 10 h/14 h. After pupation, cocoons were kept for a few days at 16 °C in complete darkness to induce diapause. Subsequently pupae were stored in a dark box at 12 °C until the beginning of the experiment. The mean pupal mass of a random sample of the population was 4.746 g ± 1.395 g (SD, N=36). Sexes have not been determined.

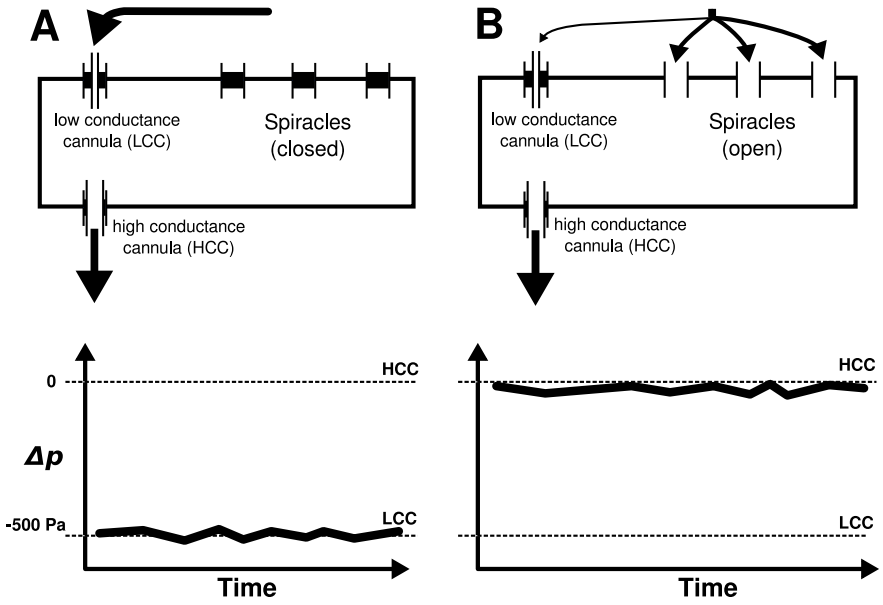

Figure 2.2.: Measurement principle of the perfusion experiment. Open spiracles bypass the flow through the cannula LCC resulting in a drop of the perfusion pressure.

2.2.2. Setup

Tracheal pressure has been used as a good measure for spiracular activity in moth pupae (Schneiderman and Schechter, 1966; Wobschall and Hetz, 2004; Hetz and Bradley, 2005; Terblanche et al., 2008). Thus, unlike Burkett and Schneiderman (1974b), we used a setup where we perfused the tracheal system through two spiracles with gases containing different oxygen and/or carbon dioxide concentrations at a constant perfusion rate. With this setup we circumvented the problem that ambient gas mixtures do not necessarily equal tracheal gas composition due to spiracle activity. Changes in perfusion pressure were recorded automatically as a measure for spiracular activity. The details of the setup are given below.

Two animals could be measured simultaneously in a Peltier thermostatted (10 °C ± 0.1 °C) brass chamber (see Figure 2.3).

Gases suitable to perfuse the tracheal system were mixed from $N_2/O_2/CO_2$ cylinders (technical grade 4.0, Air Liquide GmbH, Germany) and room air using four mass flow controllers (MKS Mass Flo®, max flow 100 ml min^{-1}, MKS Instruments Inc., USA) simultaneously. The mass flow controllers were driven by a Mass Flow Programmer (MKS 147B, MKS Instruments Inc., USA) which itself was controlled by a computer via an RS232 interface. p_{O_2} and p_{CO_2} of the mixtures were monitored prior to entering the brass chamber with the aid of an oxygen and carbon dioxide flow through sensor (O_2: Ametek S-3A/II + N37 sensor, CO_2: Ametek CD-3A + P61B sensor, Ametek, USA, now manufactured by AEI Technologies, Naperville, IL, USA).

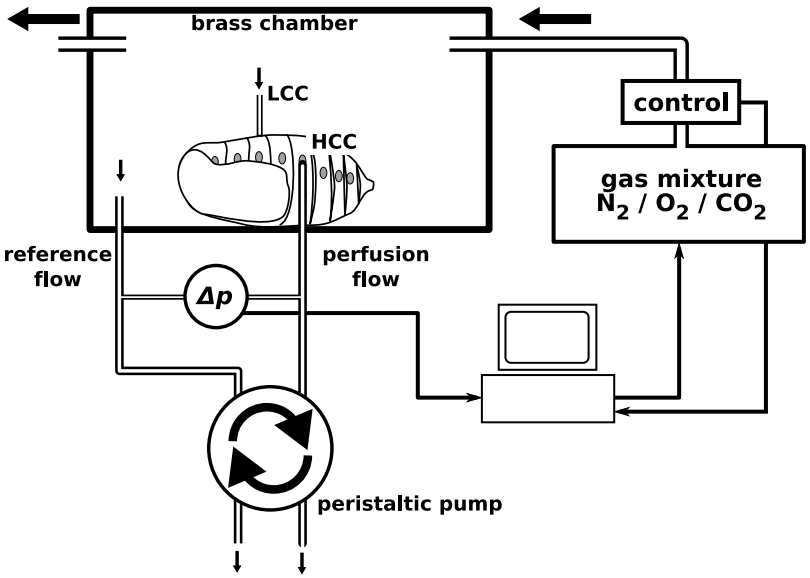

Figure 2.3.: Schema of the perfusion setup. The cannulated animal lies in a thermostatted brass chamber, where it is superfused with artificial air mixed from bottled gases. The pressure needed to perfuse the animal with a fixed volume flow is measured differentially against a constant reference flow to attenuate the pump pressure fluctuations.

In order to cannulate two spiracles, for each animal two L-shaped cannulas were constructed from bent stainless steel capillaries (OD: 0.28 mm). One of them, the low conductance cannula (LCC), was pinched at the tip, resulting in a lower flow conductance and an increased pressure difference along the cannula. The pressure drop was approximately -500 Pa at a perfusion rate of 103.2 µl min^{-1} generated by a multichannel peristaltic pump (Ismatec IPS 4, Ismatec SA, Zürich, Switzerland). The flow rate of about 100 µl min^{-1} was chosen in order to ensure that the deviation of the 'true' partial pressures of the endotracheal gas mixture from the set values was less than 0.5 kPa. The deviation was estimated based on the animals´ oxygen uptake and carbon dioxide release rates (oxygen uptake rate of 20 nmol min^{-1}). Higher flow rates, as tested during the setup evaluation, often resulted in apparent occlusion of the cannulae (i.e. perfusion pressure fell more than 500 Pa without unusual behavior of the cannulae in a subsequent check).

The perfusion has been setup such that the pump sucked air from the animal rather than pushing it through. The resulting pressure gradient of -500 kPa was considered to better match the naturally occurring subatmospheric tracheal pressure during constriction in moth pupae (Wobschall and Hetz, 2004; Hetz and Bradley, 2005; Terblanche et al., 2008). The low conductance cannula (LCC) was left open to the chamber, while the opposite high conductance cannula (HCC) was connected to the peristaltic pump line via short polyethylene tubing (PE10, 0.279 mm/0.635 mm inner/outer diameter). All flow lines were constructed from stainless steel capillaries (1.0 mm inner diameter),

except connectors made from short pieces of silicone tubing.

The peristaltic pump drove both the perfusion flow and the reference flow allowing a differential pressure measurement. This resulted in synchronization between the two flows and strongly attenuated the background pressure oscillations originating from the pump action. For the pressure measurement we used differential pressure transducers (SenSym SCX05DN, SensorTechnics, Puchheim, Germany). The sensors were connected to custom made sensor bridge amplifiers. The signal was amplified and an offset voltage was added to match sensor output to the input range of the A/D-converter board (12 bit; DT2811, Data Translation Inc., USA) in the pressure range from -2500 to 500 Pa. Accuracy and stability over 24 hours was within 20 Pa (<1 % of full scale).

The setup was fully controlled by a custom written, multithreaded Python (`http://www.python.org`) script. The script serially communicated with the mass flow programmer to automatically change the perfusion mixture every two hours. After a change of the mixture the script checked the success of the transition to the new setpoints and retried it up to three times in case of significant deviation (sometimes a mass flow controller did not properly react to its control input). At the same time the pressure data as well as the signals from the CO_2 and O_2 sensors were continuously read with 1 Hz sample rate from the A/D board in another thread and logged complete with timestamp and setpoint information to file for offline data analysis (see below).

2.2.3. Experimental Protocol

Before the preparation started, the pupae were weighed to account for water loss during the experiment. The cannula HCC was carefully inserted into the spiracle of the last immobile abdominal segment and fixed with a wax droplet as was the low conductance cannula LCC into the contra lateral spiracle. Occluded cannulas, indicated by an instantaneous huge pressure drop when connected to the pump flow, were replaced until the perfusion worked properly.

After preparation, the animals were perfused with room air and allowed to recover for at least one hour. The perfusion pressure signal was constantly monitored and recovery of the animals was assumed if it dropped to -500 Pa and stayed there continuously for more than 30 min.

The computer script controlling the experiment subsequently tested a predefined set of O_2/ CO_2 mixtures, each being active for two hours. Based on pilot trials, CO_2 varied between 0 - 6 kPa, O_2 varied from 0.5 - 20 kPa (with a higher point density between 0 and 5 kPa (see Fig. 2.5). To avoid possible hysteresis effects, random variation in the gas mixture was advisable. Otherwise, the inferred thresholds might have been biased depending on the direction of the variation. However, random variation in CO_2 evoked strong, long lasting reactions of the animals, which could be misinterpreted as flutter. Especially on large CO_2 partial pressure differences, this transient behavior lasted up to three hours. Carbon dioxide therefore had to be varied systematically from low to high partial pressures. As a result, for every carbon dioxide partial pressures all oxygen partial pressures were tested in random order before advancing to the next higher p_{CO_2}.

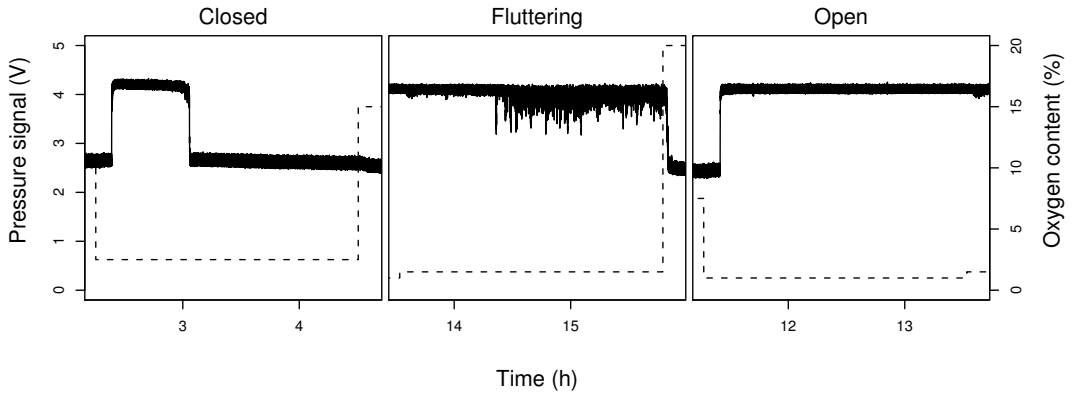

Figure 2.4.: Example pressure traces of a single perfusion showing closed, fluttering and open spiracles respectively. Dashed lines represent the reference oxygen partial pressure of the mixture. p_{CO_2} was zero in all three cases.

At least, compared to a fully systematic variation in both gas species, this approach could have demonstrated any hysteresis at the O_2 trigger.

The desired high resolution of the steady state map required a large number of test mixtures ($\approx$ 100-150, 12-16 combinations of p_{O_2} times 8-10 combinations of p_{CO_2}). Together with two hours of treatment for one gas mixture, a typical single experiment therefore lasted between 10-14 days.

After the experiment, the animal was removed from the chamber. All cannulas and wax remnants were drawn off. The pupae were weighed again to account for water loss during the experiment. The spiracles used for inserting the cannulas, now defunct and open, were sealed with a wax droplet to minimize dehydration. Subsequently, the pupae were then kept until ecclosion to see if the the experiment, especially the implantation of the cannulas, might have adversely affected normal development. Only pupae that had been injured during the preparation occasionally died before ecclosion. Otherwise, mortality rate was not influenced by the experiment.

2.2.4. Data Processing

To account for the transient reaction of the animal to a change in gas mixture and to ensure steady state spiracle behavior, the first 90 minutes of each treatment had to be discarded from the data processing. From the remaining 30 minutes, mean and standard deviation of p_{O_2} and p_{CO_2} in each gas mixture were calculated from the signals of the gas analyzers. Highly variant data due to instable gas composition (usually one of the gas cylinders accidentally ran empty) were discarded. The states “open” or “closed” were assessed manually if the perfusion pressure was invariantly at the respective level (Fig. 2.2) throughout the last 30 min of a treatment, possibly interrupted by short, singular events. Fluttering was defined as high frequency switching between open and closed spiracles (see Fig. 2.4 for examples).

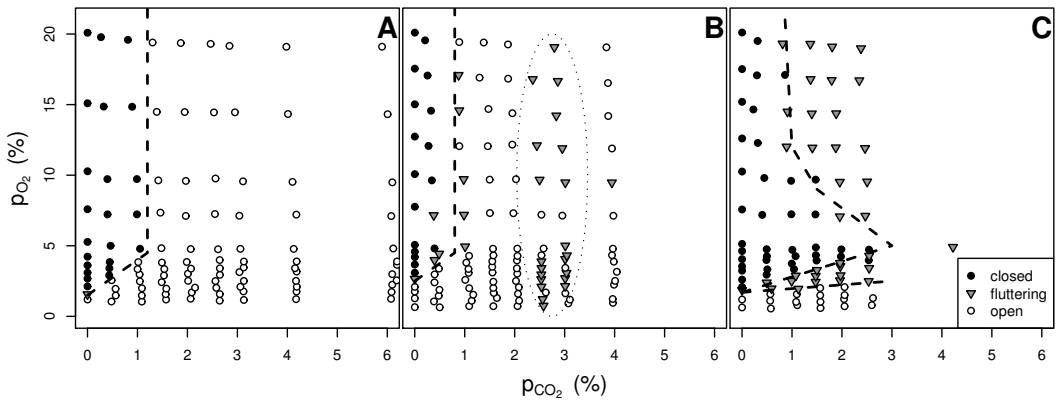

Figure 2.5.: Phase space diagrams of three different animals. Each single point corresponds to two hours perfusion. (A) typical best, no flutter region, (B) typical phase space with singular flutter along the transition, flutter in the ellipse is due to a temporarily occluded cannula, (C) atypical case with large flutter regions and negative correlation between p_{CO_2} and p_{O_2} at the top part of the transition.

The interaction between the thresholds was estimated by standard linear regression analysis of the lowest p_{O_2} per CO_2 level, which allowed permanent closure of the spiracles, against p_{CO_2}.

2.3. Results

In total, from 35 attempted experiments, eight complete perfusion runs were achieved, which tested a large range of the phase space. Therefore, numerical results are presented as mean and range.

The perfusion setup allowed non-ambiguous estimation of spiracle behavior for most gas mixtures. Usually the steady-state was reached within the first hour after changing the gas composition if the experimental protocol described in the previous section was followed. However, in pilot trials other regimes of changing the gas composition resulted in considerably longer transient response.

The duration of these transients also revealed a significant disparity in the animals' response to specific changes in the gas composition. Altering oxygen partial pressure usually resulted in a relatively quick response according to the amount of oxygen available. That is, high oxygen partial pressures resulted in closed spiracles, while severely hypoxic mixtures quickly effected steadily open spiracles. On the other hand, the reaction to changes in carbon dioxide, especially from high to low partial pressures, was considerably delayed. In an unusual case, an animal, in a pilot trial, closed the spiracles after 3 h permanent perfusion with room air, which is the steady-state behavior according to the phase space maps (see below). The immediately preceding mixture

contained a p_{CO_2} of 6 kPa, resulting in continuous spiracle opening. Obviously during this hypercapnic perfusion a tremendous load of CO_2 was generated, taking a long time to unload again in the carbon dioxide free air.

The general structure of the two-dimensional map of spiracle behavior in response to endotracheal p_{CO_2}/p_{O_2} was similar to that hypothesized in Burkett and Schneiderman (1974b). Two large areas of constricted (top left) and fully open spiracles (lower right) are clearly distinguishable in Fig. 2.5A and B.

In contrast to Burkett and Schneiderman (1974b) in six out of the eight pupae, no extended flutter area could be recognized in the map. Rather there was a sharp transition from closed to open spiracles due to a lack of O_2. A few gas mixtures with a gas composition near the transition line resulted in flutter behavior, which can possibly be attributed to small variations in the perfusion partial pressures, either from residual total pressure variations from the pump action or from variations in the mixture caused by the mass flow controllers themselves. These might have repeatedly driven the system back and forth over the threshold (Fig. 2.5B).

In one pupa, a large flutter area was associated with the transition due to high CO_2 levels. This animal showed flutter behavior between 1.5 and 3 kPa, even though the gas mixture was normoxic. Interestingly this flutter area broadened with increasing p_{O_2}. This behavior differs from the model of Burkett and Schneiderman (1974b), where the area narrows with increasing oxygen partial pressure (see Fig. 2.1, left).

A second animal showed a flutter area associated with the O_2 transition (Fig. 2.5C). In this animal a negative correlation between p_{CO_2} and p_{O_2} was observed. Unfortunately, a large and interesting part of the experiment had to be discarded due to an empty nitrogen cylinder.

The much higher resolution of our experiment compared to the previous perfusions by Burkett and Schneiderman (1974b) showed a dependency of the O_2 trigger on p_{CO_2} hypothesized by Schneiderman (1960).The minimum p_{O_2} where we observed closure of the spiracles was 2.6 kPa (1.6 - 4 kPa), increasing with a rate of 2.1 kPa/kPa of carbon dioxide (0.8 - 4.4 kPa/kPa, N = 6). Above a threshold p_{CO_2} = 1.1 kPa (<1 - 2.5 kPa) spiracles were kept open regardless of p_{O_2}.

2.4. Discussion

2.4.1. Pressure based suction perfusion

Suction perfusion (negative pressure perfusion) proved to be advantageous over traditional positive pressure perfusion Burkett and Schneiderman (1974b). Because the endotracheal pressure is sub-atmospheric most of the time, animal distension by pressure did not occur, even at relatively high flow rates. On the other hand, very high flow rates probably caused the total collapse of parts of the tracheal system, resulting in very steep pressure gradients and causing preliminary experiments to fail.

Occasionally a cannula became occluded and usually the animal simply responded with opening of spiracles, providing an alternative flow path thus avoiding any adverse effects of impaired perfusion as might happen with pressure perfusion. If the occlusion was not permanent (e.g. the wall of the tracheal manifold was pushed against the cannula opening), the cannula sometimes became functional again and the animals responded to the perfusion without a notable difference compared to undisturbed runs. Pupal shrinking as an effect of sub atmospheric pressure and tracheal compliance seems to simulate the naturally occurring movements and mechanical stresses of the pupal tracheal system much better than positive pressure perfusion (Brockway and Schneiderman, 1967).

A further advantage of our method is the preparation of the cannulas. These can be manufactured to produce a specific pressure gradient for any desired flow rate. By matching cannula flow conductance to a certain flow rate it is possible to keep endotracheal pressure within physiological bounds (Wobschall and Hetz, 2004; Levy and Schneiderman, 1966a).

The differential pressure measurement against a synchronized reference flow greatly attenuated pressure fluctuations generated from peristaltic pumps. Residual pressure differences were below 100 Pa in amplitude. This allowed us reliably to distinguish the state of the spiracles even on relatively short time scales of a few seconds.

The generation of the full pressure gradient took approximately 60 s due to the low flow rate of the peristaltic pump. The breakdown occurs almost immediately after opening of a spiracle. So even though the duration of micro-openings during flutter can be shorter than the sampling rate used (Wobschall and Hetz, 2004; Sláma, 1988, 1 Hz = 1 s *vs.* 0.2 - 1 s), any opening is registered as a deviation in the pressure signal.

Further improvements in the temporal resolution can probably be achieved by oversampling and trying to model the residual variance from the pump action. One approach might be to include additional measurements of the flow and then trying to use independent component analysis (ICA) to decompose the signal sources.

2.4.2. Carbon dioxide threshold partial pressure

The measured CO_2 thresholds for spiracle opening in the present paper are much lower than in most other reports and are among the lowest ever reported. There are several papers dealing with endotracheal p_{CO_2} in the literature.

Punt (1956) observed fully open spiracles in an atmosphere of 1.5 % CO_2 (1.52 kPa) in *Hyalophora cecropia*. Harrison et al. (1995) state that discontinuous ventilation in grasshoppers (*Taeniopoda*) ceased above an ambient p_{CO_2} of 2.9 kPa CO_2. The corresponding hemolymph p_{CO_2} triggering the opening phase was determined to be 2.26 kPa. However, hemolymph p_{CO_2} was found to be significantly influenced by ambient temperature in another grasshopper (*Melanoplus*; Harrison, 1988). A concentration of 2 - 3 % carbon dioxide (2.03 - 3.04 kPa), applied externally, resulted in fully open spiracles in *Periplaneta americana*, whereas additional ventilatory movements were not observed until CO_2 concentration reached 5 - 10 % (5.07 - 10.13 kPa; Hazelhoff, 1926; Jordan,

1927). In *Samia* pupae, DGC is fully abandoned in artificial atmospheres containing 4 % CO_2 (4.05 kPa; Terblanche et al., 2008).

Lighton (1996) provides a trigger threshold of 4 kPa, cited from Lighton and Garrigan (1995). These authors in turn cite Levy and Schneiderman (1966c) with a trigger threshold of 2 - 6 kPa. The 4 - 6 kPa of Lighton and Fielden (1996) is probably from the same source. According to Miller (1974) spiracles open at 6.4 % (6.48 kPa) with a p_{O_2} of 3.55 kPa, which seems to be the average of the data presented in Table 2 in Levy and Schneiderman (1966c).

Buck (1958), in an indirect experiment, estimated the ambient p_{CO_2} that resulted in no net gas transfer across the spiracles in the subsequent burst to be 45 mmHg (5.99 kPa) in *Agapema*. They concluded that this was the triggering carbon dioxide partial pressure.

Schneiderman and Williams (1955) described non-continuous CO_2 release in atmospheres of as high as 8 - 10 % CO_2 (8.11 - 10.13 kPa) in air at an unspecified temperature (probably 25 °C, as in other studies from these authors). From their descriptions, it is unclear whether they really observed discontinuous gas exchange with regular cycles or if it was an irregular mode of gas exchange.

In conclusion, a large number of the figures on CO_2 triggers in the literature seem to be directly or indirectly referred from the Levy and Schneiderman (1966b) data. Compared to this investigation these authors performed their experiments at a higher temperature of 25 °C (10 °C in the present study).

Levy and Schneiderman (1966c) pointed out a positive correlation of temperature and the threshold, which might in part account for the low trigger thresholds that we observed. The triggering p_{CO_2} decreased from 6.5 kPa at 25 °C by approximately 30 % to 4.5 kPa at 15 °C in *H. cecropia* pupae. Harrison (1988) found a nearly twofold increase in hemolymph p_{CO_2} ($\approx$ 3.0→5.3 kPa) from 10 to 20 °C in the grasshopper *Melanoplus bivittatus*. At higher temperatures, p_{CO_2} decreased linearly reaching about 1.5 times the low temperature values at 40 °C ($\approx$ 4.2 kPa). Part of the differences in the reported trigger thresholds might thus be due to temperature effects on the animals' acid-base control. Significantly higher experimental temperatures, however, can break diapause in untreated *Attacus* pupae, resulting in much higher metabolic rate and, eventually, abandonment of DGC (Bradley, 2008).

2.4.3. Oxygen threshold partial pressure

Despite the focus on the role of oxygen in the control of DGC, surprisingly little is known about the actual internal set points that govern spiracle opening. Schneiderman (1960) reported two different thresholds with respect to oxygen, the "O_2-open" and the "O_2-flutter" threshold respectively. The "O_2-open" threshold was defined as the lowest oxygen partial pressure, which allowed temporary closure of the spiracles, a concept that is compatible to the data in this study. The second, "O_2-flutter" threshold was defined as the highest oxygen partial pressure at which temporary spiracle opening (fluttering) occurred or inversely the lowest p_{O_2} that supports permanent closure of the spiracles.

Because definite flutter was not observed in the experiments, no "O_2-flutter" threshold could be derived.

The mean "O_2-open" threshold for Attacus was 2.6 %, which fits nicely with previous data. Schneiderman (1960) reported 2.5 % for *Samia cynthia* and 3.1 % for *Polyphemus*, based on cannulated, but non-perfused pupae. Values for minimum endotracheal p_{O_2} obtained from gas sampling in *H. cecropia* pupae showing DGC vary between 2.0 and 5.1 % independent of ambient oxygen concentration (Levy and Schneiderman, 1966b). Perfusion experiments resulted in 2 - 5 % later as well (Burkett and Schneiderman, 1974b). Direct measurement of endotracheal p_{O_2} with microelectrodes in Attacus pupae gave values around 4 - 5 kPa (Hetz et al., 1994). Using the same technology, Hetz and Bradley (2005) demonstrated active regulation of endotracheal p_{O_2} down to about 4 kPa during the flutter phase, independent of ambient oxygen partial pressure.

These low values are remarkable, because based on spiracle behavior they would correspond to the "O_2-flutter" threshold as the change is from closed to flutter. This threshold was reported to be about 12 - 15 % O_2 previously (Schneiderman, 1960; Burkett and Schneiderman, 1974b), which seems to be significantly higher. Yet the traces in Levy and Schneiderman (1966b) and Hetz and Bradley (2005) clearly show that animals start fluttering no sooner than endotracheal p_{O_2} reaches its minimum values and then actively regulate the p_{O_2} around this level. No part in the DGC-cycle was observed, where endotracheal oxygen partial pressure decreases from the "O_2-flutter" to the "O_2-open" threshold with fluttering spiracles. Yet this would have to be expected if these thresholds defined a separate part of the phase space map that resulted in spiracular flutter behavior. Since a projection of the periodic DGC into the phase space has to be a continuous, closed loop, this flutter area had to be somehow crossed to reach the "O_2-open" threshold (compare Figs. 2.1A and 2.6). An alternative explanation for extended flutter consistent with the active regulation of p_{O_2} were a slowly horizontal crossing of the flutter area. Then no decrease of p_{O_2} during fluttering had to be assumed. However, the expected minimal values would then be the 12 - 15 % of the "O_2-flutter" threshold, which are in contrast to the data presented by Levy and Schneiderman (1966c) and Hetz and Bradley (2005).

Since the phase space map does not include time as a variable it might be argued that the crossing of the fluttering area happens very fast, so the effect of a falling p_{O_2} during spiracular fluttering cannot be detected. Indeed there is some mismatch between the start of the intermittent spiracle openings and the time of a noticeable CO_2 release (Hetz et al., 1994; Wobschall and Hetz, 2004), indicating the difficulties of exactly specifying the begin of the fluttering phase from measurements of CO_2 release alone. However, in the studies that measured it, endotracheal p_{O_2} was continuously monitored, so the fast change would have become apparent as a sudden drop or jump from the "O_2-flutter" to the "O_2-open" threshold, which is not the case in both studies (Levy and Schneiderman, 1966c; Hetz and Bradley, 2005). So again, this hypothesis is not supported by the available data.

Looking closer it becomes apparent that the "O_2-flutter" threshold itself is not without problems. It was defined based on an experiment with partly cannulated (2-5 spiracles

were forced open), but not actively perfused pupae (Schneiderman, 1960). Spiracular control over the tracheal space was thus not completely eradicated, resulting in an undefined and possibly not constant endotracheal gas composition. The low reproducibility of the results even in the same individual on successive trials (Schneiderman, 1960) might be an additional indication of the weak definition of this particular threshold. Burkett and Schneiderman (1974b) used stop flow perfusion with relatively short perfusion and recovery periods of around 20 - 30 min. From my own perfusion experience this seems far too short to guarantee steady-state behavior. Even though they stated that they observed no differences between 5 and 20 min runs, this might account for the relatively large number of gas mixtures that resulted in spiracle fluttering. After preparation the animals in this study usually responded with full opening of the spiracles even when perfused with ambient air. They then started to flutter, which often lasted for 30 - 60 min before they eventually constricted. The sudden change in perfusion flow imposed by stop flow experiments might have been enough to evoke fluttering as a reaction to the mechanical disturbance.

2.4.4. Interpretation of the phase space map

Given the above difficulties, the development of a hypothesis of the DGC trajectory in a tripartite phase space seems impossible and the tripartite phase space seemingly has to be rejected in favour of a bipartite structure.

An intriguing explanation of this structure is that of two separate, interacting control systems (Fig. 2.6). Both systems possess a single threshold line each which separates the regions of the phase space where the systems force the spiracles to close or open. Constriction only occurs if endotracheal conditions are such that both systems signal closing spiracles, i.e. the white region of Fig. 2.6 with low p_{CO_2} and high p_{O_2}. As soon as one control variable is beyond the threshold the spiracles will open, even though the control input might be inconsistent (the light grey regions). Both systems are equivalent inasmuch as the O_2 control might 'override' the CO_2 control and *vice versa*.

Fig. 2.6 also presents a hypothetical trajectory of p_{CO_2} and p_{O_2} during DGC cycles. After the open phase the system is at the upper left corner point, with high p_{O_2} and low p_{CO_2}. During constriction O_2 quickly falls to the oxygen threshold while CO_2 only increases slowly. Upon hitting the O_2 threshold spiracles start fluttering. How this might work is the focus of the next chapter (chapter 3). However, CO_2 is below its respective threshold but still accumulates slowly. In the phase space this means that the curve is oscillating around the oxygen threshold, drifting to the right. After a while the CO_2 threshold is crossed and the spiracles open widely. O_2 quickly rises to nearly ambient values, followed by a slower reestablishment of the initial CO_2 conditions and the cycle starts over.

When interpreting the phase space map care has to be taken though. It represents endotracheal variables which most probably are not identical to the more important local conditions at the respective sensor. Especially for the delayed termination of the open phase additional processes resulting in a large hysteresis of the endotracheal p_{CO_2}

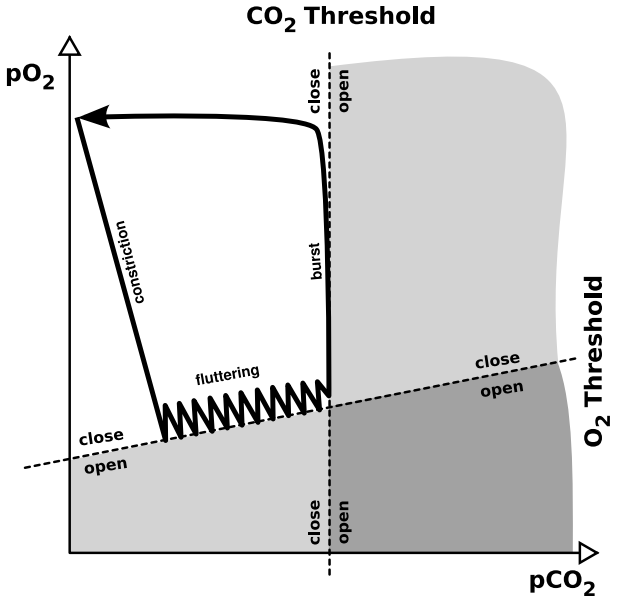

Figure 2.6.: Interpretation of the perfusion experiment. The boundary between open and closed regions consists of two interacting linear thresholds. A hypothetical trajectory of a DGC cycle is shown.

have to be assumed. Whether this hysteresis is built into the sensor (two-point control) or somehow 'generated' between sensor and tracheal space is an open question. The model in chapter 4 will present one possible way how this hysteresis might be realized.

Part III.

Theoretical Work

3. Flutter model

3.1. Introduction

The discussion of the phase space map only briefly mentioned the problem of fluttering as an oscillation phenomenon around the O_2 threshold. This chapter develops a model for how the observed patterns of CO_2 release during the flutter phase of DGC might be generated.

3.1.1. The segment as an independent oscillator

It has long been known that each segment independently controls its spiracles (van der Kloot, 1963). It is also acknowledged that the fluttering apparently has a cyclic component, which is sometimes called the micro-cycle (Schneiderman, 1960).

So the first question is, how can a single segment generate these cycles?

First of all, it is clear that when the spiracles are closed, endotracheal oxygen partial pressure falls. If the O_2-open threshold is reached, the spiracles of the segment open and O_2 flows into the tracheal system by diffusion and/or convection. This again raises the endotracheal partial pressure above the threshold. However, there has to be some hysteresis, otherwise the spiracle would immediately close again and only little O_2 would have been taken up.

Hysteresis commonly occurs when there is a time delay in the feedback loop (Glass and Mackey, 1988). In the case of the O_2 control during the flutter phase of DGC one possibility would be the diffusion time of oxygen to the O_2 sensor, which is thought to be located in the segmental ganglion (Burkett and Schneiderman, 1974b). A simple model calculation demonstrates the compatibility of the time scales.

The characteristic time scale for diffusion is (Fowkes and Mahony, 1996)

$$x = 4\sqrt{Dt} \qquad t_{ch} = \frac{x^2}{16D} \tag{3.1}$$

For a diffusion distance of about 1 cm (the radius of a medium sized *Attacus* pupa) and a diffusion coefficient of D=0.178 $cm^2\,s^{-1}$ for O_2 in air (Dejours, 1975), the resulting time scale is t=0.35 s.

Measurements of open time during flutter yield single micro-openings from 0.3 to 0.9 s (Wobschall and Hetz, 2004; Sláma, 1988). However, these small values are only achieved if the inflow has a considerable convective component, i.e. at the beginning of the flutter

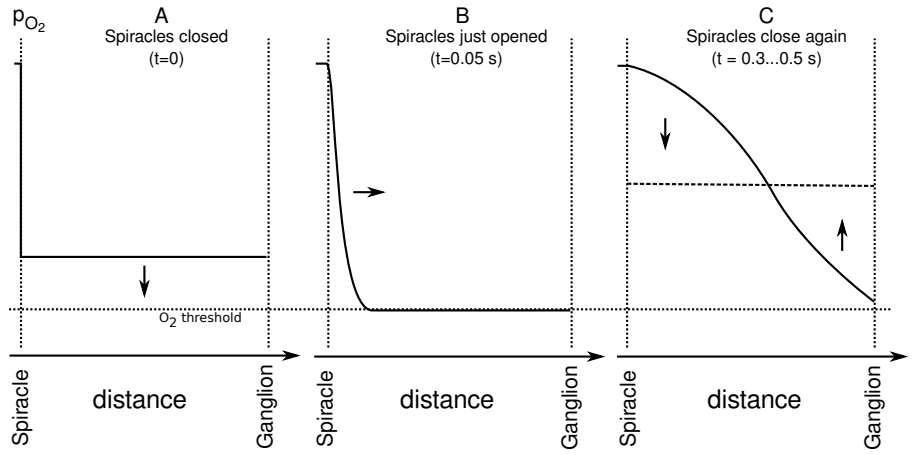

Figure 3.1.: Schematic microcycle model. When the spiracles are closed the p_{O_2} is equilibrated throughout the tracheal system and falling due to metabolic rate (A). If a threshold is reached the spiracles open and a diffusion front moves into the interior (B). However, it takes some time to reach the sensor and the mean p_{O_2} is increased significantly above the threshold after reequilibration (C).

phase. This results in a largely increased apparent diffusion coefficient for O_2. Later, when flutter phase transport has become predominantly diffusive the duration of single micro-openings is several seconds (Wobschall and Hetz, 2004) up to tens of seconds in hypoxia (Hetz, *pers. comm.*).

So the proposed model of the flutter mechanics in a single segment is as follows. Initially, endotracheal partial pressure at the ganglion is above the threshold. Due to metabolic rate the partial pressure falls slowly. Upon reaching the threshold the spiracles open and O_2 flows into the tracheal system. However, it takes a small time for the oxygen to reach the ganglion and raise the tracheal partial pressure above the threshold. During this time the spiracles of the segment are still open and a considerable amount of oxygen is taken up. Following spiracle closure it will equally distribute in the tracheal system. The O_2 partial pressure is now well above the O_2-open threshold and depending on metabolic rate it will take some time until the threshold is reached again. The result is a micro-cycle with very brief openings and a relatively long phase of closed spiracles.

As the flutter phase is thought to be controlled primarily by O_2 (Schneiderman, 1960; Hetz and Bradley, 2005) the following model is simplified to include just the dynamics of oxygen consumption and O_2 uptake via diffusion. It is assumed that p_{CO_2} is below the trigger threshold for spiracle opening and does not influence the behavior of the spiracles during the flutter phase (Schneiderman, 1960).

3.1.2. Interaction between multiple segments

The previous section described a possible way how regular micro-cycles might be generated in a single segment. However, the organization of insects is metameric, that is they consist of multiple connected segments. This connection results in the coupling of the single segment oscillators.

I propose that two mechanisms define the coupling. First of all the tracheae of multiple segments are connected and diffusion occurs along them. The endotracheal air exchanged between neighboring segments and that way is equilibrated throughout the whole animal. The diffusive conductance for this process might be quite high as the main tracheal trunks which run longitudinally along the body are relatively large.

As second mechanism which might distribute respiratory gases within the animal is circulation. Dissolved gases in the hemolymph are transported from segment to segment by the ation of the heart. This likewise results in equilibration of the endotracheal gas composition over time.

From a more abstract point of view the tracheal system during the flutter phase of the DGC might be seen as a set of oscillators that are coupled in series. Systems of this kind can exhibit a rich behavior in terms of synchronization (Pikovsky et al., 2003). The critical parameters determining the behavior are the frequencies of the free running (i.e. uncoupled) oscillators and the strength of coupling between them.

The frequency of the segmental flutter phase oscillator is mostly determined by the metabolic rate of the segment, the time delay which determines the micro-opening time and the spiracular conductance. Coupling strength is proportional to the diffusive conductance of the main tracheal stems and cardiac output.

It is clear that in biological systems these parameters are not identical in every segment. Thus slight variations in the oscillation period of multiple segments are expected. However, if these differences are small and the coupling is sufficient, passive synchronization might still occur (Pikovsky et al., 2003).

Flow through respirometry measures the total CO_2 release from the whole animal. As a summation signal it can still appear quite regular, despite the possible complexity of the rhythm of micro-openings. An example might clarify this. The observed regular opening rhythm in the respirometer may derive from a single segment micro-cycling with steady rhythm. However, it could alternatively be produced by two phase shifted segments, which just open every other beat. Without knowledge of the particular spiracle that opened, there is no way of distinguishing between both cases.

3.1.3. Working Hypothesis

The last two sections described a generation mechanism for the complex patterns of CO_2 release which are observed during the flutter phase of the DGC. The mechanism was derived solely from the morphological arrangement and the tentative mode of O_2 control (Burkett and Schneiderman, 1974b).

A simplified, quantitative model can thus be developed, which at least qualitatively can reproduce the patterns of micro-opening of the flutter phase. The model will be purely passive in the sense that no other coordination of segments occurs except by diffusion of oxygen between neighboring segments. In particular, neural coordination is explicitly excluded from the model and a segments control loop acts completely independent of other segments (Burkett and Schneiderman, 1974b).

However, if the flutter phase CO_2 release patterns are the result of a synchronization mechanism as described previously, then the theory of coupled oscillators (Pikovsky et al., 2003) allows for much more fine-grained hypotheses about the system.

For low coupling strength, synchronization is less likely. In the concrete case it is thus expected that for low internal conductance the pattern of micro-openings is less regular and more spiracles participate in the rhythm. The distribution of micro-openings should be more or less uniform over all spiracles.

For high coupling strength, synchronization does occur. The patterns will become more regular and fewer spiracles participate in the rhythm. As a result the distribution of micro-openings will concentrate on fewer spiracles and a multimodal distribution occurs.

Coupling strength between any two segments is a function of distance due to the serial organization. Neighboring segments have the highest coupling and will mutually inhibit each other. It is thus expected that the segments that still open are uniformly distributed over the whole body and some 'striping effect' does occur in the histogram of micro-openings. Between segments that open there will be other, neighboring segments that will have shut their spiracles all the time and do not take part in gas exchange. With increasing coupling strength the number of these silenced segments will increase, and consequently, the number of stripes in the histogram will decrease.

For sufficiently high coupling it is predicted that only one single spiracle opens in a regular pattern. In effect, this would be in strong agreement with the master spiracle hypothesis (Sláma, 1988).

3.1.4. Rationale of the Modelling Approach

Experimental variation of the coupling between multiple segments in an animal is not feasible to date. Also measurement of p_{O_2} in multiple segments with high time resolution require an instrumentation of the animal that most probably interferes with the phenomenon under observation.

Therefore, a test of the working hypothesis is only indirectly possible. A theoretical quantitative model, assuming the described process to be true, allows to deduce very specific predictions that might or might not contradict independent experimental data. In the first case, this would provide strong support for rejection of the working hypothesis; in the latter case the working hypothesis will be retained as a best explanation so far.

3.2. Model Specification

The theoretical model has been implemented as a hybrid delayed differential equation (DDE; Murray, 1993; Ellner and Guckenheimer, 2006) model in Matlab (The MathWorks, Inc., Natick, MA, USA). For every segment it contains two states (open and closed respectively). The segments are independent so the total number of states in the model is 2^N where N is the number of segments.

Insects are described to typically possess 10 pairs of functional spiracles after hatching (Miller, 1974), thus $N = 10$ has been used throughout the whole model analysis.

Closed state The closed state in the i-th (internal) segment can be described as

$$\frac{dM_i}{dt} = -MR_i + G_{in}\left(\frac{M_{i-1}}{\alpha v} + \frac{M_{i+1}}{\alpha v} - 2\frac{M_i}{\alpha v}\right) \quad 1 < i < N \tag{3.2}$$

where M_i is the amount of oxygen in the i-th segment, MR_i is the metabolic rate of the segment and G_{in} is the internal, intersegmental diffusive conductance of oxygen. For simplicity the tracheal volume of each segment (v) is equal and 1/Nth of total tracheal volume $v_i = \frac{V_{tr}}{N}$. α is the capacitance of oxygen in air (Piiper et al., 1971).

So basically two processes influence the segments O_2 in the closed state. The first is the reduction in O_2 due to metabolic rate, the second is diffusive equilibration between neighboring segments.

The terminal segments have limited diffusive flow and need special treatment

$$\frac{dM_1}{dt} = -MR_1 + G_{in}\left(\frac{M_2}{\alpha v} - \frac{M_1}{\alpha v}\right) \tag{3.3}$$

$$\frac{dM_N}{dt} = -MR_N + G_{in}\left(\frac{M_{N-1}}{\alpha v} - \frac{M_N}{\alpha v}\right) \tag{3.4}$$

Oxygen consumption is slow compared to the diffusive redistribution of O_2 in the tracheal system. Also, when the spiracle opens significant amounts of oxygen enter the tracheal system and lift the partial pressure well above the threshold.

It is thus assumed that O_2 is uniformly distributed in the segment before the threshold partial pressure (Förster and Hetz, 2008, terminal partial pressure) θ_i is arrived. As a result the O_2 sensor reacts immediately if p_{O_2} falls below the threshold and the spiracle opens.

An event function can be defined which detects the crossing

$$ev_i(t) = \frac{M(t)_i}{\alpha v} - \theta_i \quad i = 1 \ldots N \tag{3.5}$$

A state change occurs, if one of the components of $ev(t)$ changes its sign from positive to negative.

Open state The open state is very similar to the closed state. It additionally contains the oxygen diffusion across the open spiracle

$$\frac{dM_i}{dt} = -MR_i + G_{in}\left(\frac{M_{i-1}}{\alpha v} + \frac{M_{i+1}}{\alpha v} - 2\frac{M_i}{\alpha v}\right) + G_{sp,i}\left(p_{O_2}^{amb} - \frac{M_i}{\alpha v}\right) \quad 1 < i < N \tag{3.6}$$

$$\frac{dM_1}{dt} = -MR_1 + G_{in}\left(\frac{M_2}{\alpha v} - \frac{M_1}{\alpha v}\right) + G_{sp,1}\left(p_{O_2}^{amb} - \frac{M_1}{\alpha v}\right) \tag{3.7}$$

$$\frac{dM_N}{dt} = -MR_N + G_{in}\left(\frac{M_{N-1}}{\alpha v} - \frac{M_N}{\alpha v}\right) + G_{sp,N}\left(p_{O_2}^{amb} - \frac{M_N}{\alpha v}\right) \tag{3.8}$$

However, due to the time delay that is imposed by the diffusion time from the spiracle to the sensor (Fig. 3.1) the reaction to the O_2 inflow will not be instantaneous. This was modelled by comparing the threshold to the oxygenation state some short time τ earlier.

For the detection of closure the event function was thus

$$ev_i(t) = \frac{M_i(t-\tau)}{\alpha v} - \theta_i \quad i = 1 \ldots N \tag{3.9}$$

A state change occurs if one component of $ev(t)$ changes its sign from negative to positive (i.e. the oxygen partial pressure is above the threshold and rising)

The maximum stepsize for numerical integration of delay differential equations is the least common denominator of the delays. This significantly slowed the computations if multiple delays (one per segment) were used. For that reason the same delay τ was used for all segments.

State model The state of the spiracles can be conveniently encoded using a spiracle state vector $a = a(t)$, which can be computed from the event functions (eqs. 3.5 and 3.9). For open spiracles $a_i = 1$, for closed spiracles $a_i = 0$.

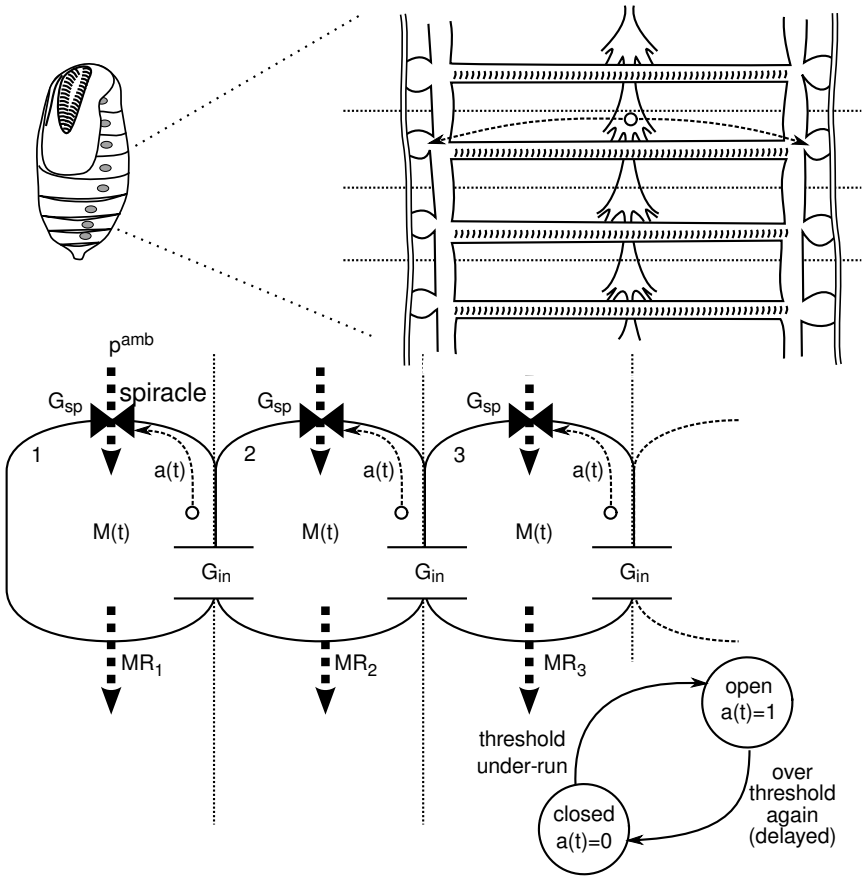

Figure 3.2.: The hybrid flutter phase model. Segments consist of a tracheal gas space with an O_2 sensor (the ganglion) attached to it which controls the spiracular valve. Neighboring segments are coupled via longitudinal tracheae. The lower right corner shows the state diagram of a single segment with the conditions determininig the state switch.

The two model states can then be combined into a single system

$$\frac{dM_i}{dt} = -MR_i + G_{in}\left(\frac{M_{i-1}}{\alpha v} + \frac{M_{i+1}}{\alpha v} - 2\frac{M_i}{\alpha v}\right) + a_i G_{sp,i}\left(p_{O_2}^{amb} - \frac{M_i}{\alpha v}\right) \quad 1 < i < N \tag{3.10}$$

$$\frac{dM_1}{dt} = -MR_1 + G_{in}\left(\frac{M_2}{\alpha v} - \frac{M_1}{\alpha v}\right) + a_1 G_{sp,1}\left(p_{O_2}^{amb} - \frac{M_1}{\alpha v}\right) \tag{3.11}$$

$$\frac{dM_N}{dt} = -MR_N + G_{in}\left(\frac{M_{N-1}}{\alpha v} - \frac{M_N}{\alpha v}\right) + a_N G_{sp,N}\left(p_{O_2}^{amb} - \frac{M_N}{\alpha v}\right) \tag{3.12}$$

Parameters It was assumed that the mean CO_2 release of a diapausing *Attacus* pupa weighing 5 g was about 50 nmol min^{-1} (e.g. Hetz, 1994; Wobschall and Hetz, 2004). Assuming a respiration ratio of 0.7 this corresponds to a total oxygen consumption of MR=71.4 nmol min^{-1}. Assuming that every segment contributes about equally the segmental metabolic rate is MR_i=7.1 nmol min^{-1}.

Th O_2 capacitance in air at 15 °C is α=0.417 mmol l^{-1} kPa^{-1} (Piiper et al., 1971). The tracheal volume has been assumed to be 241 µl (Bridges et al., 1980) at the size given.

The threshold partial pressure θ (terminal partial pressure Förster and Hetz, 2008) has been assumed to be 5 kPa for simplicity. The exact value is dependent on a number of factors, e.g. CO_2 partial pressure (Schneiderman, 1960, see also chapter 2) and metabolic rate (Hetz, 1994). However, its exact value is of minor importance as any variation will not influence the general form of the solution. Rather it will only result in a slight variation of the particular oscillation frequency.

It has been assumed that some random variation occurs in the metabolic rate of a segment as well as in its O_2 threshold. No literature values for metabolic rate distribution or the variability of O_2 thresholds in single individuals have been found. Thus the variability has been conservatively guessed to be 1 % of the respective nominal value and normally distributed.

To limit sources of noise and simplify the analysis it has been assumed that the spiracle conductance was exactly equal in each segment and thus 1/10th of the total spiracle conductance. Using the pressure rise rate during micro-openings of Δp=2.2 kPa s^{-1} (Wobschall and Hetz, 2004) and the oxygen partial pressure gradient of about $\Delta p_{O_2} \simeq$15 kPa, G_{sp}=8.8 min^{-1} has been calculated for the single spiracle conductance. Since it is assumed that only single spiracles open during flutter this number directly applies to all segments.

The opening time of spiracles during flutter is specified as 0.1 - 0.3 s (Wobschall and Hetz, 2004). However this figure applies to the pressure rise period where a significant convective component of the inflow might enhance the apparent diffusion coefficient thus shortening the opening time according to equation 3.1. τ has thus been assumed to be a slightly longer 1 s or 0.0167 min in agreement with unpublished endotracheal pressure traces of the later flutter phase of *Attacus* pupae (Hetz, unpublished).

The final parameter table thus looks as follows

ambient oxygen partial pressure	$p_{O_2}^{amb}$	$20.95\,\mathrm{kPa}$
spiracular conductance	G_{sp}	$70\,\mathrm{nmol\,min^{-1}\,kPa^{-1}}$
conductance of longitudinal tracheal trunks	G_{in}	$70\,\mathrm{nmol\,min^{-1}\,kPa^{-1}}$
metabolic rate of i-th segment	MR_i	$7.14 \cdot \mathcal{N}(1, 0.01)\ \mathrm{nmol\,min^{-1}}$
tracheal volume of i-th segment	v_i	$24.1\,\mu\mathrm{l}$
oxygen capacitance in tracheal air	α	$0.417\,\mathrm{nmol\,\mu l^{-1}\,kPa^{-1}}$
opening threshold of i-th segment	θ_i	$5 \cdot \mathcal{N}(1, 0.01)\ \mathrm{kPa}$
sensory delay	τ	$0.0167\,\mathrm{min}$

where $\mathcal{N}(1, 0.01)$ stands for normally distributed noise with mean 1 and standard deviation of 0.01.

Simulated CO_2 release To make the model results visually comparable to existing flow-through respirometry data of CO_2 release during flutter the estimation of CO_2 release by flow through respirometry has been simulated. On integration the model generates the timings of spiracle openings. Because the individual open times are brief, the openings were interpreted as a series of delta spikes. These were then convoluted with a log-normal kernel to visually simulate the washout characteristics of the respirometer chamber and the IRGA cuvette (Gray and Bradley, 2006; Lighton, 2008).

As most of the parameters are not accurately known and also because CO_2 partial pressure is not part of the model, the resulting CO_2 release rates are completely arbitrary. The purpose is solely to visualize the complexity of the generated patterns that can be achieved with the model.

3.3. Results

3.3.1. Time Series Solution

As expected for a constant metabolic rate, p_{O_2} in a single segment falls linearly until reaching the open threshold θ. Because of the delayed closing a significant amount of oxygen enters the tracheal system and the endotracheal p_{O_2} is elevated well above the threshold again (Fig. 3.3).

The time delay and the metabolic rate are fixed and so the frequency of oscillations is constant. This results in a regular rhythm in the simulated CO_2 release.

Fig. 3.4 shows the time course of endotracheal p_{O_2} for two neighboring segments with some internal conductance, i.e. the segments are coupled. In contrast to the independent segment above the two rhythms of the segments become dependent on each other and synchronize their frequency.

As was typical, the segment with the higher threshold opens more often. However in the case of Fig. 3.4 the coupling strength is too small to completely prevent the slower

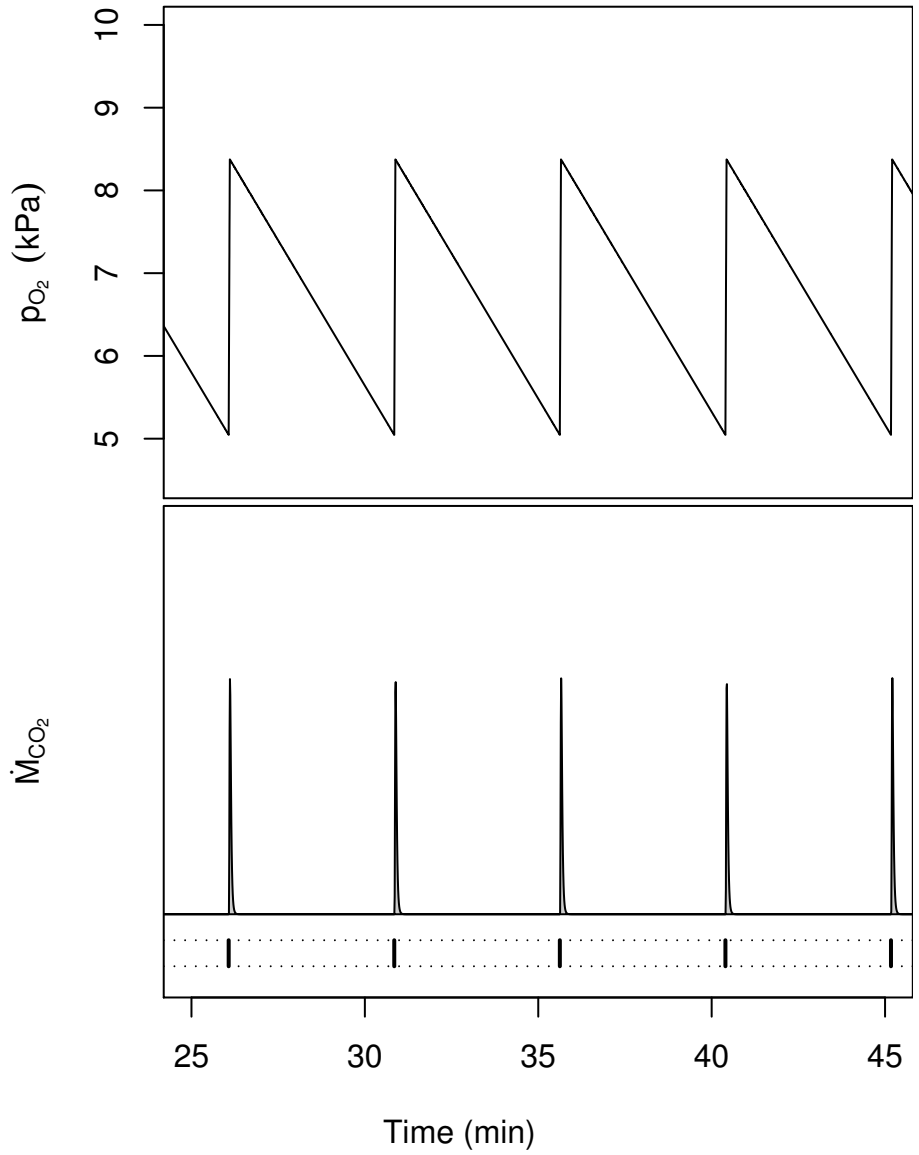

Figure 3.3.: Model solution for a single uncoupled segment. Above - Time series solution for the endotracheal p_{O_2}. Below - Simulated CO_2 release from the single segment. The control mechanism generates a regular rhythm of micro-openings. The lowermost dashes represent the opening time of the spiracle.

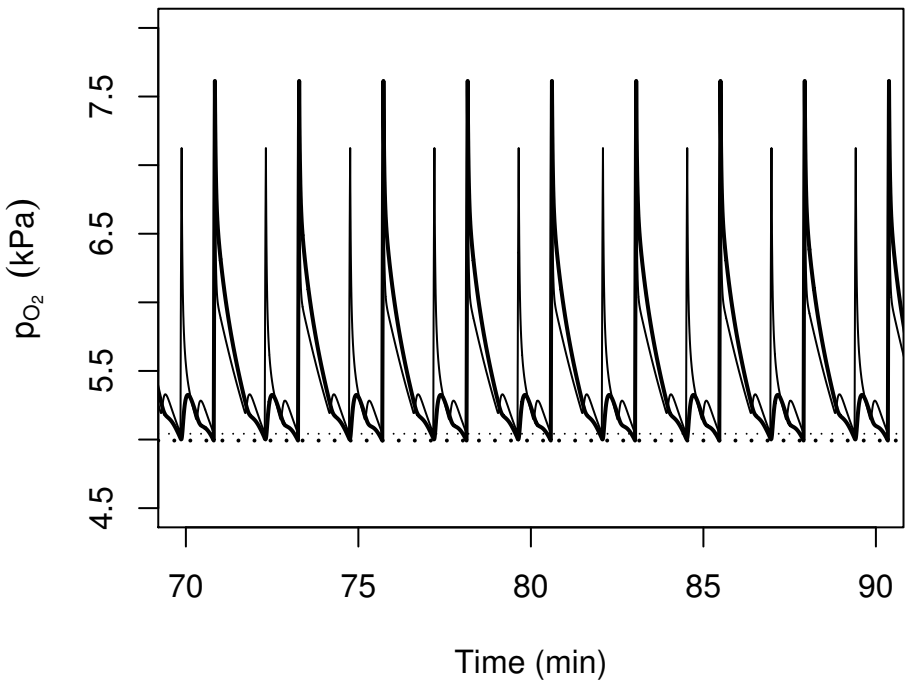

Figure 3.4.: 2:1 phase locking between segments 7 and 10 at higher coupling strength (G_{in}=200 nmol min^{-1} kPa). Segment 7 (thin line) opens with twice the frequency of spiracle 10 (thick line). Segments 8 and 9 (not shown) do not open at all. The dotted lines show the opening thresholds of segments 7 and 10 respectively.

segment from opening. The result is a 2:1 rhythm when focusing on these two segments (No. 7 and 10) only. The full (10 segment) model is shown in Fig. 3.5.

3.3.2. Distribution of open spiracles

Figs. 3.6 and 3.8 show the distribution of the spiracles which are opened during the flutter phase for different values of the coupling strength G_{in}. For uncoupled segments the event histogram accurately reflects the distribution of metabolic rate across the segments. Segments with higher metabolic rate and thus higher frequency of oscillation open more often.

Increasing coupling strength leads to partial synchronization between neighboring segments. Especially when there is considerable difference in metabolic rate or open thresholds between the segments it may happen that one segment does no longer open at all and the segments O_2 consumption is met by delivery from neighboring segments.

The total number of spiracles used is roughly proportional to the inverse of the coupling strength (Fig. 3.7). Intermediate values often led to frequency and sometimes phase locking of neighboring segments (compare Fig. 3.4).

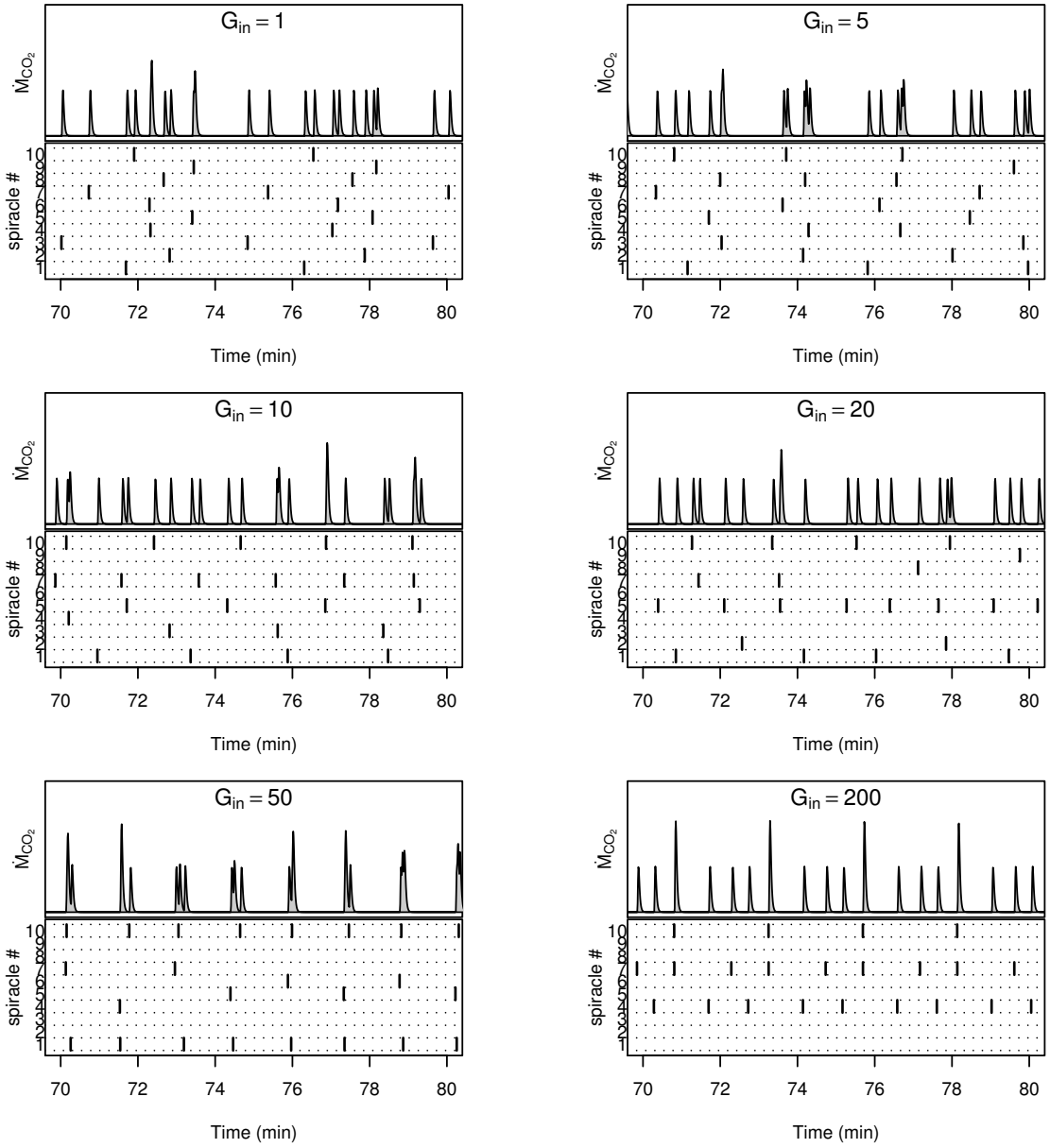

Figure 3.5.: Simulated CO_2 release for ten segments with varying internal conductance (coupling strength). The lower part of each figure shows the opening sequence of the single spiracles. For higher coupling strength the segments become partly synchronized and fewer spiracles open at all.

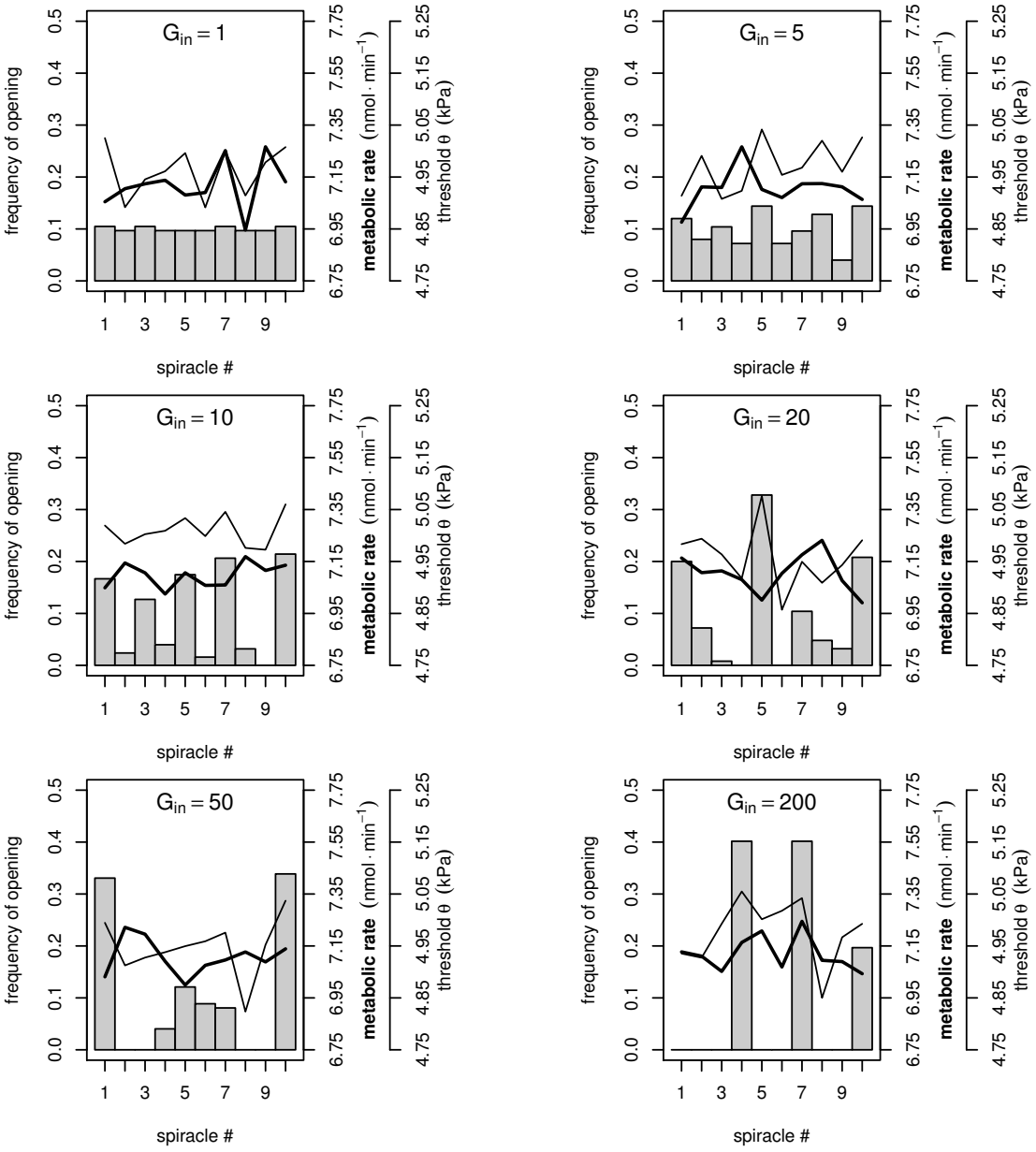

Figure 3.6.: Histograms of spiracle opening events. For higher inner conductance the 'striping' effect becomes clearly visible. Also note that the use of spiracles seemingly depends more on the O_2 threshold θ than on local metabolic rate.

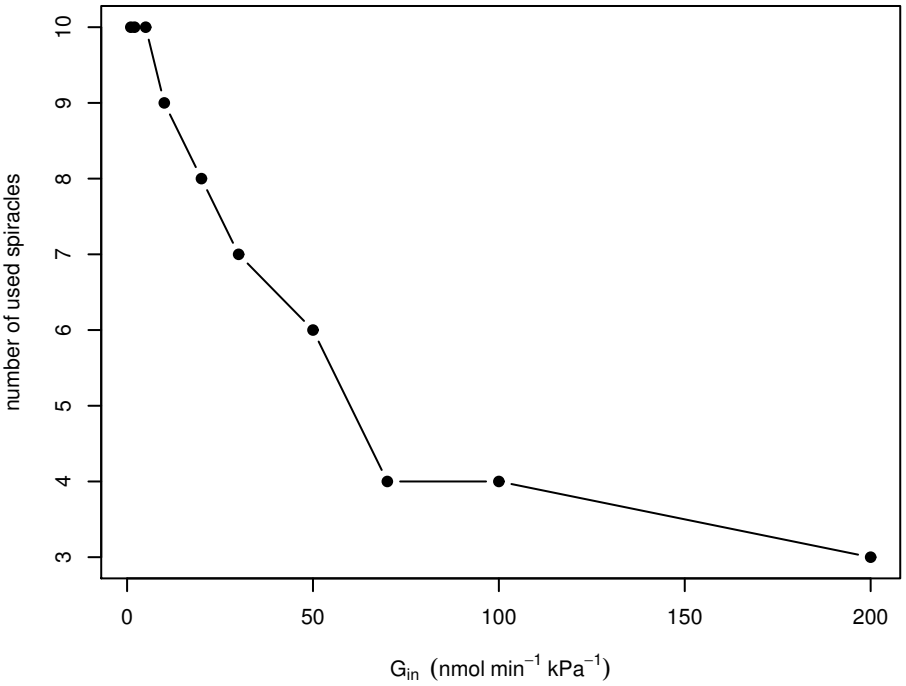

Figure 3.7.: Number of the spiracles used for fluttering at different values of the inner conductance G_{in} (coupling strength).

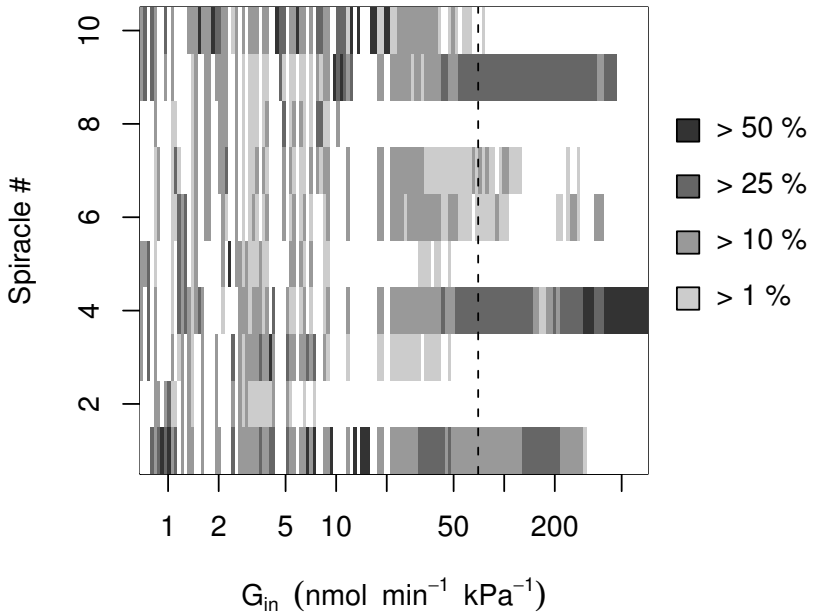

Figure 3.8.: Distribution of opened spiracles when the coupling strength (G_{in}) is varied. Higher G_{in} results in fewer spiracles used and a more regular opening pattern. Identical distributions of metabolic rate and thresholds have been used for all values of G_{in}

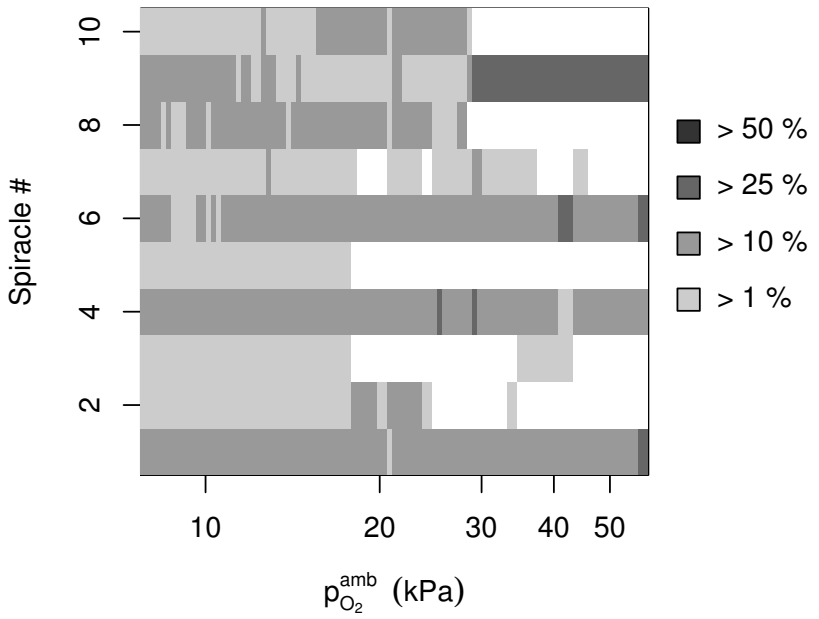

Figure 3.9.: Distribution of opened spiracles when the ambient p_{O_2} is varied. Hyperoxia has a synchronizing effect, mimicking the effect of increased coupling strength. Distributions of metabolic rate and O_2 thresholds have been identical for all values of ambient p_{O_2}.

3.3.3. The influence of ambient oxygen partial pressure

Low ambient p_{O_2} affected the spiracles in the same way than high longitudinal conductance G_{in} did - the distribution of open spiracles was more uniform and the temporal pattern became more complex (Fig. 3.9). Strong hyperoxia had a synchronizing effect.

Instead of experimental manipulation of longitudinal conductance, the model might thus be more easily tested by changing the ambient p_{O_2}. The data in Hetz and Bradley (2005) can be interpreted in this way.

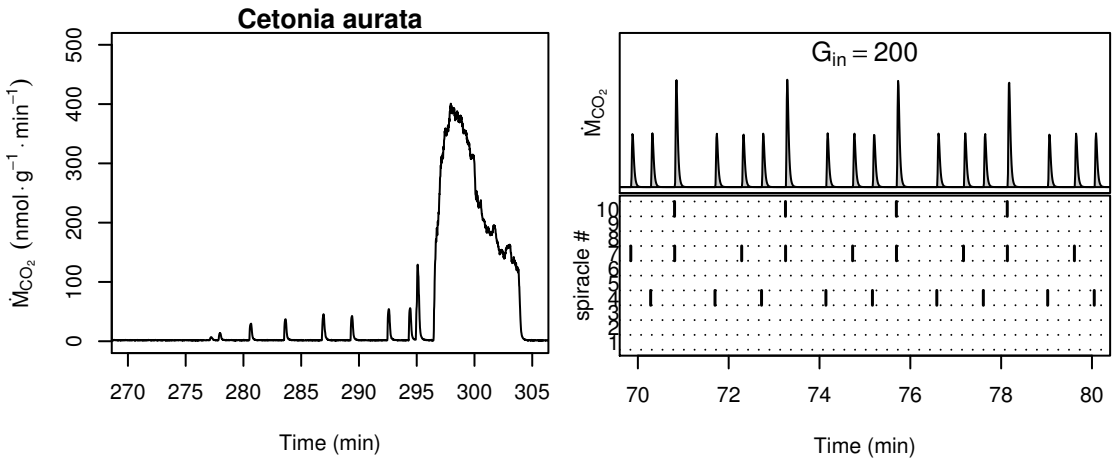

Figure 3.10.: Comparison of CO_2 release of *Cetonia aurata* measured with flow through respirometry to simulated CO_2 release of the model with very high coupling strength. Synchronized spiracles generates a regular rhythm of microopenings.

3.4. Discussion

The assumed variation in thresholds and metabolic rate between segments was 1 %. Compared to the observed variation in live insects this probably was a very conservative estimate. Woods (2009) describes the development of spiracle size in larval *Manduca sexta* and relates it to metabolic demand of the respective segments. According to him the last two abdominal spiracles on either side initally make up 70 % of the total spiracle area dropping to about 25 % in later instars. As spiracle area is thought to provide an index of local metabolic activity, similar variation in local metabolic rate might be assumed.

So far nothing is known about the variability of the O_2-open threshold in a single individual. However, the perfusion experiment has shown (Fig. 2.5; also compare Schneiderman, 1960; Burkett and Schneiderman, 1974b) that it depended on p_{CO_2} which is slowly rising during the flutter phase. Local p_{CO_2} in turn is strongly influenced by local metabolic rate. It might thus be assumed that at least some variation of local oxygen thresholds exists.

The simulated CO_2 release patterns resemble those observed in various groups of insects. High coupling strength results in regular micro-openings that are typical of beetles (Fig. 3.10). The effect that only one spiracle is used has also been described earlier (Sláma, 1988).

Decreasing coupling strength allows more spiracles to open (Fig. 3.7). Sláma (1988) shows one case of an individual that employs only the most terminal segments during fluttering. The model has shown that the specifically active spiracles depend on the distribution of metabolic rate and the O_2 thresholds (Fig. 3.6). However, for a certain coupling strength a two-segment mode was commonly observed.

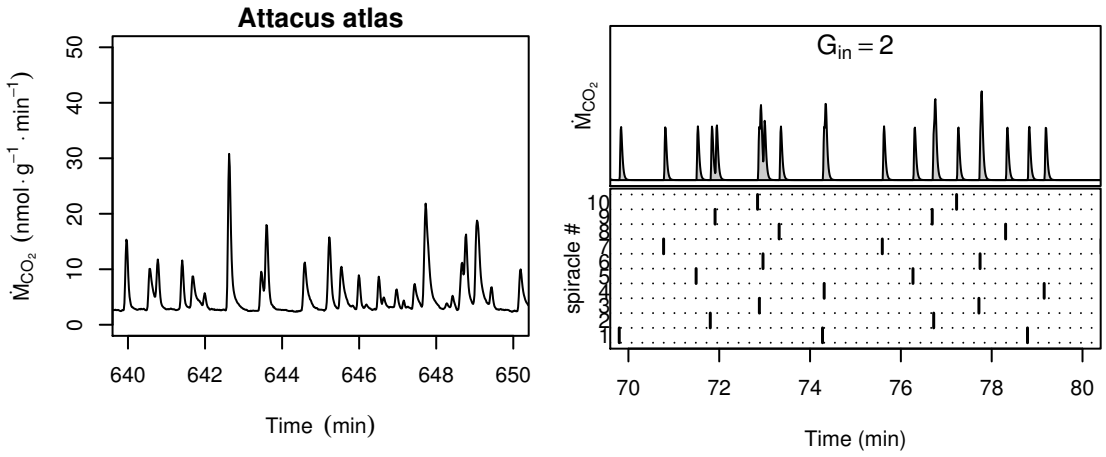

Figure 3.11.: Comparison of CO_2 release of *Attacus atlas* measured with flow through respirometry to simulated CO_2 release of the model with low coupling strength. The multiple free running segments generate an irregular pattern of microopenings.

Further decreased coupling strength allows more and more spiracles to participate in the fluttering. Due to their slightly different periods of oscillation the resulting CO_2 release pattern becomes more and more irregular (Fig. 3.11). This is a typical feature of lepidopteran DGCs. From the point of view of a single segment the oscillations are still quite regular though.

When looking closely one can see many different amplitudes of the single opening events in the *Attacus* data. On the other hand the model seems to exhibit two distinct levels only. However, it should be remembered that an equal spiracle conductance had been assumed. If one allows for some variation in that parameter too, then likewise there will be some variation in the amplitude of CO_2 release from single events. It might even be possible to use this fact to decompose a composite observation like Fig. 3.11 and classify the single events into distinct clusters corresponding to the opening of a distinct segment.

However, this is not an easy task in the absence of information about the actual number of active segments and their local parameters like metabolic rate or spiracle conductance.

It is not quite clear whether both spiracles in a segment open synchronously during flutter. From the central control mechanism by unpaired median nerve neurons (Burkett and Schneiderman, 1974b) one would expect that they do. However, as the data of Sláma (1988) show, this might not necessarily be the case. Electrophysiological recordings likewise cast doubt on the strictly synchronized action of the spiracles in a single segment (van der Kloot, 1963). If they do not, then the number of possible generators of microcycles promptly doubles.

Lastly the task is further complicated by the fact that the O_2 thresholds are influenced

by p_{CO_2} which is slowly rising with time. This means that the model thresholds change over time. In turn this alters the periods of oscillation of the segments which poses a challenge since most methods for the analysis of time series depend on the stationarity of the data. This assumption might or might not be violated depending on the speed of the CO_2 increase.

4. Carbon dioxide cycle model

4.1. Introduction

The motivation for the second model also derives from the perfusion experiment. If, as the discussion at the end of chapter 2 indicated, the feedback controls for O_2 and CO_2 are comprised of two different mechanisms then the question is what is the CO_2 mechanism and how is the internal CO_2 level sensed?

Because CO_2 hydrates in aqueous solution forming carbonic acid and by subsequent dissociation protons and bicarbonate CO_2 could possibly be sensed as a pH signal either in the hemolymph or at some specialized sensory site (Harrison, 2001). The observation of Matthews and White (2009) that after hypoxia treatment and the resulting respiratory alkalosis the normal spiracle opening behavior sets in no sooner than pre treatment hemolymph pH has been reached also indicates some form of pH control.

From the works of Hoyle (1959, 1960, 1961) and van der Kloot (1963) the most likely site for the CO_2'sensor' is the neuromuscular junction of the spiracle muscle. Both authors observed a decrease in the muscular tension if CO_2 concentration was enhanced near the neuromuscular junction of the median nerve branch that supplies the muscle. However the actual mechanism has not been revealed so far.

To check the possibility of a general pH feedback control a simple model of the insect has been created. It consists of two compartments only, the tracheal system and a lumped together hemolymph-tissue compartment ('wet' compartment, Fig 4.1). The aggregation was based on the assumption that the hemolymph plays the predominant role in the buffering of the CO_2 during the constriction and flutter phase of the DGC (Harrison et al., 1995). Furthermore, this tremendously simplifies the modelling effort as the intricate transport processes between intracellular and extracellular space can be neglected. The only form of exchange between the 'wet' compartment and the tracheal space is diffusion of CO_2 across the tracheal wall.

The 'wet' compartment posesses an aerobic metabolism generating a constant stream of CO_2 into the compartment. The CO_2 is physically dissolved and may react according to the simplified reaction scheme for CO_2 in aqueous solutions (Gibbons and Edsall, 1963)

$$CO_2 + H_2O \underset{k_{-1}}{\overset{k_1}{\rightleftharpoons}} H^+ + HCO_3^-$$

$$HB \underset{k_{-2}}{\overset{k_2}{\rightleftharpoons}} H^+ + B^-$$

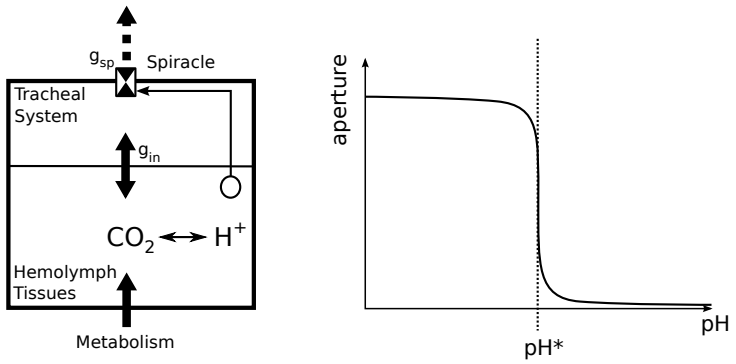

Figure 4.1.: Schema of the CO_2 control model and the feedback response function.

Protons can be buffered by an unspecified nonbicarbonate buffer B^- which is present in finite concentration in the 'wet' compartment. It is assumed that this buffer has a single pK, although most likely it will consist of a mixture of several buffering substances (Harrison, 2001; Wyatt, 1961).

It is further assumed that the pH of the wet compartment is somehow sensed and used to determine the spiracle aperture. However, bifurcation analysis (see next section) requires that the model is continuous and a state model like the fluttering model (chapter 3) can not be used. Thus, to model the thresholding phenomenon, a stiff sigmoidal response of spiracle aperture to hemolymph pH has been used. For too acidic pH (high CO_2) the spiracle opens and it closes again, when the pH is on the alkaline side of the threshold.

4.1.1. Bifurcation analysis of dynamical systems

To facilitate the analysis of the long term behavior of the CO_2 model for a given set of parameters, dynamical systems theory has been applied. It provides a range of tools that are probably only superficially known to the average physiologist.

This section therefore will present some basic facts about the analysis of dynamical systems that are crucial for the understanding of the remainder of this chapter. It has been based on chapter 5 of Ellner and Guckenheimer (2006) which is recommended as a well written and slightly expanded introduction to this vast field.

Basic terms

The goal of dynamical systems theory of ordinary differential equations is to describe the solutions of these systems in geometric terms.

Conceptually, the values of all variables in a differential equation system at a certain time can be thought of as a point in an abstract *phase space*. This point is often also called the *state of the system*. The differential equations themselves can be interpreted as rules that determine how a point moves in the phase space given its position. If one

were to follow the evolution of a specific point over time one gets a path through the phase space which is called the *trajectory* or *orbit* of that point.

Trajectories cannot intersect if the system is autonomous. That is, it does not depend on time explicitly and its state derivatives are fully defined by the state itself. However, especially in higher dimensional phase spaces (more than at least 3 variables) the trajectories can be intertwined without intersection in a very complicated way. This occurs in so called *chaotic systems*. Initially nearby trajectories get quickly separated and it becomes impossible to approximately predict the state of the system after some time without knowing the initial state exactly (butterfly effect).

For autonomous systems all points on a particular trajectory are equivalent. That is, an arbitrary point on the trajectory allows one to reconstruct the whole trajectory. Mathematically there is no difference of going forward or backward in time. So, usually one is more interested in the long term or *asymptotic behavior* of the solutions.

Often, all trajectories starting in a certain subregion of the phase space approach a common limit set for $t \to \infty$. This set is called an *attractor* of the system and the subregion of phase space is called the *basin of attraction* of the limit set. In the simplest case it may consist of a single point or *equilibrium*. Slightly more complex attractors are closed loops (*limit cycles*) or the surfaces of (multidimensional) tori in the case of *quasiperiodicity* (a superposition of multiple oscillations with non-rational frequency ratios). In chaotic systems often *strange attractors* are observed, complicated limit sets with fractal dimensions that not long ago were fashionable enough to be printed on t-shirts.

Attractors are examples of more general phase space objects. These are called *invariant sets* and are defined by the fact that any trajectory starting in the set, will never leave it. However, the asymptotic behavior of trajectories starting *near* an invariant set can be quite different. One possibility is that they approach the set, the attracting case mentioned before. Because small pertubations from the set exponentially die out, attractors are also said to be *asymptotically stable*. Alternatively *neutrally stable* trajectories remain in a bounded region of the phase space around the invariant set, i.e. the 'errors' are not getting significantly larger but also not smaller. Pertubations of *asymptotically unstable* sets tend to grow exponentially and turn the trajectory away from the invariant set, a *repellor*.

So far our view has been restricted to a fully specified system. However, often differential equation systems contain parameters and thus represent a large family of related differential equation systems. As the values of parameters change, so might the number and types of attractors of the system. Parameter vectors where such qualitative changes of the asymptotic behavior occur are called *bifurcation values* or short *bifurcations* of the system.

Over the years, studying many different systems, it became apparent that certain types of bifurcations occur repeatedly. Mathematicians have therefore tried to classify bifurcations. One often used measure for the complexity of a bifurcation is its *codimension* or codim for short. Intuitively, it is a measure how many parameters have to be

changed simultaneously to observe a specific bifurcation type. So far, all local bifurcations up to codim 2 have been completely classified Kusnetzov (1998); Guckenheimer and Holmes (1983).

Bifurcation diagrams

A convenient way to visualize the qualitative behavior of a dynamical system are *bifurcation diagrams*. Formally they represent a partition of the parameter space (or a subspace of it) into regions with equivalent qualitative behavior (Guckenheimer and Holmes, 1983).

All bifurcation diagrams have at least one axis corresponding to a parameter (the *active parameter*). Codim 1 bifurcation diagrams usually choose a measure of state (e.g. one state variable or the norm of the state) as the second axis (see Fig. 4.2). In higher codimension diagrams all axes correspond to parameters.

For a specific value of the active parameter an equilibrium is a single point in a codim 1 diagram. However, the *implicit function theorem* demands that a smooth variation of the parameter results in smooth variation of the equilibrium as long as the system is structurally stable (Kusnetzov, 1998). The result is that sets of equilibria form smooth lines in the bifurcation diagram (see also Fig. 4.2). Usually the distinction between equilibria and sets of equilibria under parameter variation becomes blurred and the term *equilibrium* is used interchangeably for the single equilibria (points) and the set of equilibria (line) in the codim 1 bifurcation diagram.

By convention the stability of equilibria is encoded in the type of line drawn. Stable equilibria appear as solid lines whereas unstable equilibria are drawn with broken or dotted lines. Multiple lines of equilibria might coexist in a diagram and they might even intersect, the two equilibria are then said to collide. One type of bifurcation that specifically might occur at these intersections is the transcritical bifurcation with an exchange of stability between two colliding equilibria (compare Fig. 4.2).

Another important type of codim 1 bifurcation is the so called Hopf bifurcation. Here a stable equilibrium becomes unstable under the parameter change and gives birth to limit cycle oscillations. By convention, the maximum and minimum of the state variable are plotted with solid lines. However, as this can be easily confused with the lines of stable equilibria, to make oscillatory solutions stand out visually, the envelope of the periodic solutions has been filled in grey (compare left side of Fig. 4.2).

Codim 1 bifurcations appear as labeled points in a codim 1 bifurcation diagram. Usually the label is just a short abbreviation of the bifurcation type (i.e. H - Hopf bifurcation, LC - limit point etc.) In general, no bifurcations with higher codimension will be present in a bifurcation diagram of lower codimension.

Fig. 4.3 visually describes the construction of codim 2 bifurcation diagrams. As the name suggests, two active parameters have to be defined. Codim 1 bifurcations are projected onto the active parameter plane $\theta - \theta_2$, where they form smooth lines due to the implicit function theorem (Kusnetzov, 1998). These lines separate parts of

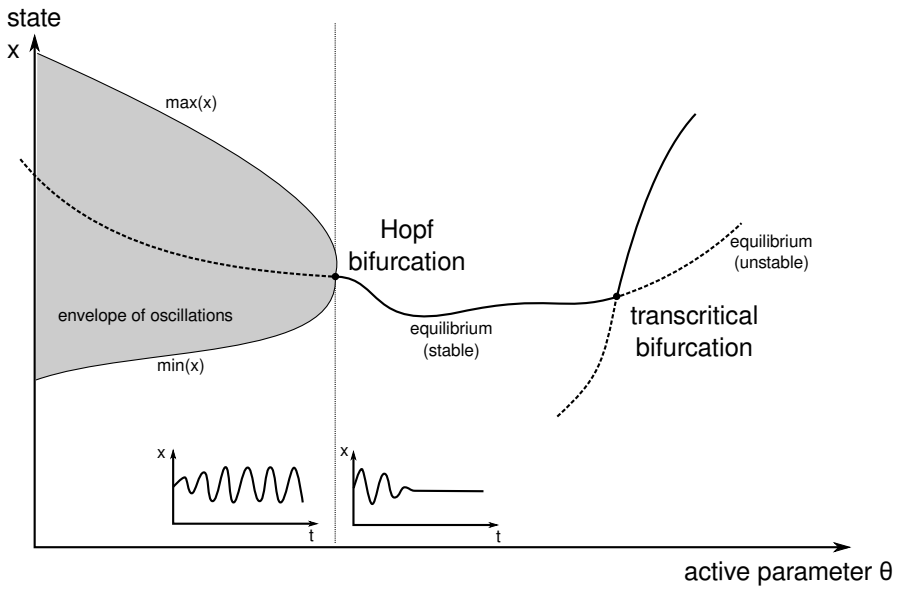

Figure 4.2.: An example codim 1 bifurcation diagram showing typical elements and two example bifurcations. The transcritical bifurcation exchanges stability between two equilibria. Hopf bifurcations separate limit cycle oscillations from stable equilibrium solutions.

the parameter (sub-)space with different qualitative behavior of the model. Codim 2 bifurcations would then appear as points on these lines.

Higher codimension diagrams are constructed in the same way. However, for more than three parameters (codimension > 3) the use of bifurcation diagrams as a means of visualization becomes meaningless.

Continuation Methods

Continuation methods provide an efficient way to derive bifurcation diagrams numerically. The goal of continuation is to compute the solutions of implicitly defined functions

$$F(x, \theta) = 0 \tag{4.1}$$

with x some state vector and θ a vector of parameters.

Equilibria and also bifurcations can be expressed in the form of eq. 4.1. For the former F simply is the vector of right hand sides of the model. It is just the definition of an equilibrium that the differentials (the left hand side of the differential equations) vanish simultaneously.

In the case of codim 1 bifurcations the system of right hand sides can be augmented by the specific mathematical condition that defines the bifurcation (a zero determinant

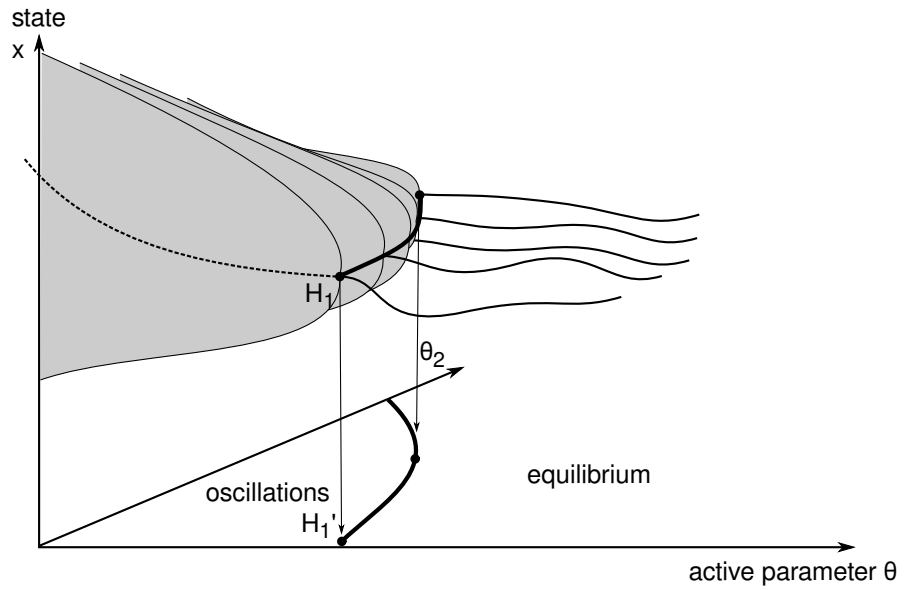

Figure 4.3.: Construction a of codim 2 bifurcation diagram near a Hopf bifurcation. A second active parameter (θ_2) is varied and the resulting set of codim 1 bifurcation diagrams is projected into the $\theta - \theta_2$ plane. Codim 1 bifurcations then appear as lines in the codim 2 diagram.

of the Jacobian matrix evaluated at the bifurcation point). This augmented system is then used as the implicit function F (Kusnetzov, 1998). The general approach of using augmented systems in principle also works for higher codimension bifurcations.

The validity of using continuation methods for bifurcation curves is again derived from the implicit function theorem (Ellner and Guckenheimer, 2006; Kusnetzov, 1998).

Various algorithms have been developed for following implicitly defined curves numerically. Predictor-corrector methods that work with an arc-length based parametrization of the curve have become standard now. These methods work by predicting a new point on the curve using a known point that lies on the curve and the tangent vector on the curve in that point (predictor step). Usually the predicted point will not lie on the curve and a Newton-like correction is employed to find a point on the curve near the predicted point (correction step).

The Matlab toolbox cl_matcont (`http://sourceforge.net/projects/matcont/`), which has been used for the analysis, implements the Moore-Penrose algorithm that is depicted in Fig. 4.4.

4.1.2. Modelling Rationale

Like in the case of fluttering (chapter 3), the process under observation is hard to study en detail experimentally. While open loop experiments like the perfusion (chapter 2) allow to investigate some parts of the involved control loops in isolation, they necessarily

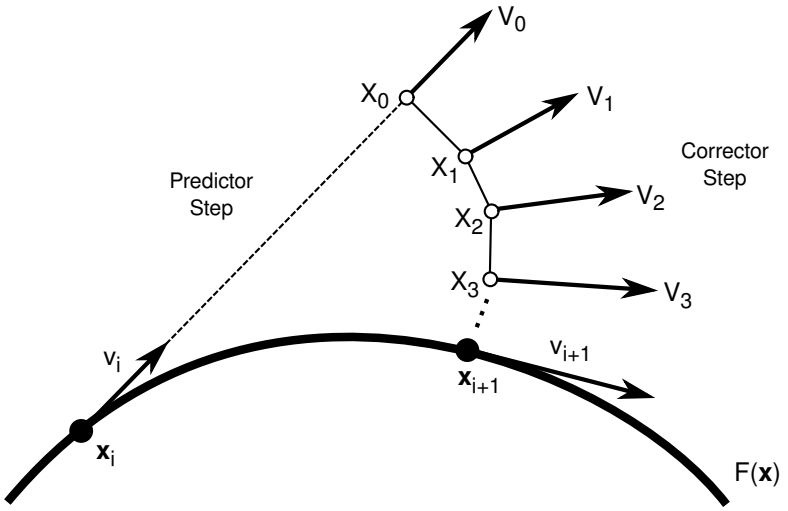

Figure 4.4.: Visualization of the Moore-Penrose algorithm for the continuation of implicitly defined functions. Moore-Penrose consists of a predictor step (arrow from x_i to X_0) and a corrector step (the iterative correction to x_{i+1}). Redrawn from Dhooge et al. (2006)

destroy the feedback. Closed loop experiments allow to only observe a very restricted set of parameters and variables in a live animal.

Again the most productive approach seems to be the deduction of specific hypotheses from a quantitative theoretical model, which might subsequently be tested on real data. For the specific case of CO_2 control, to pass the test, the model is expected to at least show oscillations for some parameters in a physiologically plausible range. Additionally, the qualitative behavior of the model should change with variation of metabolic rate (Bradley, 2008) and tracheal conductance (Hetz, 2007).

4.2. Model Specification

The equations for the raw model are derived in a straight forward way using either Fick's law of diffusion or first and second order reaction kinetics for hydration of CO_2 and the buffering reactions. See table 4.1 for a description of the model symbols.

$$\begin{aligned}\frac{dc^{ti}_{\mathrm{CO}_2}}{dt} &= \frac{MR}{V^{ti}} - k_1 c^{ti}_{\mathrm{CO}_2} + k_{-1} c^{ti}_{\mathrm{H}^+} c^{ti}_{\mathrm{HCO}_3^-} \\ &\quad - \frac{G^{in}}{V^{ti}} \left(\frac{c^{ti}_{\mathrm{CO}_2}}{\alpha^{ti}} - \frac{c^{tr}_{\mathrm{CO}_2}}{\alpha^{tr}} \right)\end{aligned} \tag{4.2}$$

$$\begin{aligned}\frac{dc^{tr}_{\mathrm{CO}_2}}{dt} &= \frac{G^{in}}{V^{tr}} \left(\frac{c^{ti}_{\mathrm{CO}_2}}{\alpha^{ti}} - \frac{c^{tr}_{\mathrm{CO}_2}}{\alpha^{tr}} \right) \\ &\quad - \mathbf{u}\left(\Delta pH\right) \frac{G^{sp}}{V^{tr}} \left(\frac{c^{tr}_{\mathrm{CO}_2}}{\alpha^{tr}} - p^{amb}_{\mathrm{CO}_2} \right)\end{aligned} \tag{4.3}$$

$$\frac{dc^{ti}_{\mathrm{H}^+}}{dt} = k_1 c^{ti}_{\mathrm{CO}_2} - k_{-1} c^{ti}_{\mathrm{H}^+} c^{ti}_{\mathrm{HCO}_3^-} + k_2 c^{ti}_{\mathrm{HB}} - k_{-2} c^{ti}_{\mathrm{H}^+} c^{ti}_{\mathrm{B}^-} \tag{4.4}$$

$$\frac{dc^{ti}_{\mathrm{HCO}_3^-}}{dt} = k_1 c^{ti}_{\mathrm{CO}_2} - k_{-1} c^{ti}_{\mathrm{H}^+} c^{ti}_{\mathrm{HCO}_3^-} \tag{4.5}$$

$$\frac{dc^{ti}_{\mathrm{B}^-}}{dt} = k_2 c^{ti}_{\mathrm{HB}} - k_{-2} c^{ti}_{\mathrm{H}^+} c^{ti}_{\mathrm{B}^-} \tag{4.6}$$

$$\frac{dc^{ti}_{\mathrm{HB}}}{dt} = k_{-2} c^{ti}_{\mathrm{H}^+} c^{ti}_{\mathrm{B}^-} - k_2 c^{ti}_{\mathrm{HB}} \tag{4.7}$$

with

$$\mathbf{u}(x) = \frac{1}{1 + e^{\sigma x}}$$

$$\Delta pH = -lg \left(\frac{c^{ti}_{\mathrm{H}^+}}{c^{*}_{\mathrm{H}^+}} \right)$$

A normalization can be applied (Buckingham, 1914), which results in a fully dimensionless system. As the variables and parameters span 4 base dimensions (length [L], mass [M], time [T], and amount of substance [N]) at most 4 parameters (the basis) can be eliminated through renormalization. Since any uncertainty in their values possibly influences a large number of the remaining variables and parameters a good choice are parameters that are accurately known or easily measurable. However, not all combinations of 4 parameters can serve as a basis. Furthermore if easily measured parameters are chosen for the basis, qualitative predictions from the model will be harder to test.

The used normalization transformations are given in table 4.2. After renormalization the system becomes

$$\frac{d\mathcal{C}}{d\tau} = \dot{\mathcal{C}} = \frac{\mu}{\upsilon} - \mathcal{C} + \kappa_1 \mathcal{H}\mathcal{A} - \frac{\gamma^{in}}{\upsilon}\left(\frac{\mathcal{C}}{\alpha} - \mathcal{T}\right) \tag{4.8}$$

$$\frac{d\mathcal{T}}{d\tau} = \dot{\mathcal{T}} = \gamma^{in}\left(\frac{\mathcal{C}}{\alpha} - \mathcal{T}\right) - \mathbf{u}\left(\mathcal{H} - 1\right)\gamma^{sp}\left(\mathcal{T} - \pi\right) \tag{4.9}$$

$$\frac{d\mathcal{H}}{d\tau} = \dot{\mathcal{H}} = \mathcal{C} - \kappa_1 \mathcal{H}\mathcal{A} + \rho\mathcal{S} - \rho\kappa_2 \mathcal{H}\mathcal{B} \tag{4.10}$$

$$\frac{d\mathcal{A}}{d\tau} = \dot{\mathcal{A}} = \mathcal{C} - \kappa_1 \mathcal{H}\mathcal{A} \tag{4.11}$$

$$\frac{d\mathcal{B}}{d\tau} = \dot{\mathcal{B}} = \rho\mathcal{S} - \rho\kappa_2 \mathcal{H}\mathcal{B} \tag{4.12}$$

$$\frac{d\mathcal{S}}{d\tau} = \dot{\mathcal{S}} = -\rho\mathcal{S} + \rho\kappa_2 \mathcal{H}\mathcal{B} \tag{4.13}$$

The differential equations are not independent. Two invariants hold which become apparent if one compares the equations for the chemical reaction systems. They result from conservation of mass ultimately. The invariants are

$$\begin{aligned} &\dot{\mathcal{B}} + \dot{\mathcal{S}} = 0 \\ &\mathcal{B} + \mathcal{S} = \mathcal{B}(0) + \mathcal{S}(0) = \beta_1 \end{aligned} \tag{4.14}$$

and

$$\begin{aligned} &\dot{\mathcal{H}} - \dot{\mathcal{A}} - \dot{\mathcal{B}} = 0 \\ &\mathcal{H} - \mathcal{A} - \mathcal{B} = \mathcal{H}(0) - \mathcal{A}(0) - \mathcal{B}(0) = \beta_2 \end{aligned} \tag{4.15}$$

respectively. If the initial conditions are treated as additional parameters, two new parameters (β_1, β_2) might be introduced, where β_1 signifies the total amount of nonbicarbonate buffer available and β_2 specifies the initial proton 'excess'. As $\mathcal{H}(0) \ll \mathcal{B}(0), \mathcal{A}(0)$; $\beta_2 \simeq (\mathcal{A}(0) + \mathcal{B}(0))$ and it could also be interpreted as a total buffer value. Using eqs. 4.14 and 4.15 two of the variables ($\mathcal{B}$ and $\mathcal{S}$) can be substituted and the final, independent differential equation system becomes

$$\dot{\mathcal{C}} = \frac{\mu}{\upsilon} - \mathcal{C} + \kappa_1 \mathcal{H}\mathcal{A} - \frac{\gamma^{in}}{\upsilon}\left(\frac{\mathcal{C}}{\alpha} - \mathcal{T}\right) \tag{4.16}$$

$$\dot{\mathcal{T}} = \gamma^{in}\left(\frac{\mathcal{C}}{\alpha} - \mathcal{T}\right) - \mathbf{u}\left(\mathcal{H}\right)\gamma^{sp}\left(\mathcal{T} - \pi\right) \tag{4.17}$$

$$\dot{\mathcal{H}} = \mathcal{C} - \kappa_1 \mathcal{H}\mathcal{A} + \rho\left(\beta_1 + \beta_2 + \mathcal{A} - \mathcal{H}\right) + \rho\kappa_2 \mathcal{H}\left(\beta_2 + \mathcal{A} - \mathcal{H}\right) \tag{4.18}$$

$$\dot{\mathcal{A}} = \mathcal{C} - \kappa_1 \mathcal{H}\mathcal{A} \tag{4.19}$$

$$\mathbf{u}(\mathcal{H}) = \frac{\mathcal{H}^{\sigma}}{1 + \mathcal{H}^{\sigma}} \tag{4.20}$$

Variable or Parameter	**Symbol**	**Dimension**
tracheal CO_2 concentration	$c^{tr}_{CO_2}$	$[N][L]^{-3}$
hemolymph CO_2 concentration	$c^{ti}_{CO_2}$	$[N][L]^{-3}$
hemolymph proton concentration	$c^{ti}_{H^+}$	$[N][L]^{-3}$
hemolymph bicarbonate concentration	$c^{ti}_{HCO_3^-}$	$[N][L]^{-3}$
hemolymph nonbicarbonate buffer concentration (deprotonized)	$c^{ti}_{B^-}$	$[N][L]^{-3}$
hemolymph nonbicarbonate buffer concentration (protonized)	c^{ti}_{HB}	$[N][L]^{-3}$
threshold proton concentration	$c^{*}_{H^+}$	$[N][L]^{-3}$
reaction rate constants		
hydration of CO_2	k_1	$[T]^{-1}$
dehydration of CO_2	k_{-1}	$[L]^3[N]^{-1}[T]^{-1}$
nonbicarbonate buffer protonation	k_{-2}	$[L]^3[N]^{-1}[T]^{-1}$
nonbicarbonate buffer deprotonation	k_2	$[T]^{-1}$
tracheal volume	V^{tr}	$[L]^3$
hemolymph volume	V^{ti}	$[L]^3$
physical CO_2 solubility in tracheal system	α^{tr}	$[N][T]^2[M]^{-1}[L]^{-3}$
physical CO_2 solubility in hemolymph	α^{tr}	$[N][T]^2[M]^{-1}[L]^{-3}$
ambient CO_2 partial pressure	$p^{amb}_{CO_2}$	$[M][L]^{-1}[T]^{-2}$
spiracular diffusive CO_2 conductance	G^{sp}	$[N][L][T][M]^{-1}$
internal diffusive CO_2 conductance	G^{in}	$[N][L][T][M]^{-1}$
metabolic rate	MR	$[N][T]^{-1}$
shape parameter of sigmoid response function	σ	1
time	t	$[T]$

Table 4.1.: Symbols used in the untransformed raw model equations. All variables can be described by the four physical dimensions time [T], length [L], mass [M] and amount of substance [N].

$$
\begin{aligned}
c^{tr}_{\mathrm{CO_2}} &= \mathcal{T} \cdot c^{*}_{\mathrm{H^+}} & k_{-1} &= \kappa_1 \cdot \frac{k_1}{c^{*}_{\mathrm{H^+}}} & p^{amb}_{\mathrm{CO_2}} &= \pi \cdot \frac{c^{*}_{\mathrm{H^+}}}{\alpha^{tr}} \\
c^{ti}_{\mathrm{CO_2}} &= \mathcal{C} \cdot c^{*}_{\mathrm{H^+}} & k_{-2} &= \kappa_2 \cdot \frac{\rho k_1}{c^{*}_{\mathrm{H^+}}} & t &= \tau \cdot \frac{1}{k_1} \\
c^{ti}_{\mathrm{H^+}} &= \mathcal{H} \cdot c^{*}_{\mathrm{H^+}} & k_2 &= \rho \cdot k_1 & G^{sp} &= \gamma^{sp} \cdot \alpha^{tr} V^{tr} k_1 \\
c^{ti}_{\mathrm{HCO_3^-}} &= \mathcal{A} \cdot c^{*}_{\mathrm{H^+}} & V^{ti} &= \upsilon \cdot V^{tr} & G^{in} &= \gamma^{in} \cdot \alpha^{tr} V^{tr} k_1 \\
c^{ti}_{\mathrm{B^-}} &= \mathcal{B} \cdot c^{*}_{\mathrm{H^+}} & \alpha^{ti} &= \alpha \cdot \alpha^{tr} & MR &= \mu \cdot c^{*}_{\mathrm{H^+}} V^{tr} k_1 \\
c^{ti}_{\mathrm{HB}} &= \mathcal{S} \cdot c^{*}_{\mathrm{H^+}}
\end{aligned}
$$

Table 4.2.: Variable substitutions used to reformulate the problem. Righthand side variables left of the · are new, dimensionless quantities that will normalize the equation system.

Normalized Variable or Parameter	**Symbol**
tracheal CO_2 concentration	$\mathcal{T}$
hemolymph CO_2 concentration	$\mathcal{C}$
hemolymph proton concentration	$\mathcal{H}$
hemolymph bicarbonate concentration	$\mathcal{A}$
time	τ
reaction rate constants	
dehydration of CO_2	κ_1
nonbicarbonate buffer protonation	κ_2
relative reaction rate of nonbicarbonate buffer deprotonation	ρ
ratio of compartment volumes	υ
ratio of CO_2 solubilities	α
ambient CO_2 partial pressure	π
spiracular diffusive CO_2 conductance	γ^{sp}
internal diffusive CO_2 conductance	γ^{in}
metabolic rate	μ
shape parameter of sigmoid response function	σ
invariance parameters	
total amount of nonbicarbonate buffer	β_1
initial proton excess ($\approx$ total amount of buffer)	β_2

Table 4.3.: Symbols used in the final, normalized model equations. The normalized variables are derived using the transformations given in table 4.2 and are all without units.

4.3. Model implementation

The model has been implemented numerically in Matlab (The MathWorks, Inc., Natick, MA, USA). Symbolic derivatives of the system, calculated in Maple (MapleSoft, Waterloo, Canada) were provided to the integrator to increase accuracy and computation speed. The continuation software cl_matcont (`http://sourceforge.net/projects/matcont/`) has been used for the bifurcation analysis of the system.

Numeric solution of the system has shown that the used control function $\mathbf{u}(\mathcal{H})$ (eq. 4.20) was infeasible for large values of σ. Even minimal deviations from the threshold concentration $\mathcal{H} = 1$ resulted in values for denominator and numerator beyond the capabilities of Matlabs internal arithmetic. This led to continued failure of the solver.

Eq. 4.20 has thus been replaced by a similarly shaped function

$$\mathbf{u}(\mathcal{H}) = \frac{1}{2} + \frac{1}{2}\tanh(\sigma \log(\mathcal{H})) \tag{4.21}$$

which proved tractable even for large shape parameters σ. Exact values for an equal dynamic range of both functions differ. However as σ is a purely technical parameter without direct biological meaning this is a neglegible issue.

4.4. Physiological parameter values

Most of the parameters in the original model are temperature dependent. As the model itself is specified isothermally a reference temperature had to be defined. 10 °C was chosen as this was the temperature of the perfusion experiment. Literature values were corrected to this temperature first if needed.

Literature values were also often normalized to body mass. If needed, 5 g was assumed as the body mass of the model animal (the mean mass of *Attacus* pupae from the perfusion experiment was 4.7 g, see chapter 2).

Threshold pH Due to extensive buffering it is assumed that the variation in hemolymph pH caused by the DGC is relatively small and that snapshot measurements of hemolymph pH provide a rough estimate of the threshold pH. A complication lies in the fact that intracellular acid-base status might differ significantly from extracelullar, i.e. hemolymph status (Harrison, 2001).

Bridges and Scheid (1982) found a mean pH of 6.57 with cycle variability of 0.04 units in whole animal homogenates of *Hyalophora cecropia*. A pH of 6.45 was observed in the hemolymph of *Agapema galbina* and *Hyalophora cecropia* pupae (Buck and Friedman, 1958). The pH of diapausing*Attacus* pupae was 6.43 (Kießling, 1997).

In normoxia the hemolymph pH of resting grasshoppers (*Schistocerca americana*) is 7.05 with alkalinization to pH 7.36 in theoretical anoxia (Greenlee and Harrison, 1998).

Harrison (1988) while investigating the temperature effects on hemolyph acid-base status found a pH of about 7.1 below 20 °C which decreased to about pH 6.9 at 40 °C. Badre et al. (2005) used a physiological saline with pH 7.2 which they state is superior for electrophysiological recordings in *Drosophila*.

Very few measurements of hemolymph pH during DGC exist. A recent study demonstrated a pH of 7.0 in rhinoceros beetles (Matthews and White, 2009). During DGC this value varied by 0.1 units. Using custom made pH-electrode Hetz and Wasserthal (1993) estimated a hemolymph pH of 6.7-6.8 in *Troides rhadamantus*. The variations within a single cycle were about 0.05 units. Harrison et al. (1995) found a change from pH 7.25 to 7.3 during the open phase in discontinuosly ventilating *Taenipoda eques* grasshoppers, which seems comparable. Even smaller changes were found in *Zophobas rugipes* pupae, where pH was between 6.9 and 7.1 with cycle variations of 0.006 to 0.017 units (Kaiser, 2002).

Overall, hemolymph pH seems to fall in the range of 6.5 to 7.5 in insects with the saturniid pupae tending to more acidic values. So, pH 6.7 has been chosen as a default.

Compartment volumes Literature values for tracheal volume are often given as percent body volume (V_r) for a given body mass. Neglecting the cuticle volume the sought ratio of compartment volumes υ can be derived directly using the correction

$$\upsilon = \frac{1 - V_r}{V_r} \tag{4.22}$$

This avoids the need of explicit tissue volumes and the assumption of specific, unknown tissue and hemolymph densities.

Relative tracheal volume in *Schistocerca americana* was between 7 % (gravid females) and 40 % (males) (Lease et al., 2006). During development of *Locusta migratoria* tracheal volume starts at 42 % and reduces to 3.8 % due to organogenesis (Clarke, 1957).

The tracheal volume of *Hyalophora cecropia* pupae has been calculated to be between 5 - 10 % from the data of Bridges et al. (1980).

The smallest relative tracheal volumes have been reported for stick insects (1.3 % Schmitz and Perry, 1999) and some beetles (Kaiser et al., 2007, *Tribolium castaneum* 0.5 %; *Eleodes obscura* 4.8 %).

So the tracheal volume seems to lie generally between 0.5 and 50 % of the body volume. For the ratio of compartment volumes this results in an observed range of $\upsilon = 1 - 199$.

However, as V^{tr} is one of the basis variables an explicit value for it is needed. Bridges et al. (1980) also provide an empirical formula for tracheal volume as function of body mass in *Hyalophora*. This has been used under the assumption of 5 g body mass. Unfortunately, no equation for the relative tracheal volume was given. For the default υ tissue volume therefore was calculated from the 5 g body mass assuming a mean density of $1\,\mathrm{g\,ml^{-1}}$.

CO_2 Solubility The gas phase CO_2 solubility α^{tr} can be calculated from the ideal gas law

$$pV = nRT \tag{4.23}$$

$$\frac{1}{RT} = \frac{n}{pV} = \alpha \tag{4.24}$$

An approximate relative tissue solubility α is directly provided by the sorption coefficient of water (Knoche, 1980). No explicit value of α^{ti} is needed.

Diffusive conductances Only a few estimates of tracheal diffusive conductance exist. Janda and Kocian (1933) have successively blocked spiracles in *Tenebrio molitor* pupae and found that even at higher temperatures (19, 23 and 33 °C) the development and oxygen consumption remained virtually unaffected even if all except one pair of spiracles were blocked. This indicates that spiracular conductance can be very high compared to metabolic rate and might not be a limiting factor in gas exchange.

Similar experiments were done by Hetz (2007) who estimated a spiracular conductance of larvae of *Samia cynthia* of 200 - 360 $\mathrm{nmol\,g^{-1}\,min^{-1}\,kPa^{-1}}$. Greenlee and Harrison (2005) likewise state a stage dependent overall maximum conductance between 80 - 250 $\mathrm{nmol\,g^{-1}\,min^{-1}\,kPa^{-1}}$ in caterpillars of the tobacco hawkmoth *Manduca sexta*.

Wobschall and Hetz (2004) state a single spiracle conductance of 70 $\mathrm{nmol\,min^{-1}\,kPa^{-1}}$ in diapausing *Attacus* pupae. Taking all 18 spiracles together, this would amount to 1260 $\mathrm{nmol\,min^{-1}\,kPa^{-1}}$ total spiracle conductance, in line with the pupal data. Standard spiracular conductance has thus been assumed to be $G^{sp} = 250\,\mathrm{nmol\,g^{-1}\,min^{-1}\,kPa^{-1}}$.

If information about spiracular conductance is scarce, information about the internal conductance of the tracheal walls can be considered completely lacking. The only reference is a morphometric analysis of larval stick insects *Carausius morosus* done by Schmitz and Perry (1999). It estimated diffusive capacity of different orders of tracheal branches by taking into account wall thickness and Krogh's diffusion coefficients for chitin and the hypodermis layer of the tracheal wall. Conversion into diffusive conductance yields G^{in}=51.3 $\mathrm{nmol\,g^{-1}\,min^{-1}\,kPa^{-1}}$ which would be about one fourth of the above spiracular conductance. However, as indicated by the small spiracles of stick insects, given the non-flying, relaxed life style of these species the diffusive conductances need not necessarily be high.

An empirical equation for the body mass dependent total conductance of the tracheal system in grass hoppers has been given in Greenlee et al. (2007). According to it, a 5 g animal had a mass specific total conductance of G_{tot}=119 $\mathrm{nmol\,g^{-1}\,min^{-1}\,kPa^{-1}}$. If it is assumed that that mass specific spiracle conductance is as above and that spiracle conductance and the internal conductance are serially connected then the internal conductance can be calculated from

$$\frac{1}{G_{tot}} = \frac{1}{G_{in}} + \frac{1}{G_{sp}} \tag{4.25}$$

The resulting value of $G_{in} = 227\,\mathrm{nmol\,g^{-1}\,min^{-1}\,kPa^{-1}}$ were comparable to spiracle conductance (G_{sp}=250 $\mathrm{nmol\,g^{-1}\,min^{-1}\,kPa^{-1}}$).

A tracheolar conductace of about $300\,\mathrm{nmol\,min^{-1}\,kPa^{-1}}$ is stated by Greenlee and Harrison (1998) in normoxia. Unfortunately, no body masses are given to transform this into a mass specific value.

Given the great uncertainty, the internal conductance has been assumed, somewhat arbitrarily, to be the same as spiracular conductance.

Reaction rate constants Recently a full evaluation of all rate constants of the CO_2 hydration reaction system has appeared (Wang et al., 2009). Activation energies and preexponential factors for the pseudo first order approximation have been computed from Arrhenius plots of the data. This allowed to calculate the reaction rate constants for arbitrary temperatures and specifically for 10 °C $k_1 = 0.0071 s^{-1}$ and $k_{-1} = 22833.7 M^{-1} s^{-1}$.

These numbers are in good agreement to Gibbons and Edsall (1963), who state $k_1 = 0.0375 s^{-1}$ and $k_{-1} = 55000 M^{-1} s^{-1}$ at 25 °C.

The reaction rate ratio between the hydration reaction and the deprotonation reaction of the nonbicarbonate buffer has been assumed to be ρ=1000 based on a remark in Gibbons and Edsall (1963).

Buffer concentrations The main buffers in insect hemolymph are proteins and bicarbonate, followed by organic phosphate and organic acids. The abundance of free amino acids in the hemolymph is insignificant for buffering in the physiological range of hemolymph pH (Harrison, 2001).

Mean bicarbonate buffer value in locusts was 23 mM/pH corresponding to a bicarbonate concentration of 10 mM (Harrison, 2001; Heisler, 1986).

Most of the buffering of the hemolymph is attributed to proteins (Harrison, 2001; Harrison et al., 1990). Additionally, concentrations of organic acids like succinate or citrate and the concentration of organic phosphate can also be high and may each exceed 30 mM. They are thought to significantly contribute to the buffer value (Harrison, 2001; Wyatt, 1961).

However, buffers are most effective if their pK is close to the buffered pH. Most pK values for organic acids lie between 4.0 and 5.5 (citrate 5.41, lactate 3.86, succinate 5.48; Williams, pKa compilation), which is more than 1 pH unit below the assumed hemolymph pH of 6.7. Better candidates are organic phosphates with pK about 6.3-6.6 and inorganic phosphate with a pK of 6.82.

The only amino acid that might significantly contribute to the buffering in the physiological range of hemolymph pH is histidine with an imidazole side chain (pK 6.1; Wyatt, 1961).

pK values of protein side chains are highly variable and dependent on the structure of the protein (e.g. Edgcomb and Murphy, 2002). Thus no general average protein pK can be inferred with some degree of confidence without knowing the relative contribution and the amino acid sequence of all the hemolymph proteins.

It has thus been decided that the unknown general buffer has the average pK of organic phosphates (6.5) and its concentration is 30 mM.

Using the pK value instead of the raw reaction rate constants k_2, k_{-2} the model parameter κ_2 can be calculated directly as

$$\kappa_2 = \frac{c^*_{H^+}}{10^{pK_2}} \tag{4.26}$$

Metabolic rate From all parameters of the model, metabolic rate is probably the most variable when observed over the whole group of insects. Because the main interest is in the DGC of diapausing lepidopteran pupae, the search for parameter values has been restricted to this group.

For *Samia cynthia* pre-pupae, the mean CO_2 release was $7.9\,\mathrm{nmol\,g^{-1}\,min^{-1}}$ with a minimum value of $5.2\,\mathrm{nmol\,g^{-1}\,min^{-1}}$ (Hetz, 2007). Diapausing pupae had a slightly higher rate of $10.35\,\mathrm{nmol\,g^{-1}\,min^{-1}}$.

Wobschall and Hetz (2004) give a mean of $60\,\mathrm{nmol\,min^{-1}}$ with with body mass about 8 g, resulting in $7.5\,\mathrm{nmol\,g^{-1}\,min^{-1}}$ for *Attacus* pupae.

Thus $10\,\mathrm{nmol\,g^{-1}\,min^{-1}}$ has been fixed as a default. At 5 g body mass total metabolic rate is then $50\,\mathrm{nmol\,min^{-1}}$.

Ambient CO_2 concentration Using the standard figure of $p_{CO_2} = 0.033$ kPa (Möller, 1991), the normalized ambient concentration of CO_2 can be calculated in a straightforward manner.

Shape parameter σ Since the spiracle control is basically all or nothing σ has been assumed to be very high ($\sigma = 10000$). This approximates a step response of the spiracle aperture to hemolymph pH.

Parameter	Symbol	Default Value
reaction rate of CO_2 hydration	k_1	$0.0071\,\mathrm{s}^{-1}$
threshold proton concentration	$c^*_{H^+}$	$199.35\,\mathrm{nM}$
tracheal volume	V^{tr}	$241\,\mu\mathrm{l}$
tracheal CO_2 capacitance	α^{tr}	$0.424\,77\,\mathrm{mM\,kPa}^{-1}$

Table 4.4.: Parameter values used to normalize the model equations according to the substitutions given in table 4.2. See text for sources.

Parameter	Symbol	Default Value
metabolic rate	μ	2434
spiracle conductance	γ^{sp}	28.5812
internal conductance	γ^{in}	28.5812
reaction rate (CO_2 dehydration)	κ_1	0.6399
reaction rate (NB buffer deprotonation)	κ_2	0.6310
amount of NB buffer	β_1	150356
total amount of buffer	β_2	-142307
CO_2 solubility ratio	α	1.247
volume ratio	υ	20.747
ambient CO_2 partial pressure	π	71.1875
relative reaction rates	ρ	1000
sigmoid shape parameter	σ	10000

Table 4.5.: Standard values for the parameters of the normalized CO_2 model. Values have been calculated from literature values and the normalization parameters (table 4.4) using the transformations given in table 4.2 which render them unitless. See text for details and sources.

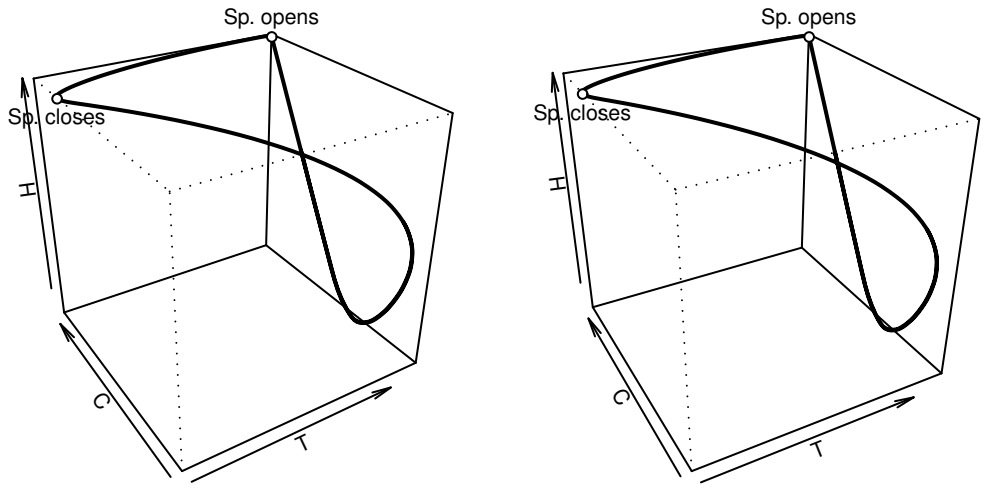

Figure 4.5.: Stereoscopic 3-d phase portrait of the steady state solution for the default parameter set. The axes show tracheal CO_2 ($\mathcal{T}$), hemolymph CO_2 ($\mathcal{C}$) and hemolymph proton concentration ($\mathcal{H}$) respectively. The solution is cyclic and rotates counterclockwise when looked from the top. Note that the cycle speed along the curve is not uniform.

4.5. Results

4.5.1. Time series solution

Fig. 4.6 shows the steady state solution for the default parameter set (see table 4.5). The solution is periodic with a period length $\Delta\tau$ about 5. This corresponds to a cycle length of about 12 min in real time. $\mathcal{A}$ and $\mathcal{H}$ show a sawtooth-like temporal pattern. Upon reaching the trigger concentration $\mathcal{H}$ =1 the spiracles open shortly, releasing a great amount of CO_2 from the tracheal system. The following reequilibration between hemolymph and tracheal space leads to a relatively large (if compared to the variation of $\mathcal{H}$ during the open phase) downward variation of both $\mathcal{A}$ and $\mathcal{H}$. Once everything is equilibrated again $\mathcal{H}$ and $\mathcal{A}$ both increase linearly until the next burst is triggered.

$\mathcal{T}$ reaches its minimum when the spiracles close. Subsequently, there is rapid reequilibration of endotracheal p_{CO_2}. The requilibration is biphasic. At first the source is physically dissolved CO_2 from the hemolymph, i.e., $\mathcal{C}$ falls sharply but $\mathcal{H}$ is less affected. Then more and more liberation of CO_2 from chemically buffered stores occurs and the reequilibration of the compartments is mostly supported by the dehydration of bicarbonate, which results in alkalinization of the hemolymph.

Fig. 4.5 shows the 3-d phase portrait of the limit cycle. The open phase consists of the small horizontal connection of the two marked points going from open to close. The phase portrait illustrates the comparatively large pH deviation that occurs as a result of the following reequilibration of p_{CO_2} between hemolymph and tracheal system (the

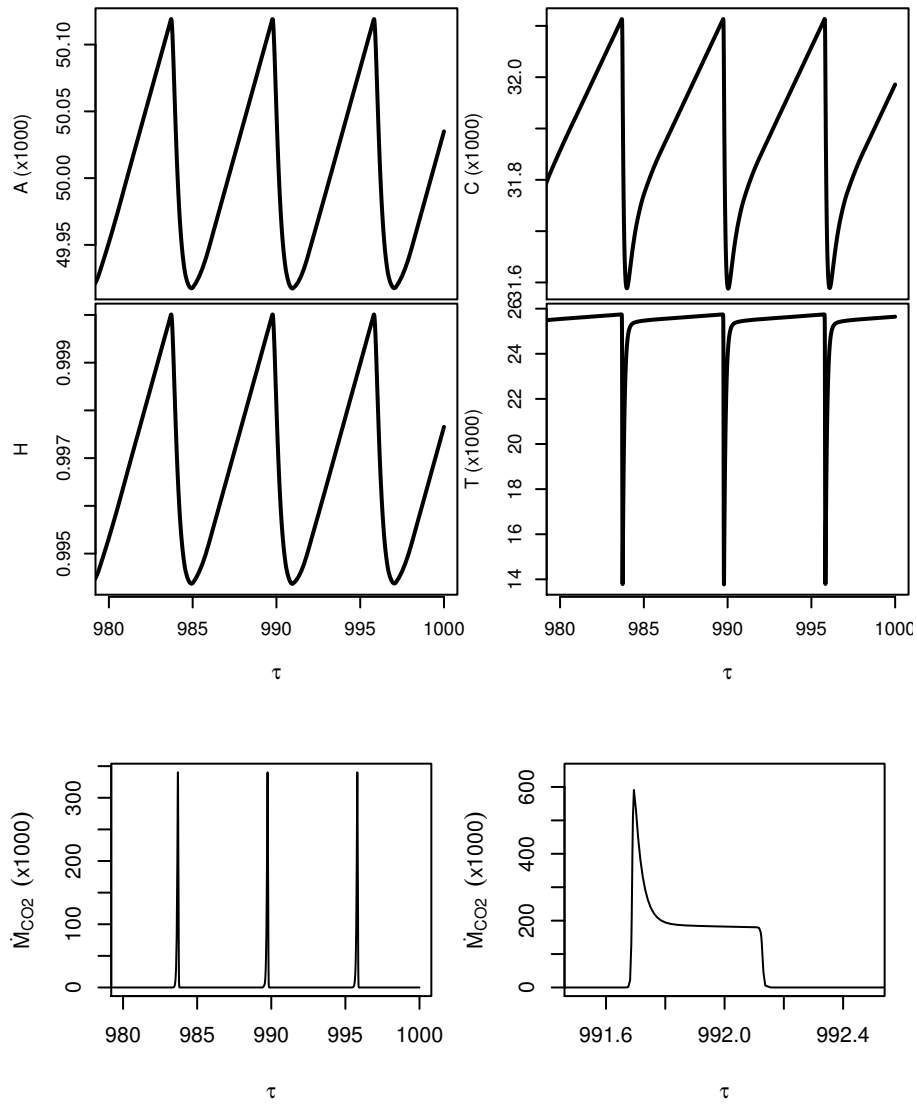

Figure 4.6.: Steady state time series solution for the default parameters. **Above**: time course of the state variables. **Below**: *left* - CO_2 release over time for the default parameters, *right* - burst shape of CO_2 release at higher metabolic rate.

large downward swing of the curve following closure of the spiracle). Also the biphasic nature of requilibration becomes visible. At last the system state increases linearly back to the opening point.

4.5.2. Bifurcation analysis

Codim 1 bifurcation diagrams

In this section selected codim 1 continuations, i.e. ones with a single active parameter are analyzed. The analysis is limited to parameters that are thought to be under the influence of the animal. This excludes mostly parameters like the relative rates of the two reaction systems ρ or their pK values. The latter might be under limited control, e.g. a variation of hemolymph composition will most probably change it. However, it can not be directly mapped to a single parameter of the model.

Active parameter μ (Metabolic Rate) Figure 4.7 shows the equilibrium continuation for the whole model state with μ as the active parameter. For very high metabolic rates a stable equilibrium exists, which lies near the equilibrium for fully open spiracles. This is not surprising as the spiracle aperture is practically one, indicating fully open spiracles.

With decreasing metabolic rate the equilibrium follows the open spiracle solution until the critical condition $\mathcal{H} = 1$ is met and spiracle regulation sets in. Further decrease of metabolic rate results in a sharp bend away from the open spiracle equilibrium solution. The equilibrium concentrations for all three tissue variables $\mathcal{A}$, $\mathcal{C}$ and $\mathcal{H}$ are then constant over a wide range of metabolic rates. Only the tracheal CO_2 concentration $\mathcal{T}$ rises with falling metabolic rate.

For continuity reasons another bend has to occur for very low metabolic rates, where the solution quickly approaches the trivial solution for μ=0. For these low values metabolic rate is small enough that a partial opening of the spiracle, some leaking, would suffice to rid the tracheal system from the generated CO_2.

Hopf bifurcations occur at H1 ($\mu = 179075.6$) and H2 ($\mu = 1217.37$) for $\sigma = 10000$ (compare Fig. 4.15). Between these two points the equilibrium becomes unstable and stable limit cycles exist. In other words the spiracle behavior has switched from continuously open to discontinuous/cyclic behavior, when passing H1 right to left.

In physical, untransformed coordinates the parameter values of H1 and H2 equal $3665\,\mathrm{nmol\,min^{-1}}$ and $24.9\,\mathrm{nmol\,min^{-1}}$ respectively.

The grey area in figure 4.7 marks the envelope of the limit cycle, i.e. the maxima and minima of the state variables.

It becomes obvious that the amplitude of the $\mathcal{H}$ oscillations is way too small. For a pH change of ± 0.05 units an envelope in the interval between 0.89 to 1.12 would have been expected.

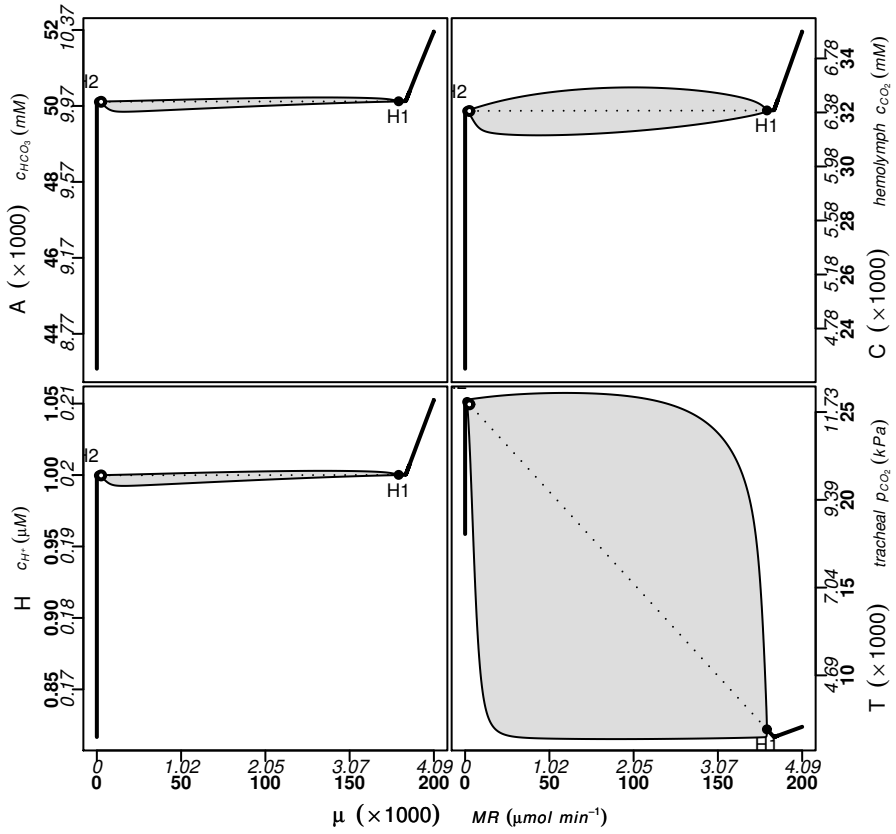

Figure 4.7.: Hopf bifurcations of the equilibrium proton concentration if metabolic rate is varied. Between the two Hopf points the equilibrium is unstable and oscillations occur. The grey area visualizes the envelope of the oscillation amplitudes. All other parameters are at their default values (table 4.5). The white circle marks the solution of the default parameter set.

The amplitudes in the limit cycles of $\mathcal{C}$ and $\mathcal{T}$ are somewhat larger. Hemolymph c_{CO_2} varies nearly symmetrically around its equilibrium concentration. The maximal amplitude is about 2000, corresponding to a Δc_{CO_2}=0.2 mM or Δp_{CO_2}=0.378 kPa.

The oscillatory envelope for $\mathcal{T}$ looks about rectangular. This means, the oscillation amplitude of that variable is nearly independent of metabolic rate. The $\Delta\mathcal{T}$ = 20000 corresponds to Δp_{CO_2}=4.7 kPa.

Figure 4.8 shows the period length of the cycles in the oscillatory region. On average the cycles are between 10 and 15 min long with a strong increase in cycle duration towards the Hopf points. It remains open whether this indicates possible homoclinic bifurcation (Guckenheimer and Holmes, 1983).

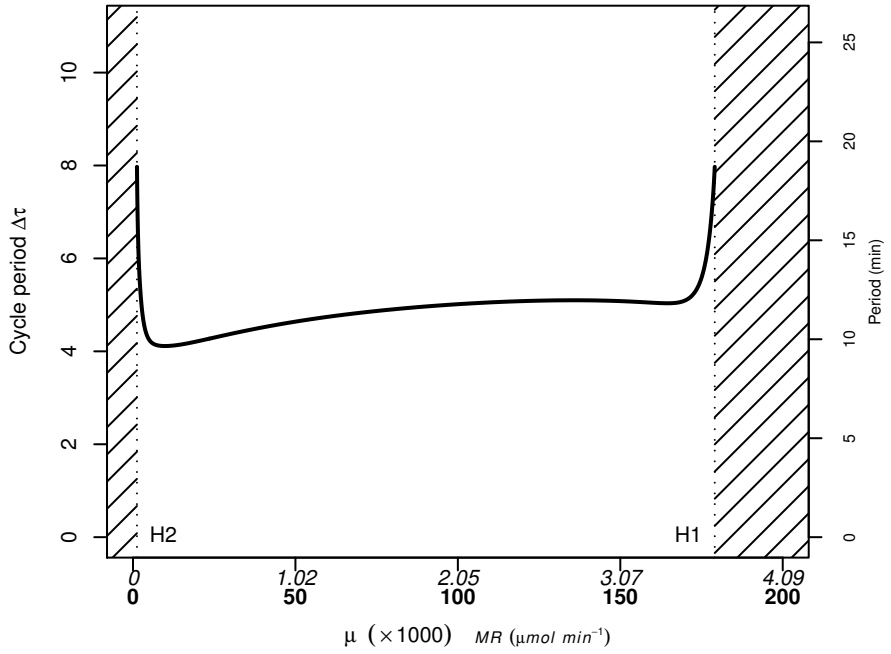

Figure 4.8.: Period length of the cycles when the metabolic rate (μ) is varied.

Active parameter υ (Tracheal Volume) The equilibrium values of all four state variables did not change under variation of υ. This could be proved in Maple (MapleSoft, Waterloo, Canada), where υ simply did not appear in the symbolic solution of the equilibrium equation system.

Active parameter β_1 (Nonbicarbonate Buffering) The codim 1 continuation with the active parameter β_1 analyzes the influence of nonbicarbonate buffering. Similar to metabolic rate 2 Hopf bifurcations occur and there exists an extensive range of buffer concentrations which drive the system into oscillations.

Contrary to metabolic rate, the bicarbonate ($\mathcal{A}$) and tissue CO_2 ($\mathcal{C}$) equilibrium concentrations correlate negatively with β_1 in the oscillatory region. However, note that β_2 (total buffer value) is constant and thus this variation of β_1 corresponds more to an exchange of nonbicarbonate and bicarbonate buffer.

The amplitude of oscillations is negligible for $\mathcal{A}$ and $\mathcal{C}$. pH changes ($\mathcal{H}$) are also small and nearly not affected by the variation of β_1. The largest amplitudes occur again in tracheal CO_2 concentration $\mathcal{T}$, with the maximum only slightly above the equilibrium value. The minimum negatively correlates with β_1.

Period length throughout the oscillatory interval is comparable to that of variations of metabolic rate. For β_1 between 50000 and 200000 the cycle duration is constant (Fig. 4.10). When the buffer concentration approaches the bifurcation values, the period length strongly increases, indicating again possible homoclinic bifurcation.

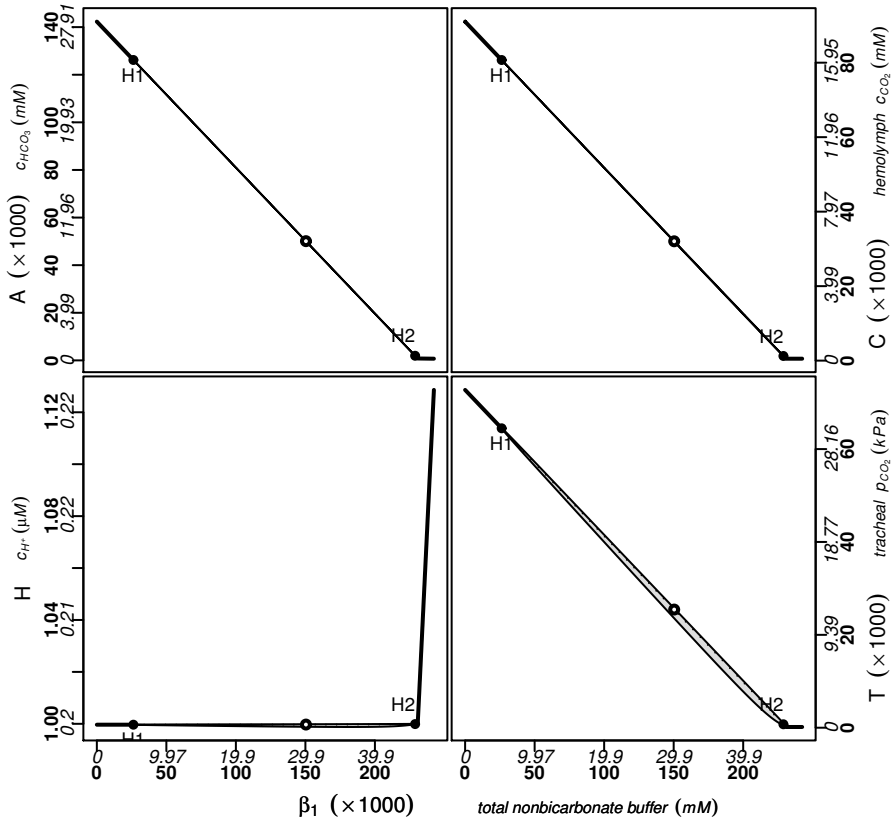

Figure 4.9.: Variation of the total amount of nonbicarbonate buffer β_1. As the total buffer value $beta_2$ is constant this corresponds to an exchange of bicarbonate and nonbicarbonate buffer. All other parameters are at their default value. The white circle marks the solution of the default parameter set (table 4.5). The grey area visualizes the envelope of oscillations.

Active parameter β_2 (Bicarbonate Buffering) Decrease of the proton excess β_2 is equivalent to an increase in the initial bicarbonate concentration as the proton concentration $\mathcal{H}$ is assumed to be approximately 1 and the total amount of nonbicarbonate buffer β_1 has not been changed.

Accordingly, the equilibrium state inversely correlates with β_2 for $\mathcal{A}$, $\mathcal{C}$ and $\mathcal{T}$. $\mathcal{H}$ is regulated close to the threshold value of $\mathcal{H}$ =1. The bifurcation diagrams look very similar to the variation of the β_1 parameter (Fig.4.9).

Two Hopf bifurcations occur for the standard parameter set at $\beta_2 = -93627$ (H1; 18.7 mM) and $\beta_2 = -246304$ (H2; 49.1 mM).

In the oscillatory parameter range the limit cycle amplitudes are negligible for $\mathcal{A}$ and $\mathcal{C}$ when compared to the variation in the equilibrium values. The amplitude for

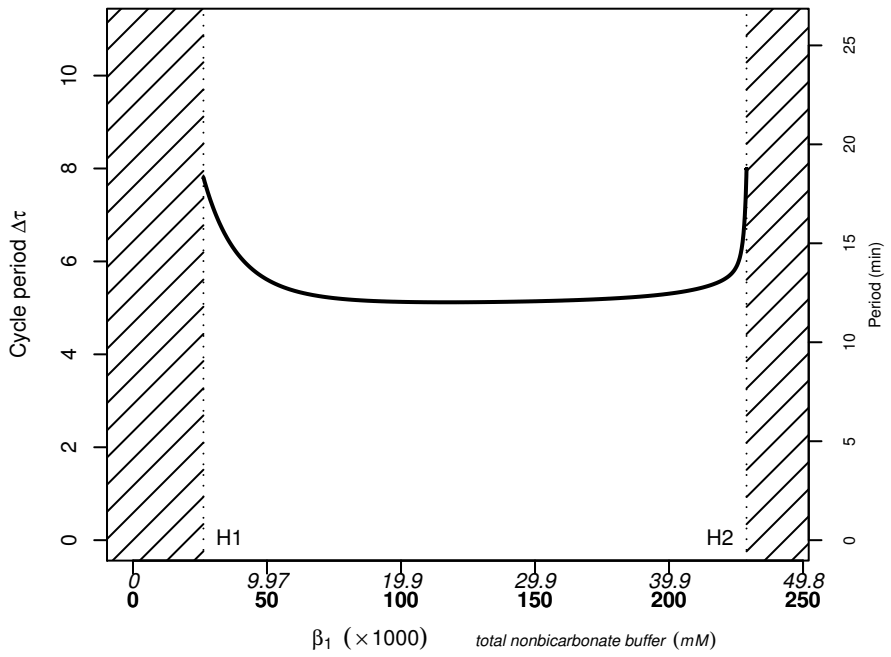

Figure 4.10.: Period length of the limit cycle oscillations when the total amount of nonbicarbonate buffer β_1 is varied. As the total buffer value $beta_2$ is constant this corresponds to an exchange of bicarbonate and nonbicarbonate buffer.

$\mathcal{H}$ is largest for points near H1, that is low total concentration of buffer. The maxima are close to the equilibrium value while the minima show somewhat larger excursions into the alkaline side. The largest amplitude is $\Delta\mathcal{H} = 0.0017$, which corresponds to approximately 0.0001 pH units.

The largest variation during a limit cycle again is observed in the tracheal CO_2 concentration $\mathcal{T}$. The shape of the amplitude envelope varies similar to $\mathcal{H}$ with the largest variation near low buffer values. The maxima of $\mathcal{T}$ stay close to the equilibrium values with excursions to lower values during the cycle.

The period length of the cycles falls with increasing β_2 from 8 (H2; 20 min) to 4.87 (11.4 min). Obviously, contrary to a mere exchange of nonbicarbonate buffer with bicarbonate (as in the previous variation of β_1), the total buffer value influences the period length. Approaching H1 the cycle length increases quickly indicating possible homoclinic bifurcation. However the approach to H2 is steady and there seems to occur a sudden termination of the cycles when passing H2 right to left.

Selected codim 2 bifurcation diagrams

The codim 2 bifurcation diagrams presented in this section take up the found Hopf points from the previous diagrams and continues them under the variation of a second

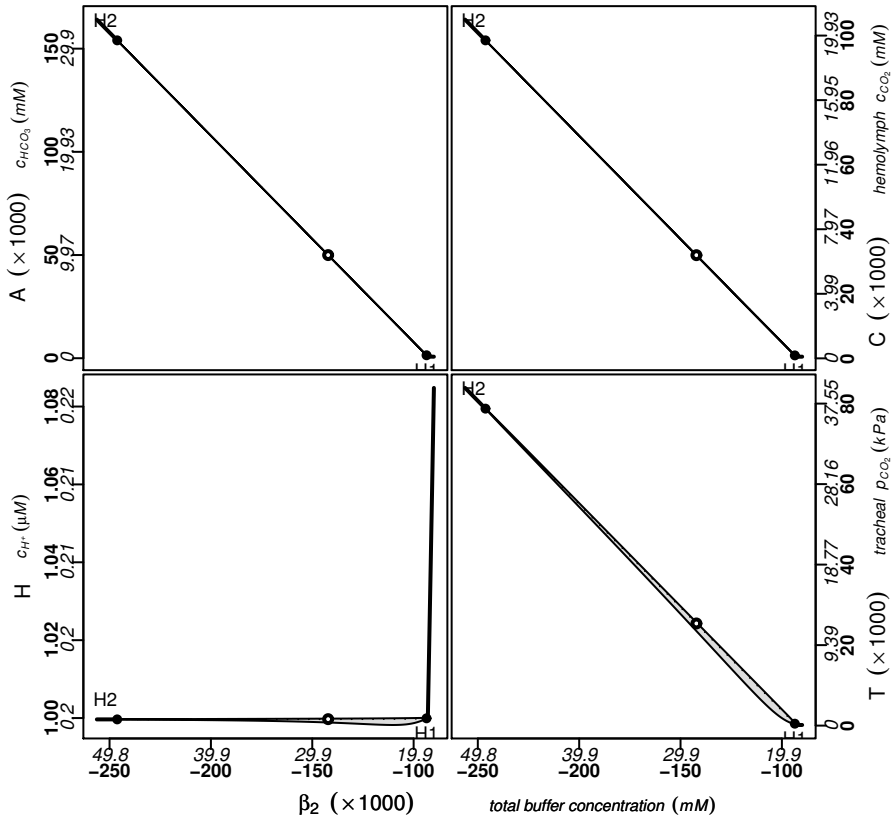

Figure 4.11.: Variation of the total buffer value β_2. As β_1 was not varied and $\mathcal{H}$ is assumed to be close to 1 this corresponds to a variation of the bicarbonate concentration. All other parameters are at their default value. The white circle marks the solution of the default parameter set (table 4.5). The grey area visualizes the envelope of oscillations.

parameter (usually μ has been used as a kind of reference parameter). The lines now no longer stand for the equilibrium values of the model state. Rather they separate the oscillatory region from the non-oscillatory region. As such they are a visualization of the qualitative change of solution behavior under two parameter variation.

A word of caution. When analysing the following codim 2 diagrams care has to be taken in the interpretation of extreme points. The exact numeric values most probably depend on the values of some or all other model parameters. The complete parameter space is 12-dimensional and all reproduced diagrams represent only tiny slices of the complete oscillatory region.

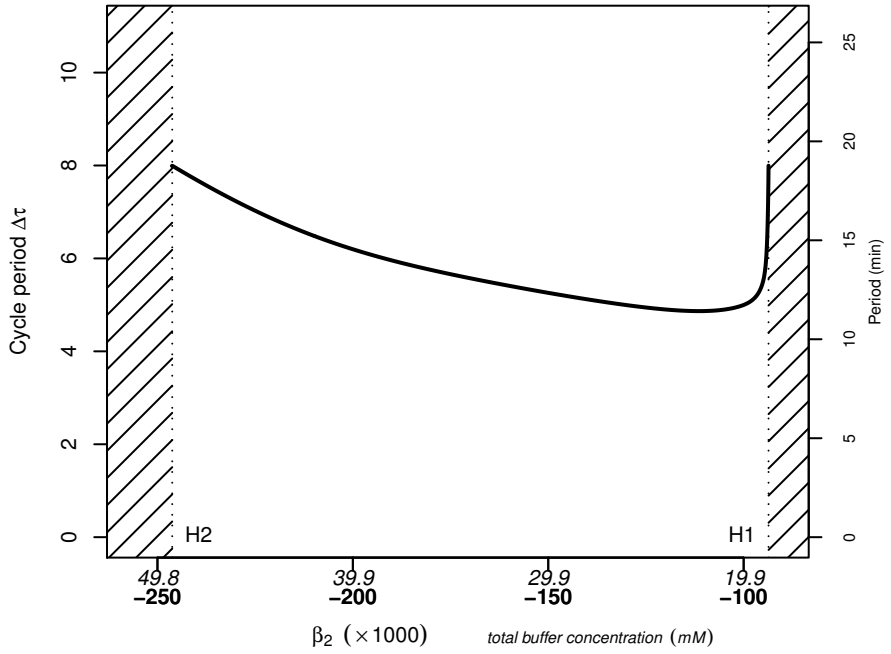

Figure 4.12.: Period length of the limit cycle oscillations when the total buffer value β_2 is varied. Since the concentration of nonbicarbonate buffer β_1 is constant, this corresponds to variation of the bicarbonate concentration.

Metabolic rate *vs.* nonbicarbonate buffering Fig 4.13 shows the codim 2 continuation of the Hopf points of Fig. 4.7 when β_1 is used as a second active parameter. The oscillatory region is a closed triangle with two borders running along the coordinate axes. These borders correspond to the stabilization of low aperture equilibria and might not be relevant biologically (see discussion).

More importantly the maximum metabolic rate that allows oscillatory solutions depends linearly and inversely on nonbicarbonate buffer concentration (β_1). Decreasing the nonbicarbonate buffer concentration destabilizes the equilibrium solution for any given metabolic rate up to a maximum of $\mu = 498895$ ($10.21\,\mu\text{mol}\,\text{min}^{-1}$), above which all solutions are stable equilibria.

Likewise a minimum nonbicarbonate buffer concentration $\beta_1 = 228926$ (45.6 mM) exists that results in continuous gas exchange irrespective of metabolic rate.

Metabolic rate *vs.* tracheal volume Even though the ratio of the compartment volumes υ had no effect on the equilibrium state, it exerts influence on the oscillatory region in the parameter space (Fig. 4.14) if all other parameters are held at their default values. Above υ about 10 (corresponding to a tracheal volume less than 9 % body volume), the range of metabolic rates μ where oscillations occur begins to shrink. Above $\upsilon = 594.1$ (<0.17 % tracheal volume) oscillations cease altogether and the gas exchange behavior

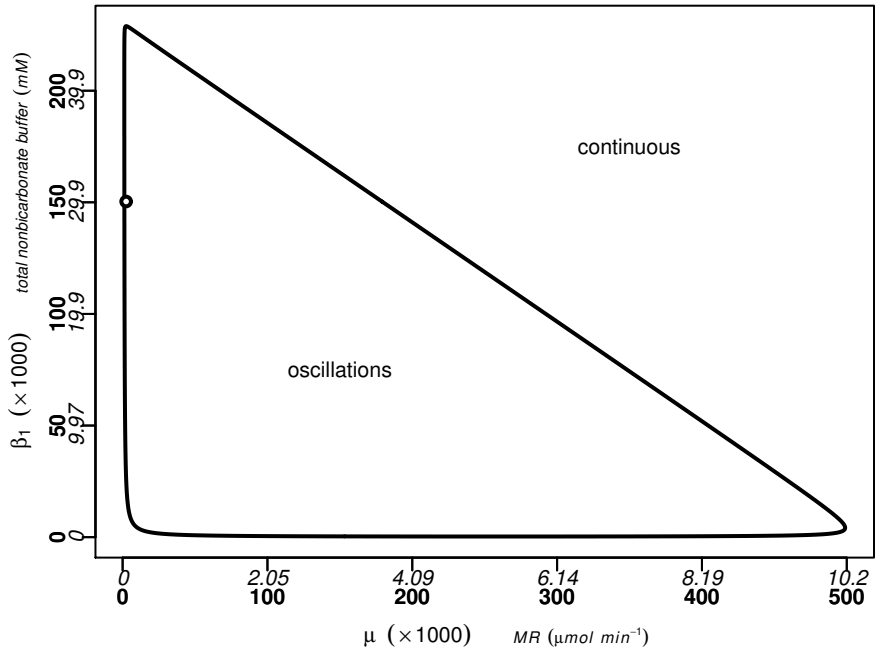

Figure 4.13.: Effect of nonbicarbonate buffering. Decreasing the nonbicarbonate buffer concentration β_1 increases the range of metabolic rates μ that result in oscillatory solutions. As the total buffer value $beta_2$ is held constant variation of β_1 corresponds to an exchange of bicarbonate and nonbicarbonate buffer. All other parameters at their default values.

will be continuous for all metabolic rates.

In the other direction, the oscillatory region is influenced for $\upsilon < 0.03$ (97.1 % tracheal volume), with no oscillations below $\upsilon = 0.0057$ (>99.4 % tracheal volume).

Shape parameter σ Fig. 4.15 shows the codim 2 bifurcation diagram for the active parameters μ and σ. Again μ has been taken as an indicator of how easily cycles do occur, i.e. if there is a large range of metabolic rates that result in oscilllations. It becomes obvious that decreasing the shape parameter σ, that is making the spiracle feedback function less switch-like, shrinks the range of oscillatory metabolic rates. Below $\sigma = 376.5$ no cycles can be observed and the equilibrium will be always stable.

Increasing σ increases the oscillatory interval. In the limit $\sigma \to \infty$ the aperture function becomes a Heaviside (Step) function and the oscillatory metabolic rates completely fill the interval from zero to the maximum metabolic rate which just allows a threshold equilibrium of $\mathcal{H}$ with fully open spiracles. By definition (i.e. $\mathbf{u}_{open}(\mathcal{H}) := 1$) this maximum metabolic rate is independent of σ.

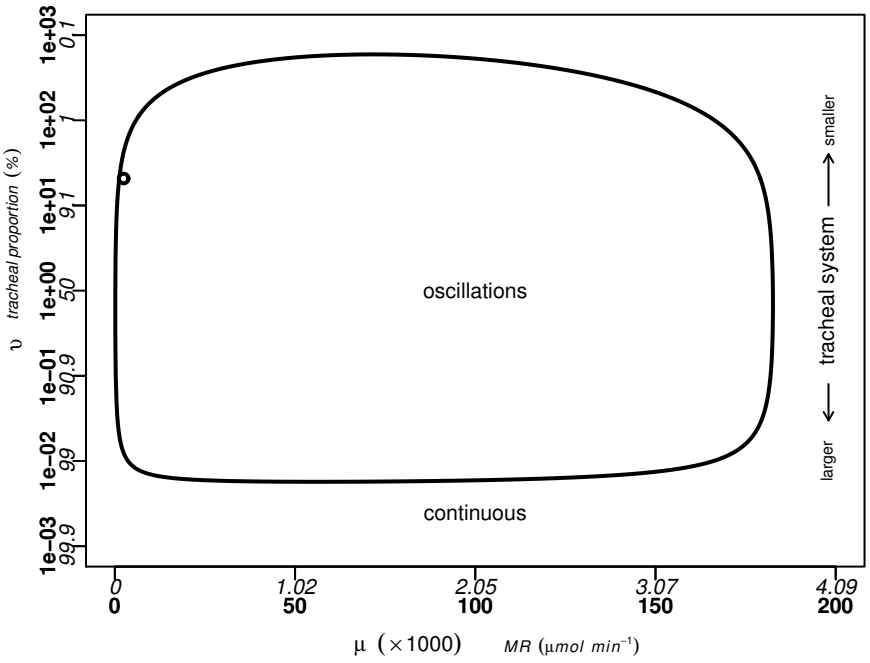

Figure 4.14.: Effect of the relative compartment size υ. The oscillatory range of metabolic rates is largest for about equal-sized compartments. Note the logarithmic ordinate.

Spiracle conductance *vs.* metabolic rate Higher spiracular conductance allows oscillatory behavior for higher metabolic rates (Fig. 4.16). The relationship is not linear and the conductance needs to increase faster than metabolic rate.

A small nonoscillatory region exists for very small metabolic rates. Hoever increasing γ_{sp} has nearly no effect in this part of the parameter space. The Hopf line is related to the low aperture solutions of Fig. 4.7 and thus shares all its problems (see discussion).

However, if one assumes that the total spiracle conductance distributes equally across 18 spiracles (Hetz, 2007), the diagram also reveals the effect of spiracle blocking. For the small metabolic rate in the default parameter set successive spiracle blocking (= going from the circle downward) has no effect onto the general patten of gas exchange. The oscillatory region simply will never be left if at least one spiracle were left open. This does not imply that the pattern will be unchanged though. Parameters like relative opening time or period length are likely influenced by the change in aperture. This was also observed by Hetz (2007).

The minimum metabolic rate to see an effect of spiracle blocking is $\mu = 33450$ ($684.6\,\mathrm{nmol\,min^{-1}}$). It has been marked by a black dot in Fig. 4.16.

Spiracle conductance *vs.* internal conductance Fig. 4.17 shows the interaction between spiracular and internal conductance how they influence the release of CO_2 from

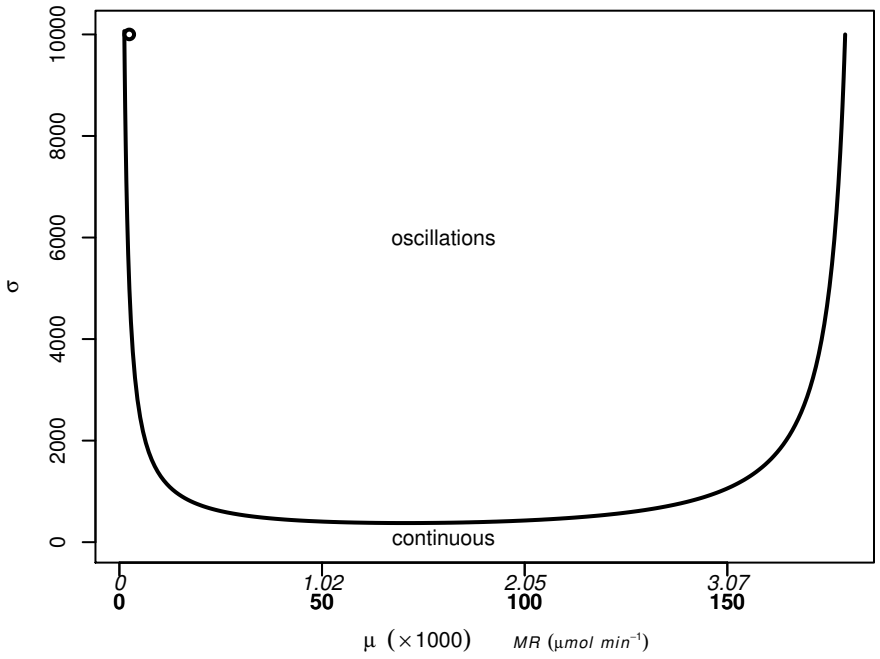

Figure 4.15.: The influence of the shape parameter σ. For very low values solutions with steady state spiracle aperture matched to metabolic rate become stable. Given the neuromuscular control mechanisms in real pupae this might be an unrealistic artifact of the control model.

the animal. The Hopf line separating oscillatory from continuous solutions is symmetric about the line of identity. The minimum conductance that allows oscillatory solutions is for both conductances $\gamma = 0.121$ (G=5.28 nmol kPa^{-1} min^{-1}). Significant interaction between both conductances occurs only for small conductances in the range $\gamma \simeq 0.2-0.5$.

Published values are around 1000 nmol kPa^{-1} min^{-1} for a 5 g pupa (Hetz, 2007) which underlines the large conductance in these animals.

Ambient p_{CO_2} Higher external partial pressure of CO_2 shrinks the range of metabolic rates that allow oscillations (Fig. 4.18). The oscillatory region itself is sawtooth shaped with two nearly linear boundaries consisting of Hopf bifurcations. In the limit $\sigma \to \infty$ the left flank seems to vanish and the oscillatory region most probably fills the complete lower triangular subspace in the quadrant.

The maximum $p^{amb}_{CO_2}$ that allows oscillations at any metabolic rate has been estimated to $\pi = 24748$ ($p^{amb}_{CO_2}$=11.63 kPa).

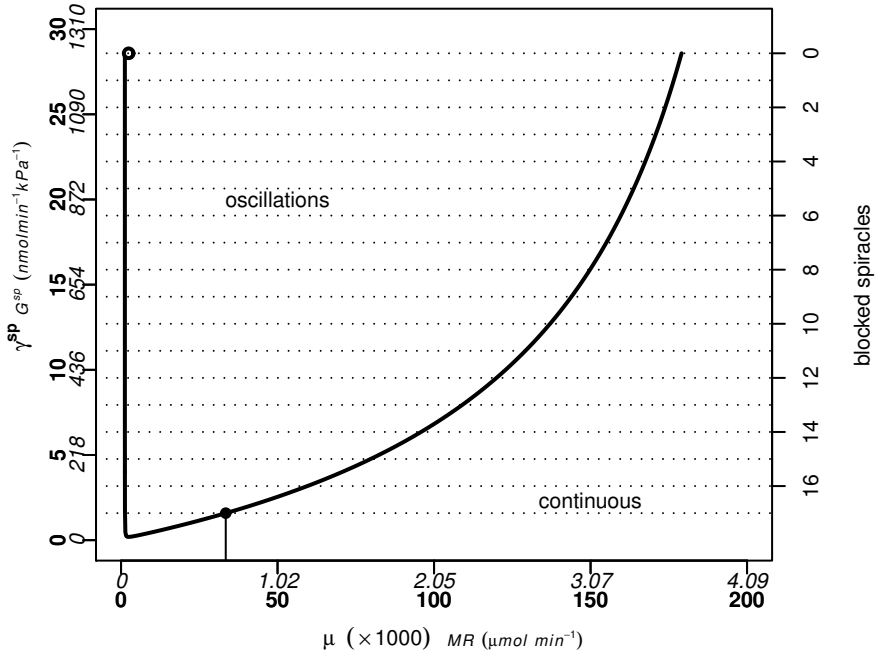

Figure 4.16.: Codim 2 bifurcation diagram for metabolic rate (μ) and spiracle conductance (γ^{sp}). Higher spiracle conductance allows oscillatory solutions at higher metabolic rates. The right axis visualizes the effect of spiracle occlusion if all spiracles were of equal size. For high enough metabolic rate spiracle occlusion (= going downwards) might result in a switch from oscillatory to continuous gas exchange, when the Hopf line is crossed. The filled dot marks the minimum metabolic rate to see a transition from oscillatory to continuous solutions due to the blocking. The open dot marks the position of the default parameters.

4.6. Discussion

4.6.1. General form of the cycles in phase space

One goal of the model has been to prove that a simple system as that of Fig. 4.1 is able to oscillate in certain regions of the parameter space. In that respect the model was quite successful. Moreover, the default parameter set, which has been assembled for diapausing *Attacus* pupae lies within the oscillatory region.

However, the model makes quantitative predictions. Looking at the numbers the model still makes quite large prediction errors when compared to experimental evidence. It turned out that in the default parameter set the DGCs persist even for very high metabolic rates (Fig. 4.7). This in turn would mean that DGC were the norm and continuous gas exchange the exception. However, numerous data prove that DGC only occurs for low metabolic rates.

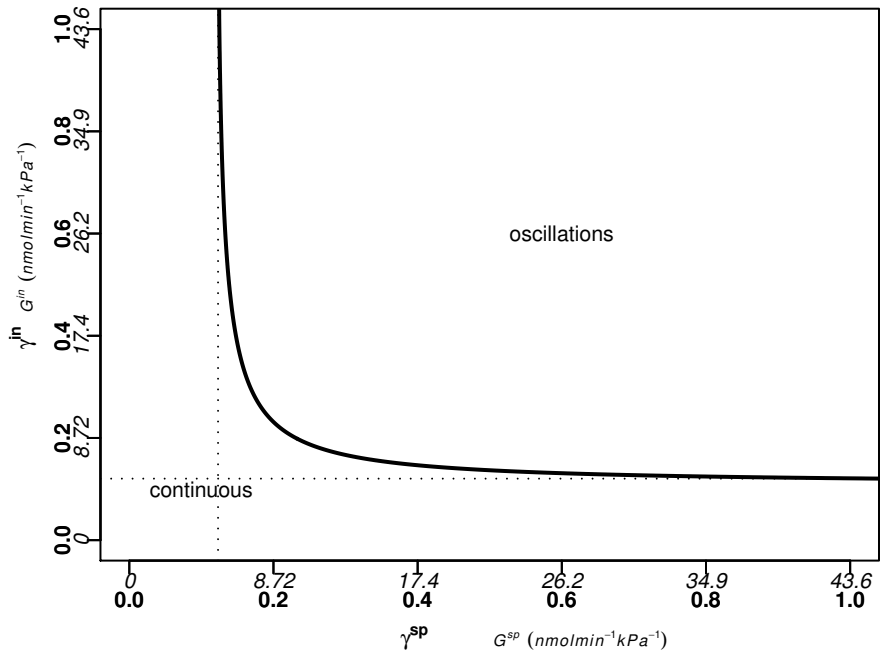

Figure 4.17.: Codim 2 bifurcation diagram showing the influence of spiracular (γ^{sp} and inner (γ^{in}) conductance. Significant interaction only occurs if both conductances are small and about the same. Otherwise the smaller of the two conductances has to be larger than a minimum value for stable oscillations.

Additionally, the amplitudes of pH fluctuations observed in the model are much too low when compared to measured data (Matthews and White, 2009; Hetz and Wasserthal, 1993). Taking even the lowest numbers from the literature (Kaiser, 2002), the model is still one to two orders of magnitude lower.

The reason might be the high concentration of buffers in the default parameter set. However, the used values for β_1 are based on hemolymph concentrations and it is believed that intracellular buffer capacity is higher than hemolymph buffering capacity (Harrison, 2001). Taking this into account the total buffering capacity of a real homogenate will probably be even higher.

On second look, the published values for organic acids of (Harrison, 2001) seem suspicious. The author refers to Wyatt (1961) with the claim that each of the organic acids may exceed 30 mM. However, in the original paper succinate is referred to only twice. The first referral is for larval *Gasterophilus* stating a succinate concentration of 41 meq/l. The second has succinate as part of the organic acid fraction of *Hyalophora* hemolymph that amounts to 25 to 35 meq/l in total. Because most organic acids have multiple carboxyl groups, the concentrations of these organic acids are lower by a factor of two to three. Succinate concentration alone is probably not higher than 20 mM

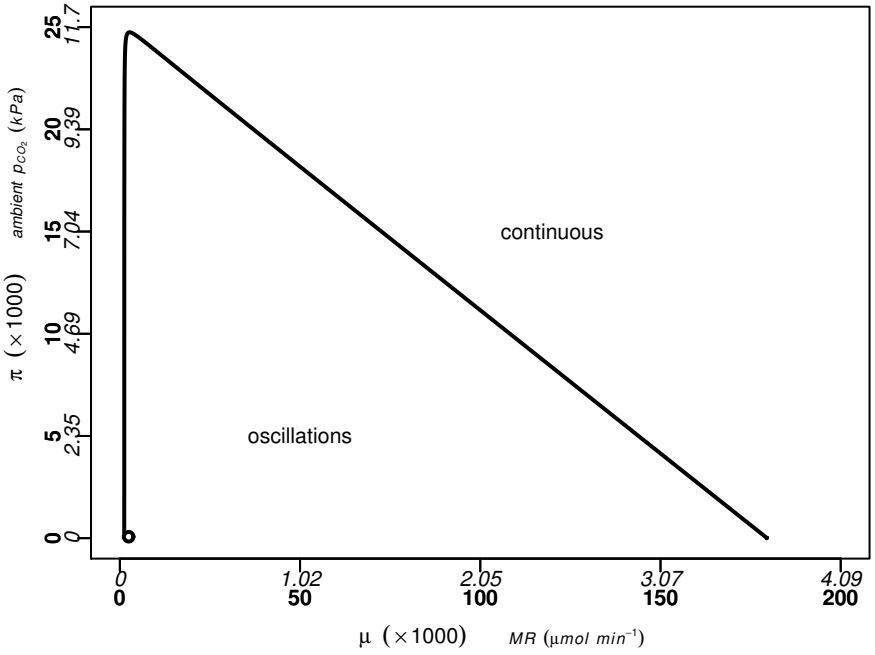

Figure 4.18.: Codim 2 bifurcation diagram showing the influence of external CO_2 partial pressure (π). Higher external p_{CO_2} decreases the range of metabolic rates (μ) that allow oscillations.

In the model the nonbicarbonate buffer concentration was assumed to be 30 mM. Since the hypothetical buffer has only a single protonation site this corresponds to 30 meq/l, a value compatible with Wyatt (1961). So this mismatch does not explain the error of the model. However, it points to the problem that estimates of hemolymph composition in a single species or even stage are often generalized to larger groups. Given the large variability this might lead to large errors when the data are combined with other physiological measurements. An accurate assay of hemolymph composition in *Attacus* including all buffering relevant chemical species seems appropriate to settle this question.

Another great unknown is the pK of the nonbicarbonate buffer. It was chosen somewhat arbitrarily to 6.5 as proteins are thought to provide the bulk of the buffer capacity (Harrison, 2001). Their pK, or more specifically the pK of the amino acid side chains that contribute to the buffering are highly variable and dependent on the geometry of the protein (Edgcomb and Murphy, 2002). The pK of imidazole, the side chain of histidine is between 6.1 and 6.9 (Wyatt, 1961; Williams, pKa data collection). The pK values for organic acids are lower, in the range of 4.5 to 5.5 (Williams, pKa data collection).

However, some preliminary calculations showed that pK_2 does not greatly influence the interval of metabolic rates with oscillatory solutions. Errors in that parameter can thus not explain the persistence of DGC at the high metabolic rates.

The model does not include temperature as a parameter. The influence of temperature variation therefore has not been checked as it would involve changing many parameters simultaneously (metabolic rate, reaction rate constants, solubilities). Using multiple sets of "default" parameters, one for every temperature, a rough picture of its influence might be obtained. However, a better alternative seems to explicitly model the temperature dependence of the respective parameters and replace them by functions of temperature.

The continuous gas exchange mode is coupled to permanent respiratory acidosis (relative to the threshold pH) in the model (Fig. 4.7). In the real animal this acidosis might be partly compensated metabolically by means of normal acid-base control (Harrison, 2001).

4.6.2. Technical problems of the model

The model showed some imperfections that are believed to be mostly of technical nature. First of all, the model solutions became stable again for parameter values that were low (see e.g. Fig 4.7). The cause is that equilibria with constant low aperture become stable. These low apertures are a result of the used sigmoidal aperture function (Fig. 4.1).

However, the spiracle opens and closes in an all-or-nothing fashion. It has been shown that once closed the spiracle conductance is zero, i.e. the spiracles are sealed hermetically (Bridges et al., 1980). From what is known about the excitation-contraction coupling of the spiracle muscle (Hoyle, 1961; van der Kloot, 1963) it is hard to imagine an excitation regime for the muscle that would allow precise control generating extremely small apertures. Even if possible, a liquid film on the lip of the valve (Kestler, 1985; Burkett and Schneiderman, 1974a) might prevent the extremely small apertures required to observe the model behavior.

In conclusion, it seems highly unlikely that these low aperture solutions are biologically relevant. More likely the used sigmoidal function is inappropriate for alkaline pH values and should be replaced by a more accurate version or an explicit dynamic model of the spiracle aperture based on the excitation-contraction coupling and biomechanical dynamics of the closing apparatus.

A second irritating problem was the unpropitious choice of the invariance parameters (β_1, β_2). The reason is that an additional constraint exists which couples both defining equations (eqs. 4.14 and 4.15) together. This constraint derives from the fact that the concentration of $\mathcal{B}$ can not be higher than β_1 for positive $\mathcal{S}$.

$$\mathcal{B} + \mathcal{S} = \beta_1 \tag{4.27}$$

$$\mathcal{B}, \mathcal{S} > 0 \tag{4.28}$$

If β_2 is fixed, this means that at some point, when β_1 is small enough, the initial concentration of $\mathcal{A}$ is varied implicitly to meet the constraint. Variation of β_1 thus reflects

more a change in the bicarbonate-nonbicarbonate ratio than a variation of nonbicarbonate buffer concentration alone. This is undesirable and a better parametrization of the initial concentrations should be found.

4.6.3. Duration of the cycles

The time scale of the oscillations is too short by about one order of magnitude (compare Figs. 4.8 and 1.2). However, the pattern itself probably stems from the different time scales of CO_2 movement – fast release from the tracheae to the outside but slow dehydration of carbonic acid in the dissolution of CO_2 from the hemolymph. The model simplified the internal structure of the animal by lumping together the intracellular and extracellular spaces. This removed an important diffusion barrier which possibly further slows down the internal release of CO_2 from the tissues and the cycle duration might be expanded.

On the other hand, the dehydration usually is facilitated by the enzyme carbonic anhydrase which speeds up the interconversion of CO_2 and bicarbonate. This enzyme is abundant in the tissues but nearly completely lacking in the hemolymph (Harrison, 2001; Buck and Friedman, 1958).

Another probably more severe limitation of the current model is the oversimplification of the processes at the neuromuscular junction of the spiracle muscle. Badre et al. (2005) have shown that extracellular pH itself seems to have little effect on the signal transduction. In contrast, increased CO_2 concentration in the saline bath did inhibit the synapse. It remains unclear, whether this is a direct CO_2 effect or, possibly, an intracellular pH effect. In the first case the whole model were based on wrong assumptions and had to be discarded. In the latter case the above argument about additional transport barriers applies and might explain the comparably long cycles that were observed in *Attacus*.

4.6.4. Switching gas exchange modes

One of the main goals of the model was to test whether a single control mechanism is capable of producing different gas exchange patterns in response to changes of respiratory parameters. This hypothesis has been put forward recently by Bradley and co-workers (Bradley, 2008; Contreras and Bradley, 2009a,b). Accordingly, for high metabolic rate continuous gas exchange is employed, switching to DGC when metabolic rate becomes low enough.

The model convincingly supports this idea. For high metabolic rate the equilibrium solution was stable, resulting in what could best be described as continuous gas exchange (Fig. 4.7). As soon as metabolic rate decreased under a critical value, a Hopf bifurcation occured and the solution became oscillatory. The form of the pattern resembles a DGC cycle without flutter phase. However, this has been expected as the model completely lacks the dynamics of O_2, which is the controlling parameter of the flutter phase (Schneiderman, 1960, also compare chapter 3).

Looking beyond metabolic rate nearly all parameters of the model influence the transition from continuous to oscillatory behavior. Biologically relevant parameters include spiracle and tracheal wall conductance (Fig. 4.17) as well as the buffering properties of the hemolymph (Fig. 4.9).

Interestingly, the ratio of compartment volumes v had only little influence on the oscillatory region (Fig. 4.14). In other words, DGC is not as dependent on tracheal volume as one might think. Only for very high or very low tracheal volume, i.e. when the model system essentially becomes a single compartment, the equilibrium is stable for all metabolic rates and the oscillatory region vanish.

Experimentally, changing metabolic rate is easily achieved in insects. This might explain why the hypothesis of Bradley (2008) has been discovered and formulated specifically for this parameter.

Similar treatment can be done in the case of spiracle conductance by blocking the spiracles (Hetz, 2007). The results likewise indicate a switch from discontinuous to continuous gas exchange if the spiracle conductance falls below a threshold. However, as the default parameters indicate, for very low metabolic rates, the conductance of a single spiracle might be just too high to observe any effect of spiracle occlusion (compare Fig. 4.16).

Replacing the nonbicarbonate buffers in the hemolymph by bicarbonate solutions (comparable to changing β_1) without severe treatment effects possibly provides a much tougher challenge. Likewise, no mechanism that allows to controllably change the internal conductance γ^{in} can be envisioned. However, in this respect it remains an interesting question, whether the proposed absorption mechanism of tracheolar fluid (Wigglesworth, 1935) significantly influences the cycle.

4.6.5. Ambient Hypercapnia

Ambient p_{CO_2} reduces the range of metabolic rates where oscillations are possible (Fig. 4.18). The external p_{CO_2} provides a limit that the animal cannot fall below with gas exchange. In the equilibrium the CO_2 release over the spiracles has to equal metabolic rate. For diffusion, this requires a fixed CO_2 gradient between the hemolymph and the outside, which is solely determined by required mass flow rate and the involved diffusive conductance.

Since spiracle conductance can only be increased up to a maximum (all spiracles fully open) and the internal conductance is believed to be about constant it becomes clear that more and more metabolic rates will be too high to sustain oscillatory solutions. DGC will be abandoned for smaller and smaller metabolic rates if external p_{CO_2} is increased.

The model predicts a maximum $p^{amb}_{CO_2}$ of 11.63 kPa, above which no DGC can be observed at all metabolic rates. This is higher than observations of spiracles in hypercapnia (Punt, 1956; Harrison et al., 1995) and might be compatible with the idea of chthonic origin of the DGC (Lighton and Berrigan, 1995).

However, the model predictions were generally one order of magnitude too large and this might also effect the $\mu - \pi$ interaction. Taking this possible error into account, the maximum ambient p_{CO_2} might be about 1 - 3 kPa comparable to the literature (e.g. Punt, 1956; Terblanche et al., 2008; Lighton, 1996, also compare the discussion on CO_2 thresholds in chapter 2).

Part IV.

Conclusions

5. Discontinuous gas exchange in lepidopteran pupae - A refined theory of mechanism

Over 50 years ago Buck published the first complete mechanistic theory of discontinuous gas exchange (Buck, 1958). Since then multiple hypotheses of DGC origin have been formulated (reviewed in Chown et al., 2006) that suggest to review also the mechanisms behind the pattern.

Using information scattered in the literature as well as the results of the previous chapters I was able to refine the original theory of the DGC control. In the following the results of this review shall be presented.

5.1. Passive generation of respiratory patterns

Since Schneiderman (1960) it is known that CO_2 and O_2 control the spiracular valve via two very different mechanisms. The emergent property hypothesis of a nonadaptive origin of DGC likewise postulates 2 independent control systems. This is also supported by the results of the perfusion experiment (chapter 2). The phase space (Fig. 5.1) can be interpreted as resulting from the interaction of two controllers, each with a separate threshold.

Two models have been created (chapters 3 and 4) which are each based on a probable physical model of the particular control. Both models generated patterns of CO_2 release that are similar to observations in real animals. However, the crucial point is that these patterns are generated passively. That is, contrary to the generation of the ventilatory rhythm where neural pattern generators are involved (Bustami, 2001), the patterns result from oscillations in the whole feedback system. The central nervous system in this case only acts as a simple sensor encoding information about endotracheal p_{O_2}.

The following sections will provide a detailed view of these two assumed feedback loops and their interaction in producing the pattern that is known as DGC. A schematic overview of the overall model is given in Fig. 5.2.

5.2. Oxygen control

The principal sensor sites for O_2 are the segmental ganglia and no conclusive evidence of peripheral oxygen effects has been found (Burkett and Schneiderman, 1974b). Possibly,

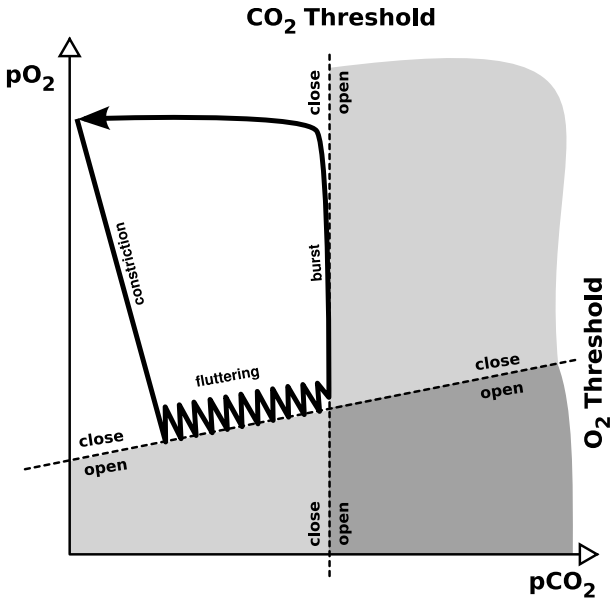

Figure 5.1.: The deduced phase space of the perfusion experiment (repeated). The control output to the spiracle (grey shading) consists of the logical disjunction (OR) of the control output of the CO_2 and O_2 feedback loop (marked at the threshold lines).

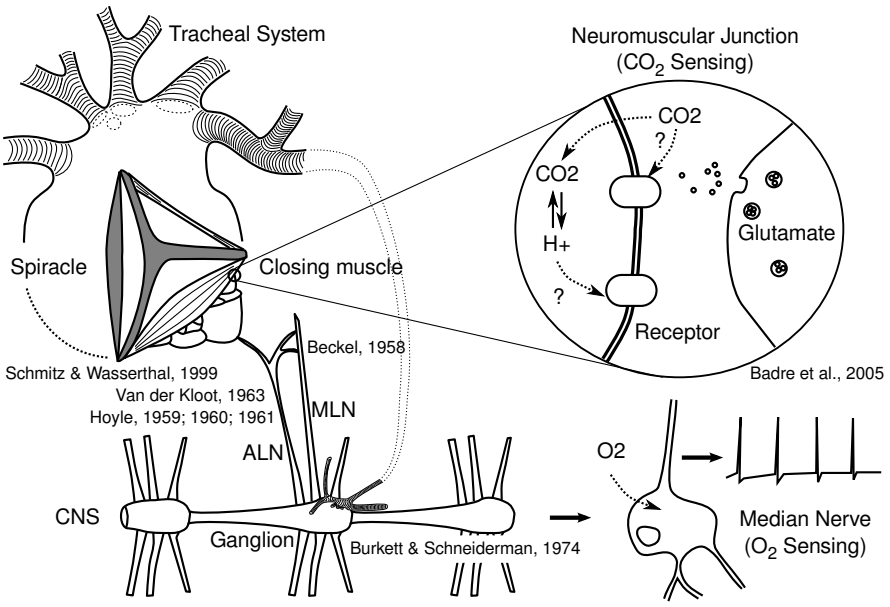

Figure 5.2.: Proposed model of spiracle control in *Attacus* pupae. Shown are the presumed locations of the CO_2 and O_2 sensor structures.

tonically firing unpaired median nerve neurons (Hoyle, 1959; van der Kloot, 1963) react to the endotracheal p_{O_2} in the ganglionic tracheae with a change of spike frequency. Higher p_{O_2} would lead to higher frequencies. However, definitive electrophysiological recordings of neuronal activity in response to oxygen are still missing. It remains unclear whether some thresholding effect occurs in unpaired neurons themselves.

The axons of the these unpaired neurons bifurcate and innervate both spiracular muscles of a segment. The neuromuscular transmission is excitatory so that high spike frequencies (high p_{O_2}) result in contraction of the spiracle muscle. Due to the morphology of the closing valve in *Attacus* this is equivalent to closing the spiracle.

From the unpaired bifurcating arrangement it can be concluded that the reaction is similar for both spiracles in a single segment. They are, however, not synchronous (Brockway and Schneiderman, 1967; van der Kloot, 1963). One resason might be different latencies of both sides.

Comparing the observations of van der Kloot (1963) and Burkett and Schneiderman (1974b), the fibres that convey the central oxygen response most probably run in the mid lateral nerves (MLN). The result is that the oxygen is completely local in the sense that the whole O_2 control loop lies within a single segment. Seemingly no neural coordination between ganglia occurs in response to hypoxia.

Somewhere in the signal transduction chain some thresholding occurs as the behavior of the spiracle valve itself is mostly all-or-nothing (Schneiderman, 1960). Candidates are either the unpaired median neurons, e.g. the neural summation generating the action potentials or some thresholding in the excitation-contraction coupling of the muscle fibres. However, the exact mechanism is irrelevant for the overall effect.

Metabolic rate steadily decreases the endotracheal p_{O_2} including the partial pressure in the ganglionic tracheae. At some point the p_{O_2} is low enough that central nervous input to the spiracles becomes insufficient to effect continuous contraction of the spiracle muscle. The muscle relaxes and the spiracle opens. Due to the subatmospheric pressure and the large gradient in partial pressure (Levy and Schneiderman, 1966c,a) oxygen flows into the tracheal system by a mix of convection and diffusion. However, the increase in O_2 availability does not instantaneously reach the ganglionic sensor site. This short delay probably determines the minimum time of micro-opening (chapter 3).

The result is integrate-and-fire type oscillations of the oxygen partial pressure within a single segment, where oscillation frequency is determined by the morphology, the metabolic rate and the actual O_2 threshold of the segment (Fig. 3.3).

It can thus be assumed that the frequencies of neighboring segments are close but not identical to each other. The diffusion along the main longitudinal tracheal stems provides a coupling mechanism. The degree of diffusion that will occur depends mainly on the diffusive conductance of the tracheae. If it is high enough, phase locking is likely and multiple segments will become synchronized even without any neural coordination (Fig. 3.4).

This passive synchronization explains why, seemingly, only few segments actually engage in gas exchange during the flutter phase (Wigglesworth, 1935; Sláma, 1988) yet

central nervous control of the spiracles is local and independent in each segment (van der Kloot, 1963; Burkett and Schneiderman, 1974b).

5.3. Carbon dioxide control

Relatively early it has been found that the action of CO_2 on the spiracle seems to be a direct one (Case, 1957; Hoyle, 1960). Preparations of the spiracle muscle with the median nerve transsected, continued to react to increased CO_2 concentrations (Beckel and Schneiderman, 1957). A suspected local reflex network could not be confirmed by morphological investigations (Schneiderman, 1960).

Later it was shown that electrical activity of the spiracle muscle ceased despite continued activity of the median nerve axons (Hoyle, 1960; van der Kloot, 1963). Only if 10 % CO_2 was blown over the muscle preparation, firing in the antero-lateral branch (ALN) ceased (van der Kloot, 1963). On the contrary, the separate perfusions of ganglia and tracheal system (Burkett and Schneiderman, 1974b) dismissed a possible central effect of CO_2 in physiological concentrations below 30 % (30.5 kPa).

It has been concluded that CO_2 directly interferes with the transmission of the electrical signals at the neuromuscular junction. However, the actual mechanism possibly remained open until Badre et al. (2005) discovered that CO_2 inhibits the postsynaptic glutamate receptors of insect skeletal muscles (Fig. 5.2). As the spiracle muscle is also of skeletal origin, the same mechanism might explain the earlier results.

Accordingly, increased local concentrations of CO_2 inhibit the neuromuscular transmission to the spiracle muscle and the muscle relaxes in the face of CO_2. Since the action is directly on the postsynaptic receptors for the neurotransmitter, no intermediate neural network or dedicated CO_2 sensor has to be assumed.

How CO_2 acts on the receptors is an open question. All that can be said so far is that extracellular pH does not influence the receptors (Badre et al., 2005). Either there is a direct inhibition of the receptors by CO_2 or, alternatively, CO_2 diffuses across the postsynaptic membrane and hydrates intracellularly forming protons and bicarbonate. The resulting acidification might effect the inactivation of the receptor. However, the intracellular compartments are usually well buffered (Harrison, 2001). On the other hand, the existence of significant amounts of carbonic anhydrase speeds up the hydration reaction and might result in transient pH disturbances that possibly lead to inhibition of the receptors.

5.4. Interaction between the two controls

Fig. 5.1 shows again the interpretation of the perfusion results (chapter 2). Without explicit knowledge of the neuromuscular transmission described in the previous two sections, it had been interpreted as the logical disjunction of two control inputs (Förster and Hetz, 2009). If either one of the two assumed control loops demanded the spiracle to

open (the grey areas of Fig. 5.1) the spiracle would open independently of the decision of the other control loop. Coincidentally, the neuromuscular junction of the spiracle muscle probably implements this type of logical connection.

A lack of oxygen possibly suppresses the electrical input to the synapse and thus the release of the neurotransmitter glutamate (Burkett and Schneiderman, 1974b). However, if there is no glutamate release presynaptically, it is just irrelevant that the postsynaptic glutamate receptors might be blocked by CO_2 (Badre et al., 2005). The result is relaxation of the muscle and the opening of the spiracle, regardless of the local p_{CO_2}.

The other way around, if sufficient oxygen is detected in the ganglion, there will be a constant stream of action potentials arriving on the median nerve axons. However, increased levels of CO_2 inhibit the postsynaptic glutamate receptors and, even though large amounts of glutamate are released into the synaptic cleft, the presynaptic activity does not result in postsynaptic potentials. Again the spiracle opens.

Only if there is sufficient electrical activation of the neuromuscular synapse (= enough O_2) and there is no inhibition of the postsynaptic receptors (= low CO_2), the muscle fibres contract and the spiracle is held closed.

5.5. Implications on DGC Origin

The developed mechanistical model is compatible with a number of hypotheses of DGC origin. As the steady emphasis on two independent control systems already foretold, it had been developed taking the emergent property hypothesis as its paradigm (Kuhn, 1996). In this respect it represents a concrete implementation of the ideas of Chown and Holter (2000).

However, several other hypotheses do not contradict the model. The oxidative damage hypothesis (Hetz and Bradley, 2005), or more specifically its postulated driving forces, can be formulated without any reference to CO_2. The underlying idea can be subsumed into the model by attaching these driving forces to the development of the oxygen dependent part of the control. It would then provide an adaptive explanation for the evolution of said O_2 control.

The fully developed DGC pattern probably does save water (Buck, 1962; Chown, 2002). Yet this aspect of the DGC might have been 'discovered' later and might not be the ultimate cause for the evolution of the two control systems. Rather it might be a secondary effect of the pattern evolution. Anyway, if the DGC pattern saves water, how is this idea different from the hygric hypothesis?

The hygric hypothesis postulates the DGC pattern as an *adaptation* to minimize respiratory water loss (Chown et al., 2006). In my view, this implies some gradual evolution of the pattern that became more and more effective in saving water. Though nowhere stated explicitly, possibly the general view held is that the pattern evolved roughly along the route continuous $\rightarrow$ cyclic $\rightarrow$ discontinuous gas exchange (though there might be multiple independent origin; Marais et al., 2005).

In contrast, the hypothesis developed here postulates an independent, possibly adaptive evolution of both control systems. Once they got into contact and began to interact the full DGC pattern appeared spontaneously, solely due to the physical properties of the animal. This might also explain the large individual variance in the patterns in some species and the seemingly multiple evolution of the pattern (Marais et al., 2005).

The tripartite pattern were an emergent phenomenon (Chown and Holter, 2000; Chown et al., 2006), which could not be explained from each of the two separate control systems alone. The new, suddenly appearing gas exchange pattern might have been beneficial to the water status of the animal. It has been retained and maybe finetuned subsequently.

6. Future questions

The central result of this work has been that the patterns of CO_2 release observed during the discontinuous gas exchange of moth pupae might be the result of simple control loops and their mutual interaction. A number of assumptions are implicit in these models, which justify further work.

One key component of the discussion of the DGC mechanics were the processes that are involved in synaptic transmission at the neuromuscular junction and their inhibition by CO_2.

van der Kloot (1963) described the spiracle muscle of *Hyalophora cecropia* pupae as autonomous. Pacemaker potentials of the muscle fibres lead to spontaneous contraction of the denervated muscle. However, this is the only description and only few other measurements of the electrical activity of the spiracle muscle exist (Hoyle, 1960). Additionally these are from insects with active ventilation and thus probably involve more sophisticated neural-spiracular control to coordinate the inspiration and expiration movements. So it remains unclear whether the possible pacemaker potentials are restricted to moth pupae as van der Kloot (1963) suggested, or whether they are a general property of the spiracle muscle.

However, the existence of pacemaker rhythms in the single fibres demands either a phase desynchronization of the fibres due to central nervous input or a direct inhibitory influence of the median nerve axons. Otherwise the contraction, which were brought about by the spontaneous electrical activity, could not be broken by central nervous input and no central nervous control of gas exchange due to O_2 could occur (Burkett and Schneiderman, 1974b).

Both alternatives are without example. Efferent input to skeletal muscles in insects is thought to be solely excitatory (Chapman, 1998). Moreover, there seems to be no general difference in the axons that reach the spiracle muscle in locusts, i.e. fast and slow axons share the same transmitter (Hoyle, 1959), most likely glutamate (Badre et al., 2005). As these axons, when stimulated, generate twitches of the muscle they definitely act excitatory.

Equally hard to imagine is the postulated desynchronization due to central nervous input. The median nerve axons reaching the spiracle muscle are polyterminal, most probably innervating every single fibre of the muscle. Even if the fibres are free running oscillators due to the pacemaker potentials, the synaptic input would provide periodic forcing and result in synchronization rather than desynchronization between the fibers.

The period of the pacemaker potentials is 1.8 - 2.2 s (van der Kloot, 1963), which would also be the period of contraction/relaxation cycles of the whole muscle if all fibres are

synchronized. Central nervous input seems to have much faster spike frequencies of 8 - 15 Hz (van der Kloot, 1963) and thus synchronization is highly likely.

Reestablishement of the spiracle muscle preparation of van der Kloot (1963) seems highly desirable to establish or refute the existence of a myogenic rhythm in the spiracle muscle of saturniid pupae and to gain a clearer understanding of the electrical events in the vicinity of its muscle fibres.

Controlled pertubation of rhythms is a powerful means of system identification. Phase response curves from single pulse pertubations and the analysis of phase locking regions from periodic stimulation reveal much of the underlying mechanisms of the oscillator (Glass and Mackey, 1988). Having the muscle preparation in place might provide a convenient tool to study the system with modern methods of synchronization theory (Pikovsky et al., 2003).

Another related question is that of the mechanism of the action of CO_2 on the neuromuscular transmission. Badre et al. (2005) found hypercapnic inhibition of postsynaptic glutamate receptors which is not based on the acidifying property of CO_2. This direct effect of CO_2 had also been concluded by Hoyle 45 years before (Hoyle, 1960).

However, the pH independent effect only applies to extracellular protons. Badre et al. (2005) explicitly mention that either a direct inhibition by CO_2 (e.g. competitive inhibition) or an intracellular pH effect due to the transmembrane diffusion of CO_2 and its subsequent hydration within the muscle fibre is possible. Because of the existence of carbonic anhydrase intracellularly the hydration reaction is accelerated and at least transiently the pH fluctuations due to CO_2 should be higher than in the extracellular medium lacking the enzyme (Badre et al., 2005). Exact knowledge of the molecular mechanism might provide insights whether or not this inhibition is coupled to intracellular acid-base homeostasis. It might also support the assumption of a pH dependent control that was the bases of the CO_2 model of chapter 4.

A more general question stems from the fact that CO_2 acts as a narcotic. Indeed this aspect of the carbon dioxide action was the original motivation that inspired the work of Badre et al. (2005). The question that arises is that if the inhibition of glutamate receptors in the postsynaptic membrane of the skeletal neuromuscular junction comprised the narcotic effect of CO_2, would that not mean that the insect during DGC is repeatedly anesthetized? Most probably this cannot be the case and it becomes clear that the CO_2 concentrations that result in muscle relaxation have to be different for different types of muscles. Otherwise the late flutter phase with high levels of CO_2 would be particularly dangerous for most insects, sitting there unable to move, perfect prey as they were.

This thread can be spun further. If multiple CO_2 thresholds existed for multiple types of skeletal muscle synapses could that not allow the pacemakers of the insect heart, which are also innervated by glutamatergic synapses(Badre et al., 2005; Dulcis and Levine, 2005), could react in a predictable way to rising levels of CO_2? According to Dulcis and Levine (2005) retrograde heartbeat is initiated by glutamatergic innervation. If this were inhibited by CO_2 at the synapses, the other pacemaker could take over and anterograde heart beat be initiated. An interesting consequence would be

an 'automatic' synchronization between respiratory (DGC) and circulatory (heartbeat reversals) patterns.

Apart from the biological questions future work is due also on the two models that have been presented here. The discussion in the previous chapter already hinted to the fact that the numeric predictions of the CO_2 model are wrong by about one order of magnitude. It remains to be evaluated whether a refined model structure which explicitly accounts for the intracellular and extracellular compartments provides better predictions. These two compartments most probably differ significantly in several aspects like buffer concentrations or the catalytic effect of carbonic anhydrase in the intracellular space.

A number of parameters are not directly accessible. However, parameters that are structurally identifiable in a model might be estimated by modern parameter estimation methods (e.g. Ljung, 1999). With the right choice of observation functions it might be possible to estimate these hard to get parameters on an individual basis allowing intraspecific comparison. However, parameter estimation methods are often sensitive to noise and it remains to be seen whether they can be successfully applied in the investigation of insect respiration.

The flutter model (chapter 3) relied on the metameric organization of insects and the degree of automatic synchronization between segments arising due to the inherent coupling between segments. So far only Lehmann and Heymann (2005) already acknowledged the possibilities for the generation of complex patterns resulting from temporal interactions of multiple spiracles.

However, the O_2 model has been only a very simple example of how the DGC pattern or parts of it might be shaped by the coupling. Similar effects can be expected if the CO_2 model were multiplied and coupled. An interesting observation in that respect is the stepwise increase of CO_2 release at the beginning of the burst in *Attacus* pupae (Hetz, 1994). Other phenomena that might possibly be explained by a metameric CO_2 model include the cyclic gas exchange pattern, where only some spiracles close and CO_2 release never goes down to zero.

As a final remark, I subscribe to Chown et al. (2006) that *"the ways in which tracheate arthropods breathe is once again a thriving area of research."* As with all science the open questions easily outnumber the answers. It is my sincere hope that this work is seen as an invitation to further develop or to challenge the ideas presented.

Acknowledgements

Classically, a number of people are thanked in this section, usually ranked to officially perceived importance. However, this work has been unusual in more than one respect so this will not be a classic acknowledgement. The problem is this. How can you fully thank someone for something when the only word in your mind is 'everything'?

Stefan Hetz not only is the one to blame for having introduced me to the fascinating research of insect respiration, he has also seen to it that my contributions might become beneficial to the field over time. However, what I hate most was that whenever you came with that idea for this exciting new experiment he either opened the drawer and handed you the data or else pulled a nearly forgotten PhD thesis from Erlangen from his shelf. Whatever you want to know of insect respiration, ask Stefan. Apart from that I enjoyed the discussions and the brainstorming sessions including the occasional big leap in thinking. I'm also sorry to his wife Martina and David and Theresa for having stolen family time sometimes.

Of course, as everyone knowing him knows, this list would not be complete without the mention of long drinks and barbecue. So here they are – longdrinks and barbecue.

My supervisor Matthias Hennig is thanked for allowing me all the freedom I enjoyed while pursuing this research. Even though often for him this meant last minute revision of grant applications or other questionably enjoying work. It is only now that I start to fully realize the level of trust this implies. He is also to thank for travel money to attend the Mara Meeting in 2008.

While talking about money it is to mention that the first two years of PhD work have been funded by a NaFöG studentship from the state of Berlin. Additionally, travel costs have been covered to present the perfusion data at the ICE 2008 in Durban.

The theoretical section benefited much from the summer school "Biomedical Modeling And Cardiovascular-Respiratory Control: Theory And Practice" organized in 2007 by Jerry Batzel, Mustafa Bachar and Franz Kappel (Graz, Austria) with funding from the Marie Curie Conferences and Training Courses program of the European Union.

Two sentences in the methods section of the perfusion experiment can definitely not express the effort necessary to establish a large moth breeding colony. A number of people have helped to feed the ever hungry caterpillars. A very big thank you goes to Gabriele Ziermann, Susanne Grübel, Kathleen Trogisch, Christian Mörbitz and Kathrin Otte. My mother and my grandmother took care of a breeding stock of *Samia cynthia* over the winter.

Kathleen Trogisch, Kathrin Otte, Deborah Friedrich, Katharina Hille and Christian Mörbitz (sorry Kriss, ladies first this time) manned the office and provided a pleasant

and fruitful working environment. It has been fun with you all and if there ever were again the chance of being taught how to teach data analysis, statistics and programming I would happily take that course again. Thanks for having an ear (and shoulder) sometimes and cake and sweets...

Rüdiger Karpinski handcrafted some custom parts of the perfusion setup. Excellent job, enjoy your retirement. Maik Kunert seamlessly continued the good work in the workshop. Many thanks for all the fresh coffee in the morning. Arnold Stern provided IT support, hardware, manuals and a Latex book that was most wanted during the preparation of this thesis.

Many colleagues have contributed indirectly by shaping my thinking about insect respiration. Thanks (in arbitrary order) go to John Lighton, Robbin Turner, Frances Duncan, Art Woods, Tim Bradley, Steve Morris, Thorsten Burmester, Jaco Klok, Jon Harrison, Phil Matthews, Jake Socha, Kendra Greenlee, Steven Chown and John Terblanche for advise, discussions, hospitality or just a nice drink at the bar.

Surely I have forgotten many more. Feel free to state your case in reward of a beer.

Bibliography

N. H. Badre, M. E. Martin, and R. L. Cooper. The physiological and behavioral effects of carbon dioxide on *Drosophila melanogaster* larvae. *Comparative Biochemistry and Physiology - Part A: Molecular & Integrative Physiology*, 140(3):363–376, 2005.

J. W. L. Beament. The active transport and passive movement of water in insects. In J. W. L. Beament, E. J. Treherne, and V. B. Wigglesworth, editors, *Advances in Insect Physiology*, volume 2, pages 67–129. Academic Press, 1964.

W. E. Beckel. *The morphology, histology and physiology of the spiracular regulatory apparatus of* Hyalophora cecropia *(L.)(Lepidoptera).* PhD thesis, Cornell University, 1955.

W. E. Beckel and H. A. Schneiderman. Insect spiracle as an independent effector. *Science*, 126(3269):352–353, 1957.

T. J. Bradley. Control of the respiratory pattern in insects. In R. C. Roach, P. D. Wagner, and P. H. Hackett, editors, *Hypoxia And The Circulation*, number 618 in Advances in Experimental Medicine and Biology, pages 211–220. Springer New York, 2008.

C. R. Bridges and P. Scheid. Buffering and CO2 dissociation of body fluids in the pupa of the silkworm moth, *Hyalaphora cecropia*. *Respiration Physiology*, 48(2):183–197, 1982.

C. R. Bridges, P. Kestler, and P. Scheid. Tracheal volume in the pupa on the saturniid moth *Hyalophora cecropia* determined with inert gases. *Respiration Physiology*, 40 (3):281–291, 1980.

A. P. Brockway and H. A. Schneiderman. Strain-gauge transducer studies on intratracheal pressure and pupal length during discontinuous respiration in diapausing silkworm pupae. *Journal of Insect Physiology*, 13(9):1413–1451, 1967.

J. Buck. Cyclic CO2 release in insects IV. a theory of mechanism. *Biological Bulletin*, 114(2):118–140, 1958.

J. Buck. Some physical aspects of insect respiration. *Annual review of entomology*, 7 (1):27–56, 1962.

J. Buck and S. Friedman. Cyclic CO2 release in diapausing pupae–III: CO2 capacity of the blood: Carbonic anhydrase. *Journal of Insect Physiology*, 2(1):52–60, 1958.

J. B. Buck and M. L. Keister. Cyclic CO2 release in diapausing *Agapema* pupae. *Biological Bulletin*, 109(1):144–163, Aug. 1955.

E. Buckingham. On physically similar systems: Illustrations of the use of dimensional equations. *Physical Review*, 4(4):345, 1914.

B. N. Burkett and H. A. Schneiderman. Discontinuous respiration in insects at low temperatures: intratracheal pressure changes and spiracular valve behavior. *Biological Bulletin*, 147(2):294–310, 1974a.

B. N. Burkett and H. A. Schneiderman. Roles of oxygen and carbon dioxide in the control of spiracular function in cecropia pupae. *Biological Bulletin*, 147(2):274–293, 1974b.

H. P. Bustami. *Ventilatorische Rhythmogenese im isolierten Insektennervensystem*. PhD thesis, Göttingen, 2001.

J. F. Case. The median nerves and cockroach spiracular function. *Journal of Insect Physiology*, 1(1):85–94, 1957.

R. F. Chapman. *The insects - structure and function*. Cambridge University Press, 4 edition, 1998.

S. L. Chown. Respiratory water loss in insects. *Comparative Biochemistry and Physiology - Part A: Molecular & Integrative Physiology*, 133(3):791–804, 2002.

S. L. Chown and P. Holter. Discontinuous gas exchange cycles in *Aphodius fossor* (Scarabaeidae): a test of hypotheses concerning origins and mechanisms. *Journal of Experimental Biology*, 203(2):397, 2000.

S. L. Chown, A. G. Gibbs, S. K. Hetz, C. J. Klok, J. R. Lighton, and E. Marais. Discontinuous gas exchange in insects: A clarification of hypotheses and approaches. *Physiological and Biochemical Zoology*, 79(2):333–343, 2006.

K. U. Clarke. On the role of the tracheal system in the post-embryonic growth of *Locusta migratoria* L. *Proceedings of the Royal Entomological Society of London. Series A, General Entomology*, 32(4-6):67–79, 1957.

J. L. Cloudsley-Thompson. Adaptations of arthropoda to arid environments. *Annual Review of Entomology*, 20(1):261–283, 1975.

H. Contreras and T. Bradley. Transitions in insect respiratory patterns are controlled by changes in metabolic rate. *Journal of Insect Physiology*, In Press, 2009a.

H. L. Contreras and T. J. Bradley. Metabolic rate controls respiratory pattern in insects. *Journal of Experimental Biology*, 212(3):424–428, 2009b.

P. Dejours. *Principles of Comparative Respiratory Physiology*. North Holland, Amsterdam, 1975.

A. Dhooge, W. Govaerts, Y. A. Kusnetzov, W. Mestrom, A. M. Riet, and B. Sautois. *MATCONT and CL MATCONT: Continuation toolboxes in Matlab*, 2006. URL `http://www.matcont.ugent.be/manual.pdf`.

D. Dulcis and R. B. Levine. Glutamatergic innervation of the heart initiates retrograde contractions in adult *Drosophila melanogaster*. *Journal of Neuroscience*, 25(2):271–280, 2005.

F. D. Duncan and M. J. Byrne. Discontinuous gas exchange in dung beetles: patterns and ecological implications. *Oecologia*, 122(4):452–458, 2000.

S. P. Edgcomb and K. P. Murphy. Variability in the pKa of histidine side-chains correlates with burial within proteins. *Proteins: Structure, Function, and Genetics*, 49(1): 1–6, 2002.

E. Edney. *Water Balance in Land Arthropods*. Springer Verlag, Berlin, 1977.

S. P. Ellner and J. Guckenheimer. *Dynamic Models in Biology*. Princeton University Press, Princeton, Oxford, 2006.

N. D. Fowkes and J. J. Mahony. *Einführung in die Mathematische Modellierung*. Springer Verlag, Heidelberg, Berlin, Oxford, 1996.

I. Fridovich. Oxygen is toxic! *BioScience*, 27(7):462–466, 1977.

T. D. Förster and S. K. Hetz. Spiracle activity in moth pupae – the role of oxygen and carbon dioxide revisited. *Journal of Insect Physiology*, In Press, 2009.

T. D. Förster and S. K. Hetz. Spiracular constriction - obeying the rules of compliance. In S. Morris and A. Vosloo, editors, *Molecules to migration: The pressures of life*, 4th CPB Meeting in Africa: Mara 2008, page 285–292. Medimond, Bologna, 2008.

B. H. Gibbons and J. T. Edsall. Rate of hydration of carbon dioxide and dehydration of carbonic acid at 25°. *J. Biol. Chem.*, 238:3502–3507, 1963.

L. Glass and M. C. Mackey. *From Clocks to Chaos - The Rhythms of Life*. Princeton University Press, 1988.

E. M. Gray and T. J. Bradley. Evidence from mosquitoes suggests that cyclic gas exchange and discontinuous gas exchange are two manifestations of a single respiratory pattern. *Journal of Experimental Biology*, 209(9):1603, 2006.

K. J. Greenlee and J. F. Harrison. Acid-base and respiratory responses to hypoxia in the grasshopper *Schistocerca americana*. *Journal of Experimental Biology*, 201(20): 2843, 1998.

K. J. Greenlee and J. F. Harrison. Development of respiratory function in the american locust *Schistocerca americana*: II. within-instar effects. *Journal of Experimental Biology*, 207(3):509, 2004.

K. J. Greenlee and J. F. Harrison. Respiratory changes throughout ontogeny in the tobacco hornworm caterpillar, *Manduca sexta*. *J Exp Biol*, 208(7):1385–1392, 2005.

K. J. Greenlee, C. Nebeker, and J. F. Harrison. Body size-independent safety margins for gas exchange across grasshopper species. *Journal of Experimental Biology*, 210(7): 1288, 2007.

J. Guckenheimer and P. Holmes. *Nonlinear Oscillations, Dynamical Systems and Bifurcations of Vector Fields*. Number 42 in Applied Mathematical Sciences. Springer Verlag, New York, 1983.

N. F. Hadley and M. C. Quinlan. Discontinuous carbon dioxide release in the eastern lubber grasshopper *Romalea guttata* and its effect on respiratory transpiration. *Journal of Experimental Biology*, 177(1):169, 1993.

J. Harrison, C. J. Wong, and J. E. Phillips. Short communication: Haemolymph buffering in the locust *Schistocerca gregaria*. *Journal of Experimental Biology*, 154:573–579, 1990.

J. Harrison, N. Hadley, and M. Quinlan. Acid-base status and spiracular control during discontinuous ventilation in grasshoppers. *Journal of Experimental Biology*, 198(8): 1755, 1995.

J. F. Harrison. Insect acid-base physiology. *Annual review of entomology*, 46(1):221–250, 2001.

J. F. Harrison, S. Camazine, J. H. Marden, S. D. Kirkton, A. Rozo, and X. Yang. Mite not make it home: tracheal mites reduce the safety margin for oxygen delivery of flying honeybees. *Journal of Experimental Biology*, 204(4):805, 2001.

J. M. Harrison. Temperature effects on haemolymph acid-base status in vivo and in vitro in the two-striped grasshopper *Melanoplus bivittatus*. *Journal of Experimental Biology*, 140(1):421, 1988.

E. H. Hazelhoff. *Regeling der Ademhaling bij Insecten en Spinnen*. PhD thesis, Rijks-Universiteit te Utrecht, Utrecht, 1926.

N. Heisler, editor. *Acid-Base Regulation in Animals*. Elsevier, 1986.

J. Heller. Sauerstoffverbrauch der schmetterlingspuppen in abhängigkeit von der temperatur. *Zeitschrift für vergleichende Physiologie*, 11(3):448–460, 1930.

G. M. Herford. Tracheal pulsation in the flea. *Journal of Experimental Biology*, 15: 327–338, 1938.

S. K. Hetz. The role of the spiracles in gas exchange during development of *Samia cynthia* (Lepidoptera, Saturniidae). *Comparative Biochemistry and Physiology - Part A: Molecular & Integrative Physiology*, 148(4):743–754, 2007.

S. K. Hetz. *Untersuchungen zu Atmung, Kreislauf und Säure-Basen-Regulation an Puppen der tropischen Schmetterlingsgattungen* Ornithoptera, Troides *und* Attacus. PhD thesis, Friedrich-Alexander-Universität Erlangen-Nürnberg, 1994.

S. K. Hetz and T. J. Bradley. Insects breathe discontinuously to avoid oxygen toxicity. *Nature*, 433(7025):516–519, 2005.

S. K. Hetz and L. T. Wasserthal. Miniaturisierte pH-sensitive Glaselektroden für die Dauermessung des Hämolymph-pH in ruhenden Schmetterlingspuppen. *Verhandlungen der Deutschen Zoologischen Gesellschaft*, page 92, 1993.

S. K. Hetz, L. T. Wasserthal, S. Hermann, H. Kaden, and W. Oelßner. Direct oxygen measurements in the tracheal system of lepidopterous pupae using miniaturized amperometric sensors. *Bioelectrochemistry and Bioenergetics*, 33(2):165–170, 1994.

G. Hoyle. The action of carbon dioxide gas on an insect spiracular muscle. *Journal of Insect Physiology*, 4(1):63–79, 1960.

G. Hoyle. Functional contracture in a spiracular muscle. *Journal of Insect Physiology*, 7(3-4):305–314, 1961.

G. Hoyle. The neuromuscular mechanism of an insect spiracular muscle. *Journal of Insect Physiology*, 3(4):378–394, Dec. 1959.

V. Janda and V. Kocian. Über den Sauerstoffverbrauch der Puppen von *Tenebrio molitor* L. *Zoologische Jahrbücher*, 52:561–589, 1933.

H. Jordan. Die Regulierung der Atmung bei Insekten und Spinnen. *Zeitschrift für vergleichende Physiologie*, 5(1):179–190, 1927.

A. Kaiser. *Effekt ontogenetischer Entwicklung und respiratorischer Veränderungen auf Zusammensetzung und Säure-Basen-Status der Flüssigkeitskompartimente von Puppen des Schwarzkäfers* Zophobas rugipes. PhD thesis, Humboldt Universität Berlin, 2002.

A. Kaiser, L. T. Wasserthal, S. K. Hetz, and N. Heisler. Spiracular movement of butterfly pupae - modulation of amplitude or of frequency. *Verhandlungen der Deutschen Zoologischen Gesellschaft*, 89:155, 1996.

A. Kaiser, C. J. Klok, J. J. Socha, W. K. Lee, M. C. Quinlan, and J. F. Harrison. Increase in tracheal investment with beetle size supports hypothesis of oxygen limitation on insect gigantism. *Proceedings of the National Academy of Sciences*, 104(32):13198, 2007.

P. Kestler. Respiration and respiratory water loss. In K. Hoffmann, editor, *Environmental Physiology and Biochemistry of Insects*, pages 137–183. Springer Verlag, Berlin, Heidelberg, 1985.

G. Kießling. *Zusammensetzung und Physiologie der Hämolymphe von Lepidopteren.* PhD thesis, Friedrich-Alexander-Universität Erlangen-Nürnberg, 1997.

W. Knoche. Chemical reactions of CO2 with water. In C. Bauer, G. Gros, and H. Bartels, editors, *Biophysics and physiology of carbon dioxide.*, pages 3–11. Springer Verlag, 1980.

T. S. Kuhn. *The structure of scientific revolutions.* The University of Chicago Press, Chicago, London, 3rd edition, 1996.

Y. A. Kusnetzov. *Elements of Applied Bifurcation Theory.* Number 112 in Applied Mathematical Sciences. Springer Verlag, 2nd edition edition, 1998.

G. N. Landis and J. Tower. Superoxide dismutase evolution and life span regulation. *Mechanisms of Ageing and Development*, 126(3):365–379, 2005.

H. M. Lease, B. O. Wolf, and J. F. Harrison. Intraspecific variation in tracheal volume in the american locust, *Schistocerca americana*, measured by a new inert gas method. *Journal of Experimental Biology*, 209(17):3476–3483, 2006.

F. Lehmann and N. Heymann. Unconventional mechanisms control cyclic respiratory gas release in flying *Drosophila*. *Journal of Experimental Biology*, 208(19):3645–3654, 2005.

R. I. Levy and H. Schneiderman. Discontinuous respiration in insects – IV. changes in intratracheal pressure during the respiratory cycle of silkworm pupae. *Journal of Insect Physiology*, 12(4):465–492, 1966a.

R. I. Levy and H. A. Schneiderman. Discontinuous respiration in insects – III. the effect of temperature and ambient oxygen tension on the gaseous composition of the tracheal system of silkworm pupae. *Journal of Insect Physiology*, 12(1):105–121, 1966b.

R. I. Levy and H. A. Schneiderman. Discontinuous respiration in insects – II. the direct measurement and significance of changes in tracheal gas composition during the respiratory cycle of silkworm pupae. *Journal of Insect Physiology*, 12(1):83–104, 1966c.

J. R. B. Lighton. Discontinuous gas exchange in insects. *Annual Review of Entomology*, 41(1):309–324, 1996.

J. R. B. Lighton. *Measuring metabolic rates - A manual for scientists.* Oxford University Press, 2008.

J. R. B. Lighton. Notes from underground: Towards ultimate hypotheses of cyclic, discontinuous gas-exchange in tracheate arthropods. *Amer. Zool.*, 38(3):483–491, 1998.

J. R. B. Lighton and D. Berrigan. Questioning paradigms: caste-specific ventilation in harvester ants, *Messor pergandei* and *M. julianus* (Hymenoptera: Formicidae). *Journal of Experimental Biology*, 198(2):521, 1995.

J. R. B. Lighton and L. J. Fielden. Gas exchange in wind spiders (Arachnida, Solphugidae): Independent evolution of convergent control strategies in solphugids and insects. *Journal of Insect Physiology*, 42(4):347–357, 1996.

J. R. B. Lighton and D. Garrigan. Ant breathing: testing regulation and mechanism hypotheses with hypoxia. *Journal of Experimental Biology*, 198(7):1613, 1995.

L. Ljung, editor. *System identification: Theory for the user*. Prentice Hall, 2nd edition, 1999.

M. Locke. The structure and formation of the cuticulin layer in the epicuticle of an insect, *Calpodes ethlius* (Lepidoptera, Hesperiidae). *Journal of Morphology*, 118(4): 461–494, 1966.

E. Marais, C. J. Klok, J. S. Terblanche, and S. L. Chown. Insect gas exchange patterns: a phylogenetic perspective. *Journal of Experimental Biology*, 208(23):4495, 2005.

P. G. Matthews and C. R. White. Rhinoceros beetles modulate spiracular opening to regulate haemolymph pH. *Comparative Biochemistry and Physiology - Part A: Molecular & Integrative Physiology*, 153(2, Supplement 1):S101–S102, 2009.

P. L. Miller. Respiration - aerial gas transport. In M. Rockstein, editor, *The physiology of insecta*, volume 6, pages 346–402. Academic Press, 2nd edition, 1974.

J. D. Murray. *Mathematical Biology*. Springer Verlag, Berlin, Heidelberg, 2nd edition, 1993.

F. Möller. *Einführung in die Meteorologie*, volume 1. BI Wissenschaftsverlag, Mannheim Wien Zürich, 1991.

C. Mörbitz and S. K. Hetz. Tradeoffs between metabolic rate and spiracular conductance in discontinuous gas exchange of *Samia cynthia* (Lepidoptera, Saturniidae). *Journal of Insect Physiology*, In Press, 2009.

W. F. Pickard. Transition regime diffusion and the structure of the insect tracheolar system. *Journal of Insect Physiology*, 20(6):947–956, 1974.

J. Piiper, P. Dejours, P. Haab, and H. Rahn. Concepts and basic quantities in gas exchange physiology. *Respiration Physiology*, 13(3):292–304, 1971.

A. Pikovsky, M. Rosenblum, and J. Kurths. *Synchronization: a universal concept in nonlinear sciences*. Cambridge University Press, 2003.

A. Punt. The influence of carbon dioxide on the respiration of *Carabus nemoralis* Müll. *Physiologia Comparata et Oecologia*, 4:130–139, 1956.

A. Schmitz and S. F. Perry. Stereological determination of tracheal volume and diffusing capacity of the tracheal walls in the stick insect *Carausius morosus* (Phasmatodea, Lonchodidae). *Physiological and Biochemical Zoology*, 72(2):205–218, 1999.

A. Schmitz and L. T. Wasserthal. Comparative morphology of the spiracles of the Papilionidae, Sphingidae, and Saturniidae (Insecta: Lepidoptera). *International Journal of Insect Morphology and Embryology*, 28(1-2):13–26, 1999.

H. A. Schneiderman. Discontinuous respiration in insects: role of the spiracles. *Biological Bulletin*, 119(3):494, 1960.

H. A. Schneiderman and A. N. Schechter. Discontinuous respiration in insects – V. Pressure and volume changes in the tracheal system of silkworm pupae. *Journal of Insect Physiology*, 12(9):1143–1170, Sept. 1966.

H. A. Schneiderman and C. M. Williams. An experimental analysis of the discontinuous respiration of the cecropia silkworm. *Biological Bulletin*, 109(1):123–143, 1955.

H. A. Schneiderman and C. M. Williams. The physiology of insect diapause. VII. the respiratory metabolism of the cecropia silkworm during diapause and development. *The Biological Bulletin*, 105(2):320, 1953.

K. Sláma. A new look at insect respiration. *Biological Bulletin*, 175(2):289–300, 1988.

A. Stabentheiner, J. Vollmann, H. Kovac, and K. Crailsheim. Oxygen consumption and body temperature of active and resting honeybees. *Journal of Insect Physiology*, 49 (9):881–889, 2003.

J. Sun, D. Folk, T. J. Bradley, and J. Tower. Induced overexpression of mitochondrial Mn-Superoxide Dismutase extends the life span of adult *Drosophila melanogaster*. *Genetics*, 161(2):661–672, 2002.

J. S. Terblanche, E. Marais, S. K. Hetz, and S. L. Chown. Control of discontinuous gas exchange in *Samia cynthia*: effects of atmospheric oxygen, carbon dioxide and moisture. *J Exp Biol*, 211(20):3272–3280, 2008.

W. R. Tschinkel. The nest architecture of the Florida harvester ant, *Pogonomyrmex badius*. *Journal of Insect Science*, 4(21), 2004.

W. G. van der Kloot. The electrophysiology and the nervous control of the spiracular muscle of pupae of the giant silkmoths. *Comparative Biochemistry and Physiology*, 9 (4):317–333, 1963.

X. Wang, W. Conway, R. Burns, N. McCann, and M. Maeder. Comprehensive study of the hydration and dehydration reactions of carbon dioxide in aqueous solution. *The Journal of Physical Chemistry A*, In press, 2009.

L. T. Wasserthal, P. Cloetens, R. Fink, and A. Rack. Physiological measurements combined with synchrotron video-radiography and x-ray-tomography for analysis of respiratory gas exchange and tracheal structure in flies. In S. F. Perry, S. Morris, T. Breuer, N. Pajor, and M. Lambertz, editors, *2nd International Congress of Respiratory Science - Abstracts & Scientific Program*, Hildesheim, Berlin, 2009. Tharax Verlag.

M. W. Westneat, O. Betz, R. W. Blob, K. Fezzaa, W. J. Cooper, and W. K. Lee. Tracheal respiration in insects visualized with synchrotron x-ray imaging. *Science*, 299:558–560, 2003.

M. W. Westneat, J. J. Socha, and W. Lee. Advances in biological structure, function, and physiology using synchrotron x-ray imaging. *Annual Review of Physiology*, 70: 119–142, 2008.

C. R. White, T. M. Blackburn, J. S. Terblanche, E. Marais, M. Gibernau, and S. L. Chown. Evolutionary responses of discontinuous gas exchange in insects. *Proceedings of the National Academy of Sciences*, 104(20):8357–8361, 2007.

V. B. Wigglesworth. *The principles of Insect Physiology.* Methuen, London, 6 edition, 1965.

V. B. Wigglesworth. The regulation of respiration in the flea, *Xenopsylla cheopis*, Roths.(Pulicidae). *Proceedings of the Royal Society of London. Series B - Biological Sciences*, 118(810):397–419, 1935.

V. B. Wigglesworth. The role of the epidermal cells in the 'migration' of tracheoles in *Rhodnius prolixus* (Hemiptera). *Journal of Experimental Biology*, 36(4):632–640, 1959.

R. Williams. pKa data compilation. URL `http://research.chem.psu.edu/brpgroup/pKa_compilation.pdf`.

A. Wobschall and S. Hetz. Oxygen uptake by convection and diffusion in diapausing moth pupae (*Attacus atlas*). *International Congress Series*, 1275:157–164, 2004.

H. A. Woods. Water loss and gas exchange by eggs of *Manduca sexta*: Trading off costs and benefits. *Journal of Insect Physiology*, In Press, 2009.

H. A. Woods, J. C. Sprague, and J. N. Smith. Cavitation in the embryonic tracheal system of *Manduca sexta*. *Journal of Experimental Biology*, 212(20):3296–3304, 2009.

G. R. Wyatt. The biochemistry of insect hemolymph. *Annual Review of Entomology*, 6 (1):75–102, 1961.

List of Figures

List of Tables

Selbständigkeitserklärung

Ich erkläre, dass ich die vorliegende Arbeit selbständig und nur unter Verwendung der angegebenen Literatur und Hilfsmittel angefertigt habe.

I declare to have completed this work all by myself and to have stated all used literature and third party contributions.

Berlin, 25. Juni 2010 Thomas Daniel Förster